Nonlinear waves in systems with $\mathcal{PT}/\mathcal{CP}$- symmetric potentials

Omar Bahaaldin Karakchi

A thesis submitted for the degree of

Doctor of Philosophy

Department of Mathematical Sciences

University of Essex

October, 2017

Acknowledgements

First of all, all thanks are due to Almighty Allah for giving me the strength and stamina to accomplish this work.

My heartfelt gratitude goes to my extremely supportive supervisor Dr Hadi Susanto, who did not only support me academically but was also a great counsellor in hard times. He always accommodated my meeting requests in his very busy schedule and replied swiftly to my inundation of emails.

The completion of my PhD journey would have been impossible without the benevolent support of my wife, who is authoring the greatest chapter in my life. I cannot thank her enough.

To the soul of my great model in life, my father, who was waiting to see me with a PhD degree. I apologise to him for not being able to be by his side during his illness. May Allah shower His mercy on his soul.

To my passionate mother, who cared tirelessly for my father in his illness when she herself was in dire need of care. Her unforgettable kindness will always be the inexhaustible source of my inspiration.

I am deeply indebted to the Chair of my Supervisory Board Dr Georgi Grahovski, who never hesitated to give advice when needed and was an outstanding example in

professionalism.

My thanks also go to Dr N. Karjanto and R. Kusdiantara for their helpful advice.

Last but not least, thanks to all my friends for their great company.

Abstract

Arguably, one of the most elementary nonlinear lattice dynamical models is the discrete nonlinear Schrödinger (DNLS) equation [1]. Particularly, the discrete system and lattice solitons are the main objects of investigation in this work.

In this thesis, we consider a chain of dimers, that is modelled by linearly coupled DNLS equations with gain and loss terms as analogues of Parity-Time ($\mathcal{PT}$) symmetric systems. We construct fundamental bright discrete solitons of the systems and explore their spectral stability. The perturbation theory is used to perform the analysis in the case of weak coupling between the lattices, which is then verified by numerical calculations. Such analysis is based on the concept of the so-called anticontinuum limit approach.

Also we consider an array of dual-core waveguides (which represent an optical realisation of a chain of dimers) with an active (gain-loss) coupling between the cores, opposite signs of the discrete diffraction in the parallel arrays, and a sufficiently large phase-velocity mismatch between them, which is necessary for the overall stability of the system. The corresponding linear array provides an optical emulation of the Charge-Parity ($\mathcal{CP}$) symmetry. The addition of the intra-core cubic nonlinearity, despite breaking the $\mathcal{CP}$-symmetry, gives rise to several families of fundamental bright discrete solitons, whose existence and stability are explored here by means of analytical and numerical methods.

We study localised solutions in a ($\mathcal{PT}$)-symmetric coupler composed by a chain of dimers, that is modelled by linearly coupled DNLS equations with gain and loss terms and with a cubic-quintic nonlinearity. We consider site-centered and bond-centered localised solutions and show that the resulting bifurcation diagrams when a parameter is varied form a snaking behaviour. Each localised solution has symmetric and antisymmetric

configurations between the arms. We analyse the width of the snaking region and provide asymptotic approximations in the limit of strong and weak coupling where good agreement is obtained.

Declaration

The work in this thesis is based on research carried out with my supervisor Dr Hadi Susanto at the university of Essex, Department of Mathematical Sciences, United Kingdom. No part of this thesis has been submitted elsewhere for any other degree or qualification, and it is all my own work, unless referenced, to the contrary, in the text.

Contents

Chapter 1

Introduction

1.1 History of soliton

The term *soliton* refers to a solitary wave propagating in a nonlinear system [2]. In [3,4], it is defined as a localised nonlinear wave. It is a special wave that is capable of travelling without dispersion, forming a rare natural phenomenon. This enables it to flow without any limitations as soon as it is formed. Soliton can be seen in both continuous and discrete systems [2].

Scientifically, soliton was discovered in August 1834 by a Scottish engineer called Scott Russell during an experiment to find design parameters for converting horse power to steam through the identification of the best canal boats in order to measure the correlation between the propelling power of the boat and its speed. In the experiment, the ropes connecting the boat with the two horses were suddenly broken, causing the boat to stop. Following this, he immediately mounted the horse to observe an extremely strange phenomenon. What he noticed was a mass of water that started to roll ahead of the boat

with high velocity and continued with this movement for around two miles without any alteration of either shape or speed [5], a wave that he later called *Wave of Translation*. Scott Russell reported his observation on that day to a senior scientist named Sir John Herschel, who did not take it seriously and presumed that it was one of many common and insignificant waves known at the time. To examine further the significance of his discovery, Russell conducted a number of laboratory experiments to simulate the wave with shallow water in a tank, which led him to the identification of the following properties:

1. Analytically, the solitary wave can be represented as a hyperbolic secant function.

2. Unlike normal waves, solitary waves can cross one another without any change, except for a small displacement to each, i.e., phase-shift, as a result of their interaction. This indicates that these waves have the capacity to interact with other similar waves while maintaining both their shapes and speeds, with only a phase shift change. This allows a large solitary wave to overtake a small one rather than merge with it, which characterises the particle-like interaction property from which the name soliton was coined in 1965, by [2].

3. Solitary waves are able to travel for long distances without dissipation.

4. The wave's speed depends on its size and width and the depth of water.

5. Two or more independent solitary waves can be produced by a sufficiently large initial mass of water.

6. In a shallow water channel of height h, a solitary wave of amplitude A travels at a speed $\sqrt{g(A+h)}$ (where g is the gravitational acceleration), implying that larger-

amplitude solitary waves move faster than smaller ones, i.e. confirming a nonlinear effect.

Throughout his life, Russell was convinced that his discovery was of great scientific significance and it was not until 20th century when his work received acceptance. At that time, his solitary waves could not be explained by the existing wave theory; it was believed that waves either vanish or rise up until they break. In fact, it was only in 1870s when solitary waves started to be theoretically investigated [6] and the most significant paper that supported Russell's discovery was written more than five decades later by Diederik J. Korteweg and his PhD student G. de Vries in 1895 [7].

A nonlinear partial differential equation (PDE) which was derived mathematically by Diederik J. Korteweg and G. de Vries and confirmed the existence of the hydrodynamic solitary wave, known as the Korteweg-de Vries (KdV) equation, modelled the evolution of waves in a shallow one-dimensional (1D) water channel, and was given by:

$$\eta_t + c\eta_x + \epsilon\eta_{xxx} + \gamma\eta\eta_x = 0, \tag{1.1}$$

where η is a wave function, $c = \sqrt{gh}$ is the velocity of small amplitude waves, $\epsilon = c(h^2/6 - T/(2\rho g))$ represents the dispersive parameter, $\gamma = 3c/(2h)$ is the nonlinear parameter, T is the surface tension and ρ is the density of water. Korteweg and de Vries showed that Eq. (1.1) had exact travelling localised solutions which agreed with Scott Russells observation. It should be noted that although Eq. (1.1) was named for Korteweg and de Vries, it was apparently first investigated (in the absence of surface tension) independently by [6].

Mathematically, the formation of a soliton in the KdV equation [7] can be explained as

follows:

In the absence of dispersive and nonlinear terms, i.e.,when $\epsilon = \gamma = 0$, the KdV equation becomes a dispersionless linear wave equation and thus has a travelling wave solution for any shape (including a localised form) at any velocity c. If one reinstates the dispersion term only, i.e., by setting $\epsilon \neq 0$ and $\gamma = 0$, different Fourier components of any initial condition will propagate at different velocities, thus the wave profile will spread out (disperse). In contrast, if one reinstates only the nonlinear term, i.e., when $\epsilon = 0$ and $\gamma \neq 0$, the wave will experience harmonic generation so that the crest of the wave moves faster than the rest; this then leads to wave breaking. However, by considering both dispersion and nonlinearity, there will be a situation such that the effect of dispersion is balanced by that of nonlinearity. In the latter case, a solitary wave can form.

Although Korteweg and de Vries were able to model Russell's solitary waves successfully, their work lost interest again due to their inability to find a general solution of their equation.

The year 1955 witnessed the exploration of the dynamics of energy equipartition in a slightly nonlinear mechanical system, i.e. a chain of equal mass particles connected by slightly nonlinear springs, through the Los Alamos MANIAC computing machine, Enrico Fermi, John Pasta and Stanislaw Ulam (FPU) [8]. It was expected that when introducing all the energy in a single mode, the small nonlinearity would lead to energy redistribution among all the modes (known as thermalisation). However, to their surprise, their numerical results ascertained that all the energy returned almost periodically to the original inter-site mode and a few nearby modes.

Interest in Russell's solitary waves was restimulated again in the post-war era by virtue

of rapid developments in digital computing. In mid 1960s applied scientists began to study nonlinear wave propagation through utilising modern digital computers, which led to the appreciation of Russell's innovative idea of the 'Wave of Translation'.

In 1965, utilising a finite difference approach, Zabusky and Kruskal [2] investigated solitary waves numerically and found out that such waves maintain their shape and speed following collision, except for a very minor change in the phase shift. It was due to this particular behaviour of these waves that the two authors decided to name such type of waves 'soliton'.

The most significant discoveries in mathematics were achieved at the hands of Gardner, Greene, Kruskal and Miura [9] in 1967. These scientists were able to find the exact solution for the soliton phenomenon, including soliton solutions of the KdV equation. The method they employed in their simulation study is known today as the inverse scattering method (ISM). The ISM, which was initially used to interpret the KdV equation only, is now implemented for generating exact soliton solutions in a variety of integrable nonlinear PDEs.

In 1972, employing the ISM, Zakharov and Shabat were able to solve the nonlinear Schrödinger equation (NLS) [10]:

$$iu_t + u_{xx} \pm \beta|u|^2 u = 0. \tag{1.2}$$

where u is a wave function and i denotes the imaginary number $\sqrt{-1}$. They showed that soliton solutions exist and are integrable. The 'plus' and 'minus' signs in the nonlinearity term refer to the so-called focusing and defocusing nonlinearities, respectively. The

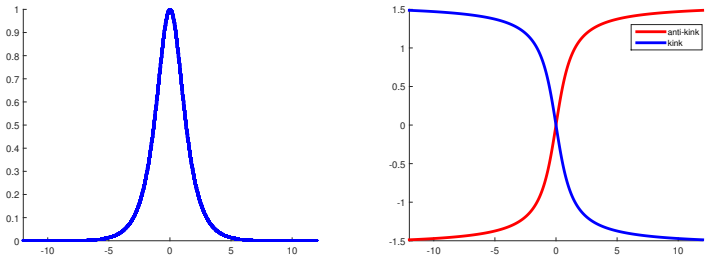

(a) A pulse of the soliton (b) A kink and anti-kink soliton

Figure 1.1: The focusing NLS shown as in (a) and the defocusing NLS as in (b).

focusing NLS permits a pulse like soliton (see Fig. 1.1 (a)), while the defocusing one has a kink-shaped soliton (see Fig. 1.1(b)). In nonlinear optics, these are known as bright and dark solitons, respectively. For the full (time-dependant) NLS, the bright solitons solution corresponds to zero boundary conditions as $|x| \longrightarrow \infty$, while dark solitons corresponds to constant boundary conditions as $|x| \longrightarrow \infty$. The name of the NLS equation comes from the similarity in form between its structure and the Schrödinger equation of quantum mechanics [11]. The NLS equation can be found as an essential model in a variety of applications. Examples include nonlinear envelope waves in hydrodynamics, nonlinear optics, nonlinear acoustics and plasma waves [12].

Also, in 1973 Ablowitz, Kaup, Newell and Segur applied ISM for solving the sine-Gordon (SG) equation [13]

$$\theta_{tt} - \theta_{xx} = \sin(\theta), \tag{1.3}$$

and presented its soliton solutions as well, which admits kink and anti-kink solitons. The SG equation is also evident in many physical applications, such as the propagation of crystal defects and the propagation of quantum units of magnetic flux (called fluxons) on long Josephson (superconducting) transmission lines [12].

Since the mid 1970s, various integrable nonlinear equations exhibiting soliton solutions have been investigated, both in continuous and discrete systems. These studies have identified the soliton phenomenon in a number of applied sciences. Despite this, examining non-integrable equations (whether continuous or discrete) is also an interesting topic for research. Apart from their distinct mathematical properties, these non-integrable equations are of overriding importance due to the fact that they appear in various useful applications. This has inspired a number of researchers to observe solitons in such systems both theoretically and experimentally.

After a delay of just less than two centuries, Scott Russell's observations and research have recently found the light in fibre-optic communication industry. The properties of the soliton wave, i.e. the fact that it does not break up, spread out or lose strength over distance, make this type of wave optimal for fibre-optic communications networks where information is carried by billions of solitons per second down fibre circuits for cable TV, telephone and computers. In recognition of his discovery, a fibre-optic cable linking Edinburgh with Glasgow now runs beneath the tow-path from which John Scott Russell had his first observations, and along the aqueduct which now bears his name.

It is noteworthy here that what we mean by a localised wave in this work is restricted to the solution of having a peak with tails decaying exponentially to 0 as the spatial coordinate x tends to $\pm\infty$, as can be seen in Fig. 1.1 (a). It is also important to highlight that the current study is devoted to the investigation of solitons in lattice systems governed by discrete nonlinear Schrödinger (DNLS) equations. Before discussing these lattice equations further, particularly, we study the DNLS equations as analogues of the so-called Parity-Time ($\mathcal{PT}$) and Charge-Parity ($\mathcal{CP}$) symmetric systems. The next sections will define and give some

background about the Parity-Time ($\mathcal{PT}$) and Charge-Parity ($\mathcal{CP}$) systems.

1.2 An introduction to $\mathcal{PT}$-symmetry with basic definitions

Space-time reflection symmetry, or $\mathcal{PT}$-symmetry, first suggested in quantum mechanics in 1998 by Bender and Boettcher [14], has become an interesting topic for research in fundamental physics.

$\mathcal{PT}$-symmetric quantum mechanics is an extension of conventional quantum mechanics into the complex domain. Hence, $\mathcal{PT}$-symmetry is not in contradiction with conventional quantum theory but is simply a complex generalisation of it. $\mathcal{PT}$-symmetric quantum mechanics was originally regarded as a purely mathematical breakthrough but with little hope of real-life applications; however, since 2007 it has interestingly become a hot research topic in experimental physics. It has now been studies experimentally in a variety of areas, such as lasers, optical wave guides, optical resonators, superconducting wires, microwave cavities, NMR, graphene, and metamaterials. Through utilising the techniques employed in these studies, there seems to be a potential of using the $\mathcal{PT}$-symmetry to develop new ways to control light, perhaps even leading to a new generation of computers run by optical beams rather than conventional electric wires. It is also possible to use it in formulating new kinds of materials and to create more advanced communication devices [15].

By $\mathcal{PT}$-symmetry we mean reflection in space, with a simultaneous reversal of time. A Hamiltonian written in the form [16]

$$H = p^2 + V(x), \tag{1.4}$$

will be $\mathcal{PT}$-symmetric if

$$V^*(-x) = V(x). \tag{1.5}$$

It can be seen that satisfies this constraint is satisfied by the Bessis and Zinn-Justin conjecture. In fact any polynomial potential will satisfy this constraint, with the condition that any even power of x has a real coefficient and odd powers have purely imaginary coefficients.

We can define the $\mathcal{P}$ and $\mathcal{T}$ operators separately. The $\mathcal{P}$ operator is defined as:

$$\mathcal{P}: \quad \begin{aligned} x &\to -x, \\ p &\to -p, \end{aligned} \tag{1.6}$$

while the $\mathcal{T}$ operator is defined as:

$$\mathcal{T}: \quad \begin{aligned} x &\to x, \\ p &\to -p, \\ i &\to -i, \end{aligned} \tag{1.7}$$

the $i \to -i$ being there to keep the commutator $[x, p] = i$ consistent. It can be noticed that $\mathcal{P}^2 = \mathcal{T}^2 = (\mathcal{PT})^2 = 1$.

The full $\mathcal{PT}$ transformation can be considered in terms of the real and imaginary parts of x. We can see that under $x = \Re(x) + i\Im(x) \to -\Re(x) + i\Im(x) = -x^*$. It appears that Hamiltonians which are symmetric under this operator may have real energies. In fact, it is true that if the eigenvectors of the Hamiltonian are also $\mathcal{PT}$-symmetric, then the eigenvalues are real. What follows shows why this should be the case.

In 1998, Bender and Boettcher [14] revealed that quantum systems with a non-Hermitian Hamiltonian can have a set of eigenstates with real eigenvalues (a real spectrum). In simpler terms, they concluded that the Hermiticity of the Hamiltonian is not a necessary condition for the realness of its eigenvalues, and the construction of new quantum mechanics is based on such Hamiltonians [14, 17, 18].

The initial point of this construction can formulated as follows. Where there are real eigenvalues of a non-Hermitian Hamiltonian, the modulus of the wave function for the eigenstates of the system is conserved in time even in regions with a complex potential. Indeed,

$$\hat{H}\psi_k = E_k\psi_k, \tag{1.8}$$

for any eigenstate of the Hamiltonian. Substituting Eq.(1.8) in the time-dependent Schrödinger equation, we obtain

$$i\frac{\partial\psi_k}{\partial_t} = E_k\psi_k. \tag{1.9}$$

Obviously, for any real E_k, the modulus of ψ_k is conserved in time. However, the eigenstates of such a Hamiltonian are not orthogonal, and the construction of self-consistent quantum mechanics based on such Hamiltonians necessitates reformulating the definitions of the scalar product and norm [19].

$\mathcal{PT}$-symmetry is a fairly recent subject. Bessis and Zinn-Justin were the first to propose the possibility that non-hermitian Hamiltonians could have a role to play. They inferred that the spectrum of the eigenvalue problem:

$$\left(-\frac{d^2}{dx^2} + ix^3\right)\psi(x) = E\psi(x), \psi(x) \in L^2(\mathfrak{R}), \tag{1.10}$$

is completely real and positive. The Hamiltonian is always Hermitian in conventional quantum mechanics, which constrains the energy spectrum to be real on the assumption of conventional boundary conditions. The non-Hermiticity of this potential implies that it is not possible to use the usual arguments for the reality of the spectrum. Bender and Boettcher [14] interpreted the reality of this spectrum to be a clue to its $\mathcal{PT}$-symmetry. In other words, the potential remains constant if we simultaneously reflect in space and reverse time.

The possibility of finding real eigenvalues in a non-Hermitian Hamiltonian has stimulated interest, particularly as the notion of $\mathcal{PT}$-symmetry seems to lend itself more to physical interpretation than the mathematical concept of hermiticity.

1.2.1 How classical physics developed into modern physics

To understand the literature on $\mathcal{PT}$-symmetric quantum mechanics, it is important to recall two novel findings in the early 20th century that transformed classical physics into what is considered today as modern physics. One of these findings was quantum mechanics, which deals with the nature of matter, the stability of atomic energy levels, the formation of molecules from the binding of atoms, and the characteristics of materials, while the other one was relativity, which is concerned with the geometry of space and time. Symmetries are an essential part of physical laws, and these two findings possess fundamental symmetries. However, while quantum mechanics has a discrete symmetry called Hermiticity, relativity has a continuous symmetry, which is expressed in terms of the Poincare' group.

The quantum interference phenomenon indicates the importance of complex numbers in interpreting physical observations in quantum mechanics. The complexity of the

Schrödinger equation stems from the fact that quantum theory makes complex numbers probabilistic rather than definite predictions. For instance, the mass of an unstable particle is displayed as a pole at a specific point in the complex plane, but the remnant of this pole is a probability distribution on the real axis, and we cannot be decisive on the mass of the particle [15].

1.2.2 Symmetries

Despite the centrality of complex numbers in quantum mechanics, the symmetries of space and time are confined to the real domain. The real four-dimensional vector (x, y, z, t) represents any point in space-time. The continuous symmetry group of space-time, known as the Poincare' group, is ten-dimensional; it includes four translations, three rotations and three possible ways of boosting the velocity. As for translations, the same experimental result will be given when repeating an experiment in a laboratory located at different points in space and time $(x + a, y + b, z + c, t + d)$. In terms of rotations, these can be around the x, y, and z axes. Hence, repeating an experiment in a laboratory that has been rotated in space will also yield the same result. Finally, the velocity of rotation can be boosted in three possible ways, along the x, y, or z axes. Again, repeating an experiment in a laboratory that is moving at a constant velocity relative to the original laboratory will yield identical results.

Along with the continuous transformations (i.e. from the Lorentz group rotations and boosts), there are also two discrete transformations of space and time variables. The first, which is called parity $\mathcal{P}$, transforms the sign of the spatial part of the four-vector $\mathcal{P} : (x, y, z, t) \rightarrow (-x, -y, -z, t)$. This symmetry operation alters one's right hand into

one's left hand; such a change cannot be accomplished by any rotation. The second, which is called time reversal $\mathcal{T}$, transforms the sign of the time component of the four-vector $\mathcal{T} : (x, y, z, t) \rightarrow (x, y, z, -t)$. In 1957, Lee and Yang were awarded a Nobel Prize for demonstrating that parity is not a symmetry of nature, and another was awarded to Cronin and Fitch in 1980 for showing that the same applies to time reversal. A left-handed laboratory can yield different experimental results from a right-handed one and a laboratory travelling backward in time can give different results from one travelling forward. After these developments, it was accepted that the correct geometrical symmetry of nature must include both $\mathcal{P}$ and $\mathcal{T}$ [15].

1.2.3 Gain and loss balanced

Typically, $\mathcal{PT}$-symmetric systems possess complex potentials and, therefore, can be regarded as non-isolated systems that interact with their environment: a potential characterised by having a positive-imaginary part and another with a negative-imaginary part. While the former describes a system that receives energy from its environment, the latter describes a system that loses energy to its environment. However, a $\mathcal{PT}$-symmetric system is unique in that the $\mathcal{PT}$-symmetry condition implies an exact balance between gain and loss. It is worth noting that a $\mathcal{PT}$-symmetric system can be produced in a laboratory by coupling two identical subsystems, one with gain and the other with loss. The resulting composite system is $\mathcal{PT}$-symmetric due to the fact that space reflection $\mathcal{P}$ causes an interchange in the subsystems and time reversal $\mathcal{T}$ alternates the roles of gain and loss. This phase transition between regions of broken and unbroken $\mathcal{PT}$-symmetry has been observed in a number of experiments, especially in the area of optics [15].

The initial theoretical and mathematical work on $\mathcal{PT}$-symmetric quantum mechanics has led to the emergence of significant experimental work in various areas of physics. It is worth mentioning that experimental work for decades in many other areas of physics, such as string theory and super-symmetry, has not succeeded to date in stimulating worthwhile experimentation. It seems that $\mathcal{PT}$-symmetry will lead to significant and continuous practical and commercial applications [15].

In Section 1.3, we will introduce the concept of $\mathcal{CP}$ violation, which forms part of the experimental work in Chapter 4.

1.3 What is $\mathcal{CP}$ violation?

$\mathcal{CP}$- can be defined as a discrete symmetry of nature comprising two essential symmetries: charge conjugation $\mathcal{C}$ and parity $\mathcal{P}$. Charge conjugation, which is the symmetry between positive and negative charge, causes the transformation of a particle into the corresponding anti-particle. For instance, if $\mathcal{C}$ is applied to an electron, a positron will be yielded; that is, $\mathcal{C}$ juxtaposes matter with anti-matter.

A basic observation of our surroundings will show that everything is composed of protons, neutrons and electrons, and these particles also form the different elements of our space, such as planets, stars and atmosphere. In other words, in our cosmos, matter exists more excessively than antimatter, conflicting the theoretical symmetry between them, which is known to particle physicists as $\mathcal{CP}$. This means that if matter and antimatter are treated alike, then nature can be said to be $\mathcal{CP}$-symmetric; on the contrary, if they are not treated equally, then $\mathcal{CP}$ is violated. In other words, if we take a particle with a positive

charge, it will be reversed into negative by C, and vice versa [20].

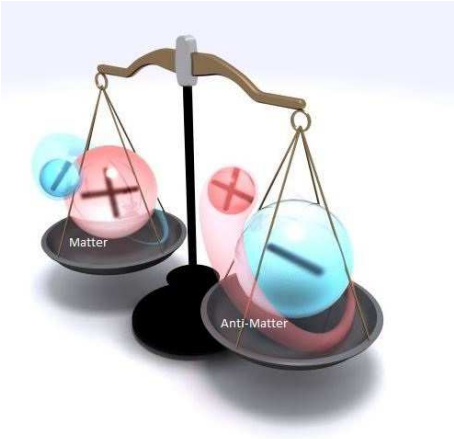

Figure 1.2: Matter if treated with antimatter alike, then nature can be said to be $\mathcal{CP}$-symmetric

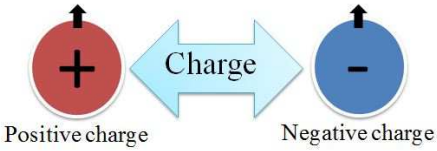

Figure 1.3: The interaction of the particles between positive and negative charge

It is worth noting that if we start with a neutral particle, C will have no charge and, consequently, no effect.

Parity, on the other hand, is slightly more difficult to describe, though more intuitive, as a symmetry of spatial coordinates is encountered when we look into a mirror. If I am right-handed, my reflection will be left-handed when I look into a mirror, which represents in particle physics an exact analogy of the $\mathcal{P}$-symmetry, where right-handed particles are transformed into left-handed ones. This means that if $\mathcal{P}$ is carried out with an electron moving with a positive velocity $\vec{v}$ from one direction to another, this electron will convert the direction of the movement with a negative velocity $-\vec{v}$. In brief, parity gives the mirror image of reality.

Therefore, when an electron moving with a velocity $\vec{v}$ undergoes a $\mathcal{CP}$ transformation, this will yield a positron moving with a velocity $-\vec{v}$. Therefore, the application of $\mathcal{CP}$ on matter will result in the mirror image of its corresponding anti-matter.

Suppose we have a "$\mathcal{CP}$-mirror," which is a device that returns the mirror image of the anti-matter (see Fig. 1.5). When looking at our image in a standard mirror, what we see is a parity transformation of ourselves.

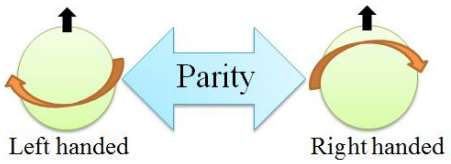

Figure 1.4: Illustration of parity time and how a left handed one will be reflected as right handed

Figure 1.5: An illustration of what can be seen in a $\mathcal{CP}$-mirror

The combination of $\mathcal{C}$ and $\mathcal{P}$ on a left-handed particle with a negative charge would result in its transformation into a right handed particle with a positive charge.

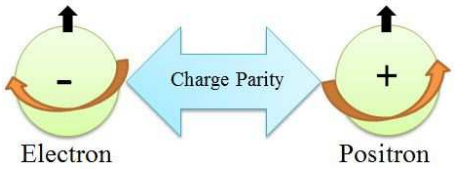

Figure 1.6: The combination of charge parity

Our intuitive expectation is that our "anti-self" will wave back at us in the $\mathcal{CP}$-mirror. That is, $\mathcal{CP}$ is expected to be an effective symmetry of nature. But does this prove to be the case?

$\mathcal{CP}$ was not discovered until 1964, when Fitch, Cronin and collaborators [21] were studying the decays of neutral kaons, which are particles comprising a strange quark and a down anti-quark. Despite the fact that the effect they noticed was tiny, only one part in a thousand, it was extremely important, as it revealed that matter and anti-matter are intrinsically different, and the researchers were awarded a Nobel Prize in 1980.

1.4 Outline of the thesis

We started our work in Chapter 1 by showing the history about solitons. Then, we gave an introduction with definitions to the $\mathcal{PT}$- and $\mathcal{CP}$-symmetry.

An introduction to stationary solutions of the DNLS in 1D is going to be given in Chapter 2 where their profile and stability analysis are studied and good agreements are shown between the numerical and analytical calculations.

In Chapter 3, we study the existence and stability of fundamental bright discrete solitons in a $\mathcal{PT}$-symmetric coupler composed by a chain of dimers that is modelled by linearly coupled DNLS with gain and loss terms. We use a perturbation theory for small coupling

between the lattices to perform the analysis, which is then confirmed by numerical calculations. Such analysis is based on the concept of the so-called anticontinuum limit approach. We consider the fundamental onsite and intersite bright solitons. Each solution has symmetric and antisymmetric configurations between the arms. The stability of the solutions is then determined by solving the corresponding eigenvalue problem. We conclude that both symmetric and antisymmetric onsite mode can be stable for small coupling, in contrast to the reported continuum limit, where the antisymmetric solutions are always unstable. The instability is either due to the internal modes crossing the origin or the appearance of a quartet of complex eigenvalues. In general, the gain-loss term can be considered parasitic as it reduces the stability region of the onsite solitons. Additionally, we analyse the dynamic behaviour of the onsite and intersite solitons when unstable, where typically it is either in the form of travelling solitons or soliton blow-ups.

In Chapter 4, we also consider a chain of dimers with a complex coupling between the arms modelling a dual-core optical waveguide with opposite signs of the group-velocity-dispersion in the two cores, and a phase-velocity mismatch between them. The corresponding linear system is an optical realisation of the $\mathcal{CP}$-symmetry. The addition of the intra-core cubic nonlinearity despite breaking the symmetry gives rise to fundamental bright discrete solitons. Here, we explore their existence and spectral stability. Asymptotic analysis in the case of weak coupling between the dimers as well as between the arms is presented. We also present discrete solitons that have no corresponding solutions in the continuum limit.

Snakes in a $\mathcal{PT}$-symmetric chain of dimers are presented in Chapter 5. We study localised solutions in a $\mathcal{PT}$-symmetric coupler composed by a chain of dimers, which is

modelled by linearly coupled DNLS with gain and loss terms and with a cubic-quintic nonlinearity. We consider site-centered and bond-centered localised solutions and show that the resulting bifurcation diagrams when a parameter is varied form a snaking behaviour. Each localised solution has symmetric and antisymmetric configurations between the arms. The critical gain/loss coefficient above which the $\mathcal{PT}-$symmetry is broken corresponds to the overlapping bifurcation diagrams. We analyse the width of the snaking region and provide asymptotic approximations in the limit of strong and weak coupling where good agreement is obtained.

Finally, Chapter 6 summarises the main findings in the thesis and concludes with suggestions for further research.

Chapter 2

Discrete nonlinear Schrödinger (DNLS) equation in one-dimension

In the previous chapter, we have briefly discussed some properties and definitions of solitons. In this chapter, we intend to give a brief introduction to DNLS, then to show some previous results of the lattice solitary waves in the DNLS equation with cubic nonlinearity in one-dimension (1D), in particular the profile and stability of fundamental bright discrete solitons.

In physics, quantum mechanics or particle physics are used to describe discrete phenomena, such as the interaction of the elementary particles of matter (e.g. electrons and atoms). However, it is almost impossible to apply a quantum-mechanical approach to most natural phenomena involving billions of such particles. This means that even modern state-of-art computers cannot perhaps explain all the interaction between these objects. For this reason, macroscopic approaches of classical physics are utilised to account for most natural phenomena, where a particular physical system is described by means of averaged

macroscopic quantities. In spite of this, it is still possible to describe many macroscopic systems by means of some type of a discrete model.

The year 1938 witnessed the first study of discrete dynamical systems by Frenkel and Kontorova, who employed a discrete model for describing the motion of dislocations inside a crystal [22]. Following this study, discrete models have been utilised in a variety of systems in physics, biology and chemistry. For instance, they have been used to account for the transfer of heat in lattices [8, 23], to justify vibrations in crystal lattices [24, 25], and to examine the dynamic transitions of the structural phase in crystals [26,27]. Additionally, discrete models have also been tapped into for predicting nonlinear localisation phenomena in atomic lattices [28,29] and molecular chains [30]. In 2001, Abdullaev et. al. made use of a discrete Schrödinger-like model in order to predict the existence of nonlinearly self-trapped states in Bose-Einstain condensates [31], and these predictions were further experimentally examined in [32].

In biology, on the other hand, discrete nonlinear models have been exploited to explain the contraction of proteins [33, 34], and more recently the localisation and transport of vibrational energy in DNA molecules [35].

Discrete periodic structures are becoming more significant in optics due to the fact that they enjoy the distinct optical properties of photonic crystal fibres and coupled waveguide arrays [36, 37]. An example of the development of a discrete model is the existence of an array of weakly coupled identical waveguides. The propagation of an optical beam in a waveguide array causes a a linear superposition of the Floquet-Bloch modes of the structure [38], each of which has its specific propagation constant and profile [39]. The problems in weakly coupled arrays can be handled in a more simplified way through

making use of the fact that most of the energy in the first order band tends to localise to the higher index waveguide regions. For this reason, the optical field can undergo a process of decomposition into a superposition of discrete modes that are associated with individual channels. In addition, it is often the case that the optical field can be approximated by analysing the phase and amplitude of each mode [40]. The exchange in optical energy among individual waveguides takes place as a result of the overlap of their modal fields and is formed through introducing a coupling term into the discrete equations.

The theoretical foundations of linear properties of light propagation in 1D waveguide chains (known as linear discrete diffraction) were introduced in 1965 by Jones [41] and then these properties were examined experimentally several years later in gallium arsenide waveguide arrays [42]. Nonlinear optical properties of waveguide arrays were first studied in 1988 by Christodoulides and Joseph, who proposed that light can trap itself in a nonlinear waveguide array through the Kerr nonlinear effect, leading to the formation of discrete soliton (DS) [43]. Discrete solitons in Kerr media were investigated experimentally for the first time in 1998 by Eisenberg et. al. [44], which has stimulated extensive research in the area. So far, discrete solitons have also been the subject of experimental observation in media with photorefractive [45], quadratic [46] and orientational nonlinearities [47].

DNLS equation describes a particularly simple model for a lattice of coupled anharmonic oscillators. In this chapter, DNLS equation can be defined as any equation that can be generated from a nonlinear Schrödinger (NLS) equation of general form [48]

$$i\frac{\partial u}{\partial t} + \Delta u + f(|u|^2)u = 0, \tag{2.1}$$

through utilising finite-difference approximation to the operators acting on the space-time-dependent continuous field. In Eq.(2.1), $\Delta = \nabla^2$ is the Laplace operator acting in one, two, or three spatial dimensions, and f is a quite general function that, for most purposes, is taken to be differentiable and with $f(0) = 0$. In the most well-known case of cubic nonlinearity, $f(|u|^2) = \pm|u|^2$, Eq. (2.1) is often referred to as the NLS equation, and is integrable with the Inverse Scattering Method if the number of spatial dimensions is one. In this work, the term DNLS equation is used to refer to the set of coupled ordinary differential equations arising from discretising all spatial variables in Eq.(2.1), while keeping the continuity of the time-variable t.

Some properties and analytical calculations on lattice solitary waves in the DNLS equation with cubic nonlinearity was studied in [49] in the presence of parametrically driving (PDNLS) equation where the existence and stability of fundamental bright and dark discrete solitons in the DNLS equation was considered.

The simplest and clearest example of a DNLS equation can be derived by replacing the Laplacian operator in Eq.(2.1) with the corresponding discrete Laplacian. Thus, Eq.(2.1) can alternatively be written in the following form which is in one spatial dimension where our work will be began by considering the DNLS equation given by:

$$\dot{u}_n = i\sigma|u_n|^2 u_n + i\epsilon\Delta_2 u_n, \tag{2.2}$$

$u_n = u_n(t)$, is a complex-valued wave function (complex mode amplitude of the oscillator) at site $n \in \mathbb{Z}$ [48]. The index n is the range over the 1D lattice where the lattice can either be infinite ($n = 0, \pm1, \pm2, ...$) or finite ($n = -N, -N+1, \ldots, N$). In the case of finite lattice, periodic

boundary conditions, $u_{-N-1} = u_N$ and $u_{N+1} = u_{-N}$ are usually assumed. The overdot is the time derivative, $i = \sqrt{-1}$, $\epsilon > 0$ is the distance constant coefficient of the horizontal linear coupling (coupling constant between two adjacent sites), $\Delta_2 u_n = (u_{n+1} - 2u_n + u_{n-1})$ is the discrete Laplacian term in one spatial dimension. The nonlinearity coefficient is denoted by σ (anharmonic parameter), which can be scaled to +1 without loss of generality due to the case of focusing nonlinearity that we consider. Bright discrete soliton solutions satisfy the localisation conditions $u_n \to 0$ as $n \to \pm\infty$.

This set of differential-difference equations with purely diagonal ("on-site") nonlinearity is sometimes referred to as the diagonal DNLS (DDNLS) equation, but since it is the most studied example of a DNLS equation at all, it is often simply named as the DNLS equation.

It is worth mentioning here that discrete soliton was first studied in 1962 by Perring and Skyrme (see [50]) who examined the discrete sine-Gordon equation derived originally by Frenkel and Kontorova in 1939 (see [12, 51]). It is also noteworthy that in early DNLS studies, when breathers in discrete systems were still obscure, these solutions were often called solitons.

Stationary solutions of the DNLS equations are special solutions of the form

$$u_n(t) = A_n e^{i\omega t}, \tag{2.3}$$

such that ω represents the light propagation constant (oscillation frequency) and A_n is the stationary amplitude (independent of time).

Substituting Eq.(2.3) into Eq.(2.2) gives an algebraic set of equations for A_n, i.e.

$$\omega A_n = A_n^3 + \epsilon(A_{n+1} - 2A_n + A_{n-1}). \tag{2.4}$$

Despite the fact that the stationary DNLS Eq. (2.2) were found by Holstein in 1959 in his significant work on polarons in molecular crystals [52], the first systematic study of its single-peak breather solution as an exact solution to the fully discrete equations was conducted by Scott and MacNeil in 1983 [53]. Later and independently, a more general method was developed by Aubry, MacKay and co-workers along these lines to address the breather problem in arbitrary systems of coupled oscillators [54, 55].

Due to the fact that the DNLS equation can be generally applied and exists in a variety of physical fields, new researchers trying to investigate it have not always been aware of previous findings, which has caused many of its properties to be rediscovered independently and appear in different contexts in the literature.

The feature of Eq. (2.4) makes the DNLS a relatively simple model to work with. For small periodic lattices up to $N = 4$, the resulting equations can be solved exactly to obtain all the families of stationary solutions as a function of ω and σ (for fixed N) with an interesting bifurcation structure [56]. However, for a large or infinite lattice the solutions must be found by numerical methods such as shooting or spectral methods. These solutions can then be examined as a function of the parameters of the equation by means of numerical continuation methods (see [57] for a complete list of solutions for $N = 6$). If σ is small enough, localised solutions are found, which decay exponentially for large n. As these solutions possess a periodic time behaviour ($A_n e^{i\omega t}$), they are conveniently called "breather"

solutions [48]. Another motivation is that the DNLS equation can be obtained from the discrete Klein-Gordon equation, describing a lattice of coupled anharmonic oscillators, via a multiscale expansion in the limits of small-amplitude oscillations and weak inter-site coupling [58–60]. The discrete breathers of this lattice are then represented as stationary solutions to the DNLS equation.

To find solutions to Eq.(2.4), many approaches exist. Iteratively, the time-independent solutions can be calculated using Newton-Raphson method. In order to obtain the localised solutions to Eq. (2.4) and hence find the discrete solitons governed by the DNLS equation, we need to find

$$\overline{X} = [A_{-N}\ A_{-N+1} \ldots A_{-N-1}\ A_N]^T \ \text{ for which } \ [f_{-N}\ \ldots\ f_N]^T = [0\ \ldots\ 0]^T,$$

where we define

$$f_n = A_n^3 - (2\epsilon + \omega)A_n + \epsilon(A_{n+1} + A_{n-1}),$$

$$f_{-N} = A_{-N}^3 - (2\epsilon + \omega)A_{-N} + \epsilon(A_{-N+1} + A_N) \ \text{ and } \ f_N = A_N^3 - (2\epsilon + \omega)A_N + \epsilon(A_{N-1} + A_{-N}).$$

For $2N + 1$ waveguide arrays, Newton-Raphson method can be written as follows:

$$\overline{X}_{k+1} = \overline{X}_k - J^{-1}_{(2N+1)\times(2N+1)}\ [f_{-N}\ f_{-N+1}\ \ldots\ f_N]^T, \tag{2.5}$$

where $J = \begin{pmatrix} \frac{\partial f_{-N}}{\partial A_{-N}} & \cdot & \cdot & \frac{\partial f_{-N}}{\partial A_N} \\ \cdot & \cdot & \cdot & \cdot \\ \cdot & \cdot & \cdot & \cdot \\ \frac{\partial f_{2N+1}}{\partial A_{-N}} & \cdot & \cdot & \frac{\partial f_{2N+1}}{\partial A_N} \end{pmatrix}$.

The iteration (2.5) is performed until a convergent criterion is achieved.

Now, we need to consider the stability of the obtained solutions of the DNLS for Eq. (2.2). The stability of such solutions in time can be investigated by looking at general perturbations in the rotating frame of the solutions [61]. Once such discrete solitary-wave solutions have been found, their linear stability is determined by solving a corresponding eigenvalue problem. To do so, we introduce $u_n = (A_n + \zeta B_n(t))e^{i\omega t}$ where $|\zeta| \ll 1$, and substitute it into Eq. (2.2) to obtain the following linearised equation:

$$\dot{B}_n = i(A_n^2\overline{B}_n + 2A_n^2 B_n - (2\epsilon + \omega)B_n + \epsilon(B_{n+1} + B_{n-1})), \tag{2.6}$$

where $\overline{B}_n$ represents the conjugate of B_n and the overdot is the derivative with respect to t. This reduces the linear stability problem to a study of a linear eigenvalue problem. It is perhaps to be expected that the stability of a branch of stationary solutions can change at a bifurcation point.

There are two fundamental solutions of the equations: single-site peaked ('site-centred') and two-site peaked ('bond-centred'). We present the plot the two types of solitons in Fig.2.1.

For the case of an infinite lattice, both solutions in Fig. 2.1 can be smoothly continued versus coupling ϵ (or, equivalently by rescaling, versus ω), without encountering any bifurcations. As there are no bifurcations, the site-centred solution is stable and the bond-centred unstable for all ϵ in the infinite chain. For $\epsilon \to 0$, the site-centred solution will be completely localised at the central site with all other oscillator amplitudes being zero, while the bond-centred solution becomes completely localised on the two central sites.

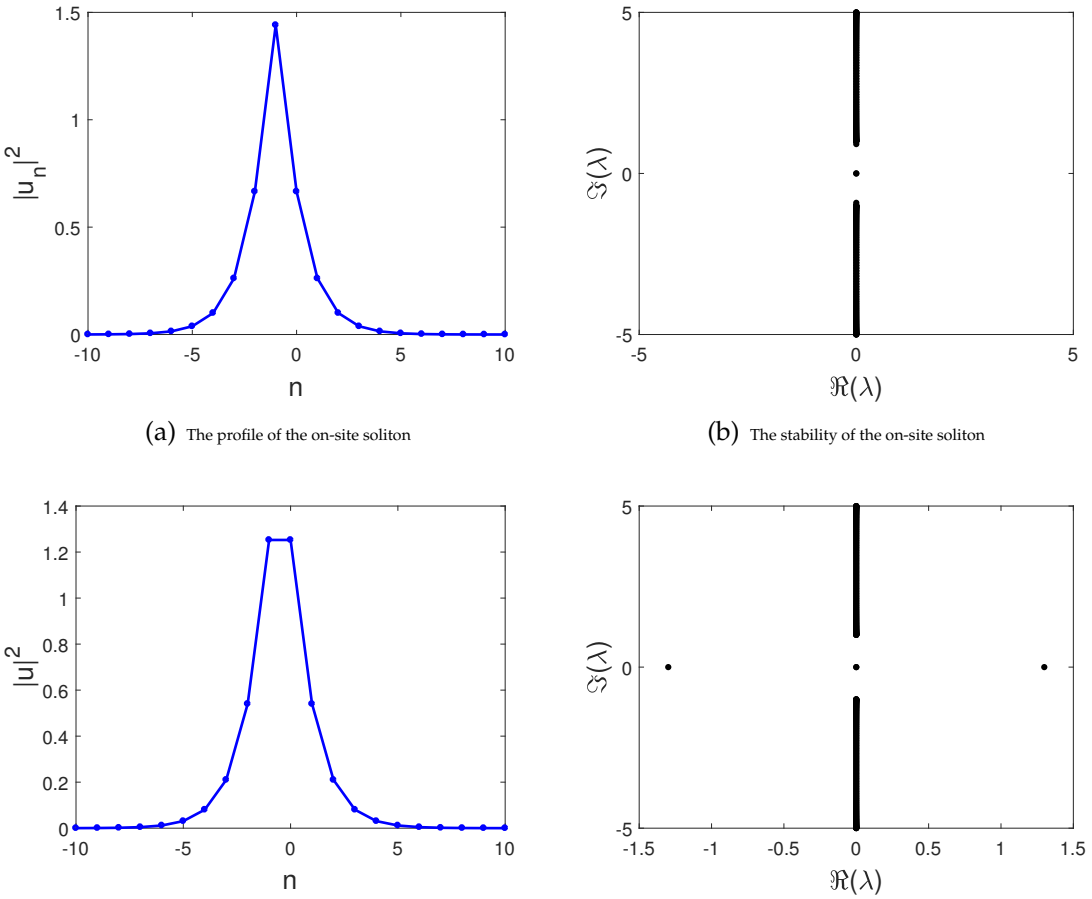

(a) The profile of the on-site soliton

(b) The stability of the on-site soliton

(c) The profile of the inter-site soliton

(d) The stability of the inter-site soliton

Figure 2.1: A general representation for the profile of the site-centred and bond-centred solitons with their spectrum for $\omega = 1$ and $\epsilon = 1$.

For $\epsilon \to \infty$, both solutions are smoothly transformed into the same soliton solution of the continuous NLS.

To find the stability, write the Eq. (2.6) as

$$\left(\dot{B}_{-N} \quad \ldots \quad \dot{B}_N \quad \overline{\dot{B}}_{-N} \quad \ldots \quad \overline{\dot{B}}_N\right)^T = M\left(B_{-N} \quad \ldots \quad B_N \quad \overline{B}_{-N} \quad \ldots \quad \overline{B}_N\right)^T, \tag{2.7}$$

where M is the Jacobian matrix. The matrix M is written as follows:

$$M = \begin{pmatrix} M_{11} & M_{12} \\ \\ M_{21} & M_{22} \end{pmatrix},$$

where

$$M_{11} = \begin{pmatrix} i(2A_{-N}^2 - c) & \epsilon & 0 & \dots & \epsilon \\ \epsilon & i(2A_{-N+1}^2 - c) & \epsilon & \dots & 0 \\ 0 & \epsilon & i(2A_{-N+2}^2 - c) & \dots & 0 \\ \vdots & \vdots & \vdots & \ddots & \vdots \\ \epsilon & 0 & 0 & \dots & i(2A_{N)}^2 - c) \end{pmatrix},$$

$$M_{12} = \begin{pmatrix} iA_{-N}^2 & 0 & 0 & \dots & 0 \\ 0 & iA_{-N+1}^2 & 0 & \dots & 0 \\ 0 & 0 & iA_{-N+2}^2 & \dots & 0 \\ \dots & \dots & \dots & \ddots & \vdots \\ 0 & 0 & 0 & \dots & iA_N^2 \end{pmatrix}, \quad M_{21} = \begin{pmatrix} -iA_{-N}^2 & 0 & 0 & 0 \\ 0 & -iA_{-N+1}^2 & 0 & 0 \\ 0 & 0 & -iA_{-N+2}^2 & 0 \\ . & . & . & . \\ 0 & 0 & 0 & -iA_N^2 \end{pmatrix},$$

$$M_{22} = \begin{pmatrix} -i(2A_{-N}^2 - c) & \epsilon & 0 & \dots & \epsilon \\ \epsilon & -i(2A_{-N+1}^2 - c) & \epsilon & \dots & 0 \\ 0 & \epsilon & -i(2A_{-N+2}^2 - c) & \dots & 0 \\ \dots & \dots & \dots & \ddots & \vdots \\ \epsilon & 0 & 0 & \dots & -i(2A_N^2 - c) \end{pmatrix}, \text{ where } c = -(2\epsilon + \omega).$$

From solving $MB = \lambda B$, we obtain the eigenvalues of M. The stability of the solution u_n is determined by the eigenvalues, i.e., u_n is stable only when the real part $\Re(\lambda) \leq 0$ for all eigenvalues λ [62].

2.1 Asymptotic analysis of localised solutions

Perturbation theory has been used in the field of nonlinear optics, i.e. lattice equation [63]. The evolution equation has been used to calculate a first-order correction by starting from a zeroth-order solution. It is possible then to identify a parameter, say ϵ, such that the

solution is available and it is simple to some extent for $\epsilon = 0$. The parameter ϵ is used to keep track of terms of different order. Then, the question is about how this solution is different for non-zero but small ϵ. In this case, the variable of the system requires to be non-dimensionalised, and then special cases that can function as a starting point for approximating the solution in the neighbouring cases need to be found. These cases are frequently obtained by setting some of the parameters equal to zero, which applies in our case as the exact solutions of the lattice equations are available in the anticontinuum (AC) limit $\epsilon = 0$. Once an exact solution is achieved, the approximate solution can be generated in the form of a perturbation expansion for the first few terms, and this operation can be infinitely repeated.

We only focus here on the two fundamental localised solutions, i.e., the one-excited site (onsite) and the in-phase two-excited site (intersite) bright solitons. In practice, perturbation theory is rarely extended to the fourth order; usually for the first two or three terms. A standard form of a perturbation expansion is in a power series of a small perturbation parameter. The aim of this work is to study the existence and stability of the solitons. To implement this, we can expand A_n in the stationary Eq. (2.4) as:

$$A_n = A_n^{(0)} + \epsilon A_n^{(1)} + \epsilon^2 A_n^{(2)} + \dots, \tag{2.8}$$

where $A_n^{(0)}$ is the exact solution in the AC limit. Upon substituting the above expansion into Eq.(2.4), by considering $\omega = 1$ and collecting the terms in successive powers of ϵ, we obtain a number of order equations from which the solutions $A_n^{(1)}, A_n^{(2)}$, etc. can be solved

iteratively. For the onsite soliton, we set

$$A_n^{(0)} = \begin{cases} 0, & \text{if } n \neq 0, \\ \pm 1, & \text{if } n = 0, \end{cases} \tag{2.9}$$

to obtain the leading order correction, $A_n^{(1)}$:

$$A_n^{(1)} = \frac{\Delta_2 A_n^{(0)}}{(1 - 3A_n^{(0)^2})}, \tag{2.10}$$

from which we can get that:

$$A_{-1}^{(1)} = A_0^{(1)} = A_1^{(1)} = \pm 1.$$

However, for the intersite soliton, we set

$$A_n^{(0)} = \begin{cases} 0, & \text{if } n \neq -1, 0, \\ \pm 1, & \text{if } n = -1, 0, \end{cases} \tag{2.11}$$

and we obtain:

$$A_{-2}^{(1)} = A_1^{(1)} = \pm 1,$$

and

$$A_{-1}^{(1)} = A_0^{(1)} = \pm \frac{1}{2}.$$

2.2 Stability analysis

Next, we will also determine the eigenvalues of the discrete solitons analytically using asymptotic expansions. By substituting

$$A_n = A_n^{(0)} + \epsilon A_n^{(1)} + \epsilon^2 A_n^{(2)} + \ldots, \quad B_n(t) = K_n(t) + iL_n(t), \tag{2.12}$$

into Eq.(2.6), we obtain

$$\begin{aligned} \dot{K}_n(t) &= (-(A_n^{(0)})^2 - 2\epsilon A_n^{(0)} A_n^{(1)} + (2\epsilon + \omega))L_n(t) - \epsilon(L_{n+1}(t) + L_{n-1}(t)), \\ \dot{L}_n(t) &= (3(A_n^{(0)})^2 + 6\epsilon A_n^{(0)} A_n^{(1)} - (2\epsilon + \omega))K_n(t) + \epsilon(K_{n+1}(t) + K_{n-1}(t)), \end{aligned} \tag{2.13}$$

which have to be solved for the eigenvalue λ and the corresponding eigenvector $[\{K_n\}, \{L_n\}]^T$. As the stability matrix of the eigenvalue problem (2.13) is real valued, $\overline{\lambda}$ and $-\lambda$ are also eigenvalues with corresponding eigenvectors $[\{\overline{K_n}\}, \{\overline{L_n}\}]^T$ and $[\{K_n\}, \{-L_n\}]^T$.

The spectrum of Eq.(2.13) will consist of continuous spectrum and discrete spectrum (eigenvalue). To investigate the former, we consider the limit $n \to \pm\infty$, the procedure is shown in the following section.

2.2.1 Continuous spectrum

We introduce a plane-wave expansion

$$K_n = \hat{k} e^{\lambda t} e^{ikn}, \quad L_n = \hat{l} e^{\lambda t} e^{ikn}, \tag{2.14}$$

and substitute the above equations into Eq.(2.13), from which one can obtain the dispersion relations

$$\lambda\hat{k} = (2\epsilon + \omega)\hat{l} - 2\epsilon\hat{l}\cos(k), \quad \lambda\hat{l} = -(2\epsilon + \omega)\hat{k} + 2\epsilon\hat{k}\cos(k), \tag{2.15}$$

which can be written in a matrix form as follows:

$$\lambda \begin{pmatrix} \hat{k} \\ \hat{l} \end{pmatrix} = \begin{pmatrix} 0 & 2\epsilon(1-\cos(k)) + \omega \\ -2\epsilon(1-\cos(k)) - \omega & 0 \end{pmatrix} \begin{pmatrix} \hat{k} \\ \hat{l} \end{pmatrix}. \tag{2.16}$$

By calculating the eigenvalues of the above matrix, this in turn shows that the continuous band lies between $\pm i[\omega, \omega + 2\epsilon]$.

2.2.2 Discrete spectrum

In this section, we are going to consider the inter-site soliton only, because there is no eigenvalues bifurcating from the origin for small ϵ.

To solve Eq.(2.13) for the discrete spectrum, $\dot{K}_n(t)$, $\dot{L}_n(t)$ are replaced by $\lambda_n K_n$ and $\lambda_n L_n$, respectively. By using perturbation expansions, we write

$$\begin{aligned} K_n &= K_n^{(0)} + \sqrt{\epsilon}K_n^{(1)} + \epsilon K_n^{(2)} + \dots, \\ L_n &= L_n^{(0)} + \sqrt{\epsilon}L_n^{(1)} + \epsilon L_n^{(2)} + \dots, \\ \lambda_n &= \lambda_n^{(0)} + \sqrt{\epsilon}\lambda_n^{(1)} + \epsilon\lambda_n^{(2)} + \dots. \end{aligned} \tag{2.17}$$

At leading orders, we obtain

$$
\begin{aligned}
\lambda^{(0)}K_n^{(0)} &= (-(A_n^{(0)})^2+\omega)L_n^{(0)},\\
\lambda^{(0)}K_n^{(1)} &= (-(A_n^{(0)})^2+\omega)L_n^{(1)}-\lambda^{(1)}K_n^{(0)},\\
\lambda^{(0)}K_n^{(2)} &= (-(A_n^{(0)})^2+\omega)L_n^{(2)}-2(A_n^{(0)}A_n^{(1)}-1)L_n^{(0)}-(L_{n+1}^{(0)}+L_{n-1}^{(0)})\\
&\quad -\lambda^{(1)}K_n^{(1)}-\lambda^{(2)}K_n^{(0)},
\end{aligned}
\tag{2.18}
$$

and

$$
\begin{aligned}
\lambda^{(0)}L_n^{(0)} &= (3A_n^{(0)})^2-\omega)K_n^{(0)},\\
\lambda^{(0)}L_n^{(1)} &= (3A_n^{(0)})^2-\omega)K_n^{(1)}-\lambda^{(1)}L_n^{(0)},\\
\lambda^{(0)}L_n^{(2)} &= (3A_n^{(0)})^2-\omega)K_n^{(2)}+2(3A_n^{(0)}A_n^{(1)}-1)K_n^{(0)}+(K_{n+1}^{(0)}+K_{n-1}^{(0)})\\
&\quad -\lambda^{(1)}L_n^{(1)}-\lambda^{(2)}L_n^{(0)}.
\end{aligned}
\tag{2.19}
$$

We can re-write the above equations as:

$$
\lambda^{(0)}\begin{pmatrix}K_n^{(0)}\\ L_n^{(0)}\end{pmatrix} = \begin{pmatrix}0 & -(A_n^{(0)})^2+\omega\\ 3(A_n^{(0)})^2-\omega & 0\end{pmatrix}\begin{pmatrix}K_n^{(0)}\\ L_n^{(0)}\end{pmatrix},
\tag{2.20}
$$

$$
\lambda^{(0)}\begin{pmatrix}K_n^{(1)}\\ L_n^{(1)}\end{pmatrix} = \begin{pmatrix}0 & -(A_n^{(0)})^2+\omega\\ 3(A_n^{(0)})^2-\omega & 0\end{pmatrix}\begin{pmatrix}K_n^{(1)}\\ L_n^{(1)}\end{pmatrix}+\begin{pmatrix}-\lambda^{(1)} & 0\\ 0 & -\lambda^{(1)}\end{pmatrix}\begin{pmatrix}K_n^{(0)}\\ L_n^{(0)}\end{pmatrix},
\tag{2.21}
$$

and,

$$\begin{aligned}\lambda^{(0)}\begin{pmatrix}K_n^{(2)}\\ L_n^{(2)}\end{pmatrix} &= \begin{pmatrix}0 & -(A_n^{(0)})^2+\omega\\ 3(A_n^{(0)})^2-\omega & 0\end{pmatrix}\begin{pmatrix}K_n^{(2)}\\ L_n^{(2)}\end{pmatrix}+\begin{pmatrix}-\lambda^{(1)} & 0\\ 0 & -\lambda^{(1)}\end{pmatrix}\begin{pmatrix}K_n^{(1)}\\ L_n^{(1)}\end{pmatrix}\\ &+\begin{pmatrix}-\lambda^{(2)} & -2(A_n^{(0)}A_n^{(1)}-1)\\ 2(3A_n^{(0)}A_n^{(1)}-1) & -\lambda^{(2)}\end{pmatrix}\begin{pmatrix}K_n^{(0)}\\ L_n^{(0)}\end{pmatrix}\\ &+\begin{pmatrix}0 & 1\\ -1 & 0\end{pmatrix}\begin{pmatrix}K_{n-1}^{(0)}\\ L_{n-1}^{(0)}\end{pmatrix}+\begin{pmatrix}0 & 1\\ -1 & 0\end{pmatrix}\begin{pmatrix}K_{n+1}^{(0)}\\ L_{n+1}^{(0)}\end{pmatrix}.\end{aligned} \tag{2.22}$$

From Eq.(2.20), we obtain that

$$L_n^{(0)}=\begin{cases}0, & n\neq -1,0,\\ C_1, & n=-1,\\ C_2, & n=0,\end{cases}$$

and $K_n^{(0)}=0$.

From Eq.(2.21), we then obtain

$$L_n^{(1)}=\begin{cases}0, & n\neq -1,0,\\ C_3, & n=-1,\\ C_4, & n=0,\end{cases}$$

and

$$K_n^{(1)} = \begin{cases} 0, & n \neq -1, 0, \\ \frac{C_1 \lambda^{(1)}}{2}, & n = -1, \\ \frac{C_2 \lambda^{(1)}}{2}, & n = 0, \end{cases}$$

Now, from Eq.(2.22) and by using Fredholm alternative [64], we obtain

$-(\lambda^{(1)})^2 C_1 + 2C_1 + 2C_2 = 0$ and $-(\lambda^{(1)})^2 C_2 + 2C_2 + 2C_1 = 0$, implying that the next order correction to the eigenvalue $\lambda^{(0)} = 0$ is

$$\lambda^{(1)} = \begin{cases} 0, \\ \mp 2. \end{cases}$$

So, the eigenvalues of the intersite soliton is $\lambda = \pm 2\sqrt{\epsilon} + O(\epsilon)$.

We have compared the numerical results of the eigenvalue with the analytic calculations in Fig. 2.2. One can observe good agreement for small ϵ

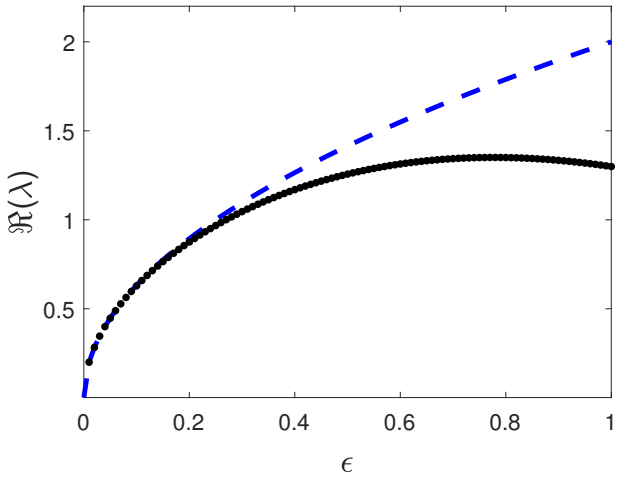

Figure 2.2: Comparison between numerical and analytical calculations of the eigenvalue of the intersite soliton (see Fig. 2.1 when $\omega = 1$). The approximation is shown in the dashed blue line.

To conclude, a systematic method to determine the stability of discrete solitons by computing the eigenvalues of the corresponding linear eigenvalue problem has been presented. We have compared the analytical results with numerical computations, where good agreement has been obtained. The method presented here will play an important part in the analytical studies of Chapter 3, 4 and 5, where we extend it to coupled DNLS equations.

Chapter 3

Bright solitons in a $\mathcal{PT}$-symmetric chain of dimers

3.1 Introduction

A system of equations is $\mathcal{PT}$-symmetric if it is invariant with respect to combined parity ($\mathcal{P}$) and time-reversal ($\mathcal{T}$) transformations. The symmetry is interesting as it forms a particular class of non-Hermitian Hamiltonians in quantum mechanics [65], that may have a real spectrum up to a critical value of the complex potential parameter, above which the system is in the 'broken $\mathcal{PT}$-symmetry' phase [14, 18, 66].

The most basic configuration having $\mathcal{PT}$-symmetry is a dimer, i.e. a system of two coupled oscillators where one of the oscillators has damping losses and the other one gains energy from external sources. Considerably dimers are also the most important $\mathcal{PT}$-systems as the concept of $\mathcal{PT}$-symmetry was first realised experimentally on dimers consisting of two coupled optical waveguides [67, 68] (see also the review [69] for $\mathcal{PT}$-

symmetry in optical applications). The experiments have been rapidly followed by many other observations of $\mathcal{PT}$-symmetry in different branches of physics, from mechanical to electrical analogues (see the review [70]).

When nonlinearity is present in a $\mathcal{PT}$- system, nontrivial behaviours may emerge that cease to exist in the linear case, such as the presence of blow-up dynamics in the parameter region of the unbroken phase in the linear counterpart [71–73]. When nonlinear dimers are put in arrays where elements with gain and loss are linearly coupled to the elements of the same type belonging to adjacent dimers, one can also obtain a distinctive feature in the form of the existence of solutions localised in space as continuous families of their energy parameter [74]. The system therefore has two arms with each arm described by a discrete nonlinear Schrödinger equation with gain or loss. Here, we study the nonlinear localised solutions, which loosely we also refer to as bright discrete solitons, and their stability analytically and numerically.

In the continuous limit, the coupled equations without gain-loss have been studied in [75–78], where it has been shown that the system admits symmetric, antisymmetric and asymmetric solitons between the arms. Unstable asymmetric solutions bifurcate from the symmetric ones through a subcritical symmetry breaking bifurcation, which then become stable after a tangent (saddle-center) bifurcation. When one adds a gain and loss term in each arm, one obtains $\mathcal{PT}$-symmetric couplers, which have been considered in [79–83]. In the presence of the linear-gain and loss terms, asymmetric solitons cease to exist, while antisymmetric solitons are always unstable [82], even though those with small amplitudes can live long due to weak underlying instability [79]. Symmetric solitons can be stable in a similar fashion to those in the system without gain-loss [82].

The stability of bright discrete solitons in $\mathcal{PT}$-symmetric couplers was discussed in [74] using variational methods, where it was shown that symmetric onsite solutions can be stable and there is a critical solution amplitude above which the $\mathcal{PT}$-symmetry is broken. The case when the polarity of the $\mathcal{PT}$-symmetric dimers is staggered along the chain is considered in [84]. The same equations without gain and loss were considered in [85] where the symmetric soliton loses its stability through the symmetry-breaking bifurcation at a finite value of the energy, similarly to that in the continuous counterpart [75–78]. Recently a similar $\mathcal{PT}$-chain of dimers with a slightly different nonlinearity was derived [86] to describe coupled chains of parametrically driven pendula as a mechanical analogue of $\mathcal{PT}$-symmetric systems [87]. The stability of bright discrete solitons was established through the applications of the Hamiltonian energy and an index theorem. The nonlinear long-time stability of the discrete solitons was also established using the Lyapunov method in the asymptotic limit of a weak coupling between the pendula [88].

In this work, we determine the eigenvalues of discrete solitons in $\mathcal{PT}$-symmetric couplers analytically using asymptotic expansions. The computation is based on the so-called method of weak coupling or anti-continuum limit. The application of the method in the study of discrete solitons was formulated rigorously in [54] for conservative systems. It was then applied to $\mathcal{PT}$-symmetric networks in [89, 90]. However, no explicit expression of the asymptotic series of the eigenvalues for the stability of discrete solitons has been presented before. Here, in addition to the asymptotic limit of weak coupling between the dimers, we also propose to consider expansions in the coefficient of the gain-loss terms. In this case, explicit computations of the asymptotic series of the eigenvalues become possible.

This chapter is outlined as follows. In Section 3.2, we present the mathematical model.

In Section 3.3, we use perturbation theory for small coupling to analyse the existence of fundamental localised solutions. Such analysis is based on the concept of the so-called anticontinuum limit approach. The stability of the solitons is then considered analytically in Section 3.4 by solving a corresponding eigenvalue problem. In this section, in addition to small coupling, the expansion is also performed under the assumption of small coefficient of the gain-loss term due to the non-simple expression of the eigenvectors of the linearised operator. The findings obtained from the analytical calculations are then compared with the numerical counterparts in Section 3.5. We also produce stability regions for all the fundamental solitons numerically. In this section, we present the typical dynamics of solitons in the unstable parameter ranges by direct numerical integrations of the governing equation. We present the conclusion in Section 3.6.

3.2 Mathematical model

The governing equations describing $\mathcal{PT}$-symmetric chains of dimers are of the form [74]

$$\begin{aligned} \dot{u}_n &= i\sigma|u_n|^2 u_n + i\epsilon\Delta_2 u_n + \gamma u_n + iv_n, \\ \dot{v}_n &= i\sigma|v_n|^2 v_n + i\epsilon\Delta_2 v_n - \gamma v_n + iu_n. \end{aligned} \tag{3.1}$$

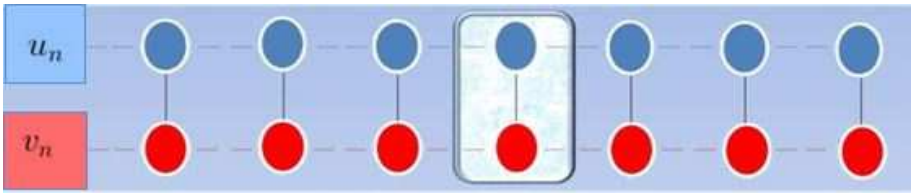

Figure 3.1: Sketch of the govering Eq. (3.1). The integrable dimers are indicated in the light blue box.

The derivative with respect to the evolution variable (i.e., the propagation distance, if we consider their application in fiber optics) is denoted by the overdot, $u_n = u_n(t)$, $v_n = v_n(t)$ are complex-valued wave function at site $n \in \mathbb{Z}$, $\epsilon > 0$ is the constant coefficient of the horizontal linear coupling (coupling constant between two adjacent sites), $\Delta_2 u_n = (u_{n+1} - 2u_n + u_{n-1})$ and $\Delta_2 v_n = (v_{n+1} - 2v_n + v_{n-1})$ are the discrete Laplacian term in one spatial dimension, the gain and loss acting on complex variables u_n, v_n are represented by the positive coefficient γ, i.e. $\gamma > 0$. The nonlinearity coefficient is denoted by σ, which can be scaled to +1 without loss of generality due to the case of focusing nonlinearity that we consider. Bright discrete soliton solutions satisfy the localisation conditions $u_n, v_n \to 0$ as $n \to \pm\infty$.

The focusing system has static localised solutions that can be obtained from substituting

$$u_n = A_n e^{i\omega t}, \quad v_n = B_n e^{i\omega t}, \tag{3.2}$$

into (3.1) to yield the equations

$$\begin{aligned} \omega A_n &= |A_n|^2 A_n + \epsilon(A_{n+1} - 2A_n + A_{n-1}) - i\gamma A_n + B_n, \\ \omega B_n &= |B_n|^2 B_n + \epsilon(B_{n+1} - 2B_n + B_{n-1}) + i\gamma B_n + A_n, \end{aligned} \tag{3.3}$$

where A_n, B_n are complex-valued and the propagation constant $\omega \in \mathbb{R}$.

3.3 Solutions of weakly coupled equations

In the uncoupled limit, i.e. when $\epsilon = 0$, the chain (3.1) becomes the equations for the dimer. The static Eq. (3.3) has been analysed in details in [89,91], where it was shown that there is

a relation between ω and γ above which there is no time-independent solution to (3.3) (see also the analysis below). When ϵ is nonzero, but small enough, the existence of solutions emanating from the uncoupled limit can be shown using the Implicit Function Theorem. The existence analysis of [86] can be adopted here despite the slightly different nonlinearity as the Jacobian of our system when uncoupled shares a rather similar invertible structure (see also [89, 90] that have the same nonlinearity in the governing equations but different small coupling terms). However, below we will not state the theorem and instead derive the asymptotic series of the solutions.

Using perturbation expansion, solutions of the coupler (3.3) for small coupling constant ϵ can be expressed analytically as

$$A_n = A_n^{(0)} + \epsilon A_n^{(1)} + \dots, \quad B_n = B_n^{(0)} + \epsilon B_n^{(1)} + \dots. \tag{3.4}$$

By substituting the above expansions into Eq. (3.3) and collecting the terms in successive powers of ϵ, one obtains from the equations at $O(1)$ and $O(\epsilon)$, respectively

$$A_n^{(0)} = B_n^{(0)}(\omega - B_n^{(0)}B_n^{*(0)} - i\gamma), \quad B_n^{(0)} = A_n^{(0)}(\omega - A_n^{(0)}A_n^{*(0)} + i\gamma), \tag{3.5}$$

and

$$\begin{aligned} A_n^{(1)} &= B_n^{(1)}(\omega - 2B_n^{(0)}B_n^{*(0)} - i\gamma) - {B_n^{(0)}}^2 B_n^{*(1)} - \Delta_2 B_n^{(0)}, \\ B_n^{(1)} &= A_n^{(1)}(\omega - 2A_n^{(0)}A_n^{*(0)} + i\gamma) - {A_n^{(0)}}^2 A_n^{*(1)} - \Delta_2 A_n^{(0)}. \end{aligned} \tag{3.6}$$

It is well-known that there are two natural fundamental solutions representing bright

discrete solitons that may exist for any ϵ, from the anticontinuum to the continuum limit, i.e. an intersite (two-excited-site) and onsite (one-excited-site) bright discrete mode. Here, we will study these two fundamental modes.

3.3.1 Intersite soliton

In the uncoupled limit, the mode structure $A_n^{(0)},\ B_n^{(0)}$ for the intersite soliton is of the form

$$A_n^{(0)} = \begin{cases} \hat{a}_0 e^{i\phi_a} & n = 0, 1, \\ 0 & \texttt{otherwise}, \end{cases} \qquad B_n^{(0)} = \begin{cases} \hat{b}_0 e^{i\phi_b} & n = 0, 1, \\ 0 & \texttt{otherwise}, \end{cases} \tag{3.7}$$

with [91]

$$\hat{a}_0 = \hat{b}_0 = \sqrt{\omega \mp \sqrt{1-\gamma^2}}, \quad \sin(\phi_b - \phi_a) = \gamma, \tag{3.8}$$

which is an exact solution of Eq. (3.5). Note that (3.8) will have no real solution when $|\gamma| > 1$. This is the broken region of $\mathcal{PT}$-symmetry. The parameter ϕ_a can be taken as 0, due to the gauge phase invariance of the governing Eq. (3.1) and henceforth $\phi_b = \arcsin\gamma,\ \pi - \arcsin\gamma$. The former phase corresponds to the so-called symmetric configuration between the arms, while the latter is called antisymmetric one. Herein, we also refer to the symmetric and antisymmetric soliton as soliton I and II, respectively. Eq. (3.8) informs us that $\omega > \sqrt{1-\gamma^2} > 0$ and $\omega > -\sqrt{1-\gamma^2}$ are the necessary condition for soliton I and II, respectively.

For the first order correction due to the weak coupling, writing

$$A_n^{(1)} = \tilde{a}_{n,1} e^{i\phi_a}, \quad B_n^{(1)} = \tilde{b}_{n,1} e^{i\phi_b},$$

and substituting it into Eq. (3.6) will yield

$$\tilde{a}_{n,1} = \tilde{b}_{n,1} = \begin{cases} 1/(2\hat{a}_0) & n = 0, 1, \\ 1/\hat{a}_0 & n = -1, 2, \\ 0 & \texttt{otherwise}. \end{cases} \tag{3.9}$$

Eqs. (3.4),(3.7),(3.8),(3.9) are the asymptotic expansion of the intersite solitons. One can continue the same calculation to obtain higher order corrections. Here, we limit ourselves to the first order correction only, which is sufficient to determine the leading order behaviour of the eigenvalues later.

3.3.2 Onsite soliton

For the onsite soliton, i.e., a one-excited-site discrete mode, one can perform the same computations to obtain the mode structure of the form

$$A_n^{(0)} = \begin{cases} \hat{a}_0 e^{i\phi_a} & n = 0, \\ 0 & \texttt{otherwise}, \end{cases} \qquad B_n^{(0)} = \begin{cases} \hat{b}_0 e^{i\phi_b} & n = 0, \\ 0 & \texttt{otherwise}, \end{cases} \tag{3.10}$$

with (3.8). After writing $A_n^{(1)} = \tilde{a}_{n,1} e^{i\phi_a}$, $B_n^{(1)} = \tilde{b}_{n,1} e^{i\phi_b}$, the first order correction from (3.6) is given by

$$\tilde{a}_{n,1} = \tilde{b}_{n,1} = \begin{cases} 1/\hat{a}_0 & n = 0, \pm 1, \\ 0 & \texttt{otherwise}. \end{cases} \tag{3.11}$$

3.4 Stability analysis

After we find discrete solitons, their linear stability is then determined by solving a corresponding linear eigenvalue problem. To do so, we introduce the linearisation ansatz $u_n = (A_n + \zeta(K_n + iL_n)e^{\lambda t})e^{i\omega t}$, $v_n = (B_n + \zeta(P_n + iQ_n)e^{\lambda t})e^{i\omega t}$, $|\zeta| \ll 1$, and substitute this into Eq. (3.1) to obtain from the equations at $O(\zeta)$ the eigenvalue problem

$$\begin{aligned}
\lambda K_n &= -(A_n^2 - \omega)L_n - \epsilon(L_{n+1} - 2L_n + L_{n-1}) + \gamma K_n - Q_n, \\
\lambda L_n &= (3A_n^2 - \omega)K_n + \epsilon(K_{n+1} - 2K_n + K_{n-1}) + \gamma L_n + P_n, \\
\lambda P_n &= -(\Re(B_n)^2 + 3\Im(B_n)^2 - \omega)Q_n - \epsilon(Q_{n+1} - 2Q_n + Q_{n-1}) \\
&\quad - (2\Re(B_n)\Im(B_n) + \gamma)P_n - L_n, \\
\lambda Q_n &= (3\Re(B_n)^2 + \Im(B_n)^2 - \omega)P_n + \epsilon(P_{n+1} - 2P_n + P_{n-1}) \\
&\quad + (2\Re(B_n)\Im(B_n) - \gamma)Q_n + K_n,
\end{aligned} \tag{3.12}$$

which have to be solved for the eigenvalue λ and the corresponding eigenvector $[\{K_n\}, \{L_n\}, \{P_n\}, \{Q_n\}]^T$. As the stability matrix of the eigenvalue problem (3.12) is real valued, $\overline{\lambda}$ and $-\lambda$ are also eigenvalues with corresponding eigenvectors $[\{\overline{K_n}\}, \{\overline{L_n}\}, \{\overline{P_n}\}, \{\overline{Q_n}\}]^T$ and $[\{K_n\}, \{-L_n\}, \{P_n\}, \{-Q_n\}]^T$ with $\gamma \to -\gamma$, respectively. Therefore, we can conclude that the solution u_n is (linearly) stable only when $\Re(\lambda) = 0$ for all eigenvalues λ.

3.4.1 Continuous spectrum

The spectrum of (3.12) will consist of continuous spectrum and discrete spectrum (eigenvalue). To investigate the former, we consider the limit $n \to \pm\infty$, introduce the plane-wave

ansatz $K_n = \hat{k}e^{ikn}, L_n = \hat{l}e^{ikn}, P_n = \hat{p}e^{ikn}, Q_n = \hat{q}e^{ikn}$, $k \in \mathbb{R}$, and substitute the ansatz into (3.12) to obtain

$$\lambda \begin{bmatrix} \hat{k} \\ \hat{l} \\ \hat{p} \\ \hat{q} \end{bmatrix} = \begin{bmatrix} \gamma & \xi & 0 & -1 \\ -\xi & \gamma & 1 & 0 \\ 0 & -1 & -\gamma & \xi \\ 1 & 0 & -\xi & -\gamma \end{bmatrix} \begin{bmatrix} \hat{k} \\ \hat{l} \\ \hat{p} \\ \hat{q} \end{bmatrix}, \tag{3.13}$$

where $\xi = \omega - 2\epsilon(\cos k - 1)$. The equation can be solved analytically to yield the dispersion relation

$$\lambda^2 = 4\epsilon\omega(\cos k - 1) - 4\epsilon^2(\cos k - 1)^2 - \omega^2 - 1 + \gamma^2 \pm (4\epsilon(\cos k - 1) - 2\omega)\sqrt{1-\gamma^2}. \tag{3.14}$$

The continuous spectrum is therefore given by $\lambda \in \pm[\lambda_{1-}, \lambda_{2-}]$ and $\lambda \in \pm[\lambda_{1+}, \lambda_{2+}]$ with the spectrum boundaries

$$\lambda_{1\pm} = i\sqrt{1 - \gamma^2 + \omega^2 \pm 2\omega\sqrt{1-\gamma^2}}, \tag{3.15}$$

$$\lambda_{2\pm} = i\sqrt{1 - \gamma^2 + 8\epsilon\omega + 16\epsilon^2 + \omega^2 + 2\sqrt{1-\gamma^2}(\pm\omega - 4\epsilon)}, \tag{3.16}$$

obtained from (3.14) by setting $k = 0$ and $k = \pi$ in the equation.

3.4.2 Discrete spectrum

Following the weak-coupling analysis as in Section 3.3, we will as well use similar asymptotic expansions to solve the eigenvalue problem (3.12) analytically, i.e. we write

$$\square = \square^{(0)} + \sqrt{\epsilon}\square^{(1)} + \epsilon\square^{(2)} + \dots, \tag{3.17}$$

with $\square = \lambda, K_n, L_n, P_n, Q_n$. We then substitute the expansions into the eigenvalue problem (3.12).

At order $O(1)$, one will obtain the stability equation for the dimer, which has been discussed for a general value of γ in [91]. The expression of the eigenvalues is simple, but the expression of the corresponding eigenvectors is not, which makes the result of [91] rather impractical to use. Therefore, here we limit ourselves to the case of small $|\gamma|$ and expand (3.17) further as

$$\square^{(j)} = \square^{(j,0)} + \gamma\square^{(j,1)} + \gamma^2\square^{(j,2)} + \dots,$$

$j = 0, 1, 2, \dots$. Hence, we have two small parameters, i.e. ϵ and γ, that are independent of each other. For the sake of presentation, the detailed calculations are shown in the Appendix. Below we will only cite the final results.

3.4.2.1 Intersite soliton I

The intersite soliton I (i.e. the symmetric intersite soliton) has three pairs of eigenvalues for small ϵ and γ. One pair bifurcate from the zero eigenvalue. They are asymptotically given by

$$\lambda = \sqrt{\epsilon}\left(2\sqrt{\omega - 1} + \gamma^2/\left(2\sqrt{\omega - 1}\right) + \dots\right) + O(\epsilon), \tag{3.18}$$

and

$$\lambda = \begin{cases} \left(2\sqrt{\omega-2} - \gamma^2 \frac{\omega-4}{2\sqrt{\omega-2}} + \ldots\right) + \epsilon\left(\sqrt{\omega-2} - \gamma^2 \frac{\omega}{4\sqrt{\omega-2}} + \ldots\right) + O(\epsilon)^{3/2}, \\ \\ \left(2\sqrt{\omega-2} - \gamma^2 \frac{\omega-4}{2\sqrt{\omega-2}} + \ldots\right) + \epsilon\left(\frac{1}{\sqrt{\omega-2}} - \gamma^2 \frac{\omega}{4(\omega-2)^{3/2}} + \ldots\right) + O(\epsilon)^{3/2}. \end{cases} \tag{3.19}$$

3.4.2.2 Intersite soliton II

The intersite soliton II, i.e. the intersite soliton that is antisymmetric between the arms, has three pairs of eigenvalues given by

$$\lambda = \sqrt{\epsilon}\left(2\sqrt{\omega+1} - \gamma^2/\left(2\sqrt{\omega+1}\right) + \ldots\right) + O(\epsilon), \tag{3.20}$$

and

$$\lambda = \begin{cases} i\left(2\sqrt{\omega+2} - \gamma^2 \frac{\omega+4}{2\sqrt{\omega+2}} + \ldots\right) \\ -i\epsilon\left(\sqrt{\omega+2} + \gamma^2 \frac{3\omega^4+35\omega^3+136\omega^2+208\omega+108}{8\sqrt{\omega+2}\left(\omega^3+6\omega^2+12\omega+8\right)} + \ldots\right) + O(\epsilon)^{3/2}, \\ \\ i\left(2\sqrt{\omega+2} - \gamma^2 \frac{\omega+4}{2\sqrt{\omega+2}} + \ldots\right) \\ +i\epsilon\left(\frac{1}{\sqrt{\omega+2}} + \gamma^2 \frac{\omega^4+21\omega^3+104\omega^2+184\omega+108}{8\sqrt{\omega+2}\left(\omega^3+6\omega^2+12\omega+8\right)} + \ldots\right) + O(\epsilon)^{3/2}. \end{cases} \tag{3.21}$$

3.4.2.3 Onsite soliton I

The onsite soliton has only one eigenvalue for small ϵ given asymptotically by

$$\lambda = \left(2\sqrt{\omega-2} - \gamma^2 \frac{\omega-4}{2\sqrt{\omega-2}} + \ldots\right) + \epsilon\left(\frac{2}{\sqrt{\omega-2}} - \gamma^2 \frac{\omega}{2(\omega-2)^{3/2}} + \ldots\right) + \ldots. \tag{3.22}$$

3.4.2.4 Onsite soliton II

As for the second type of the onsite soliton, we have

$$\lambda = i\left(2\sqrt{\omega+2} - \gamma^2\frac{\omega+4}{\sqrt{\omega+2}} + \dots\right) + 2i\epsilon\left(\frac{1}{\sqrt{\omega+2}} - \gamma^2\frac{\omega}{(\omega+2)^{3/2}} + \dots\right) + \dots. \tag{3.23}$$

3.5 Numerical results

We have solved the steady-state Eq. (3.3) numerically using Newton-Raphson method and analysed the stability of the numerical solution by solving the eigenvalue problem (3.12). Here we will compare the analytical calculations obtained above with the numerical results.

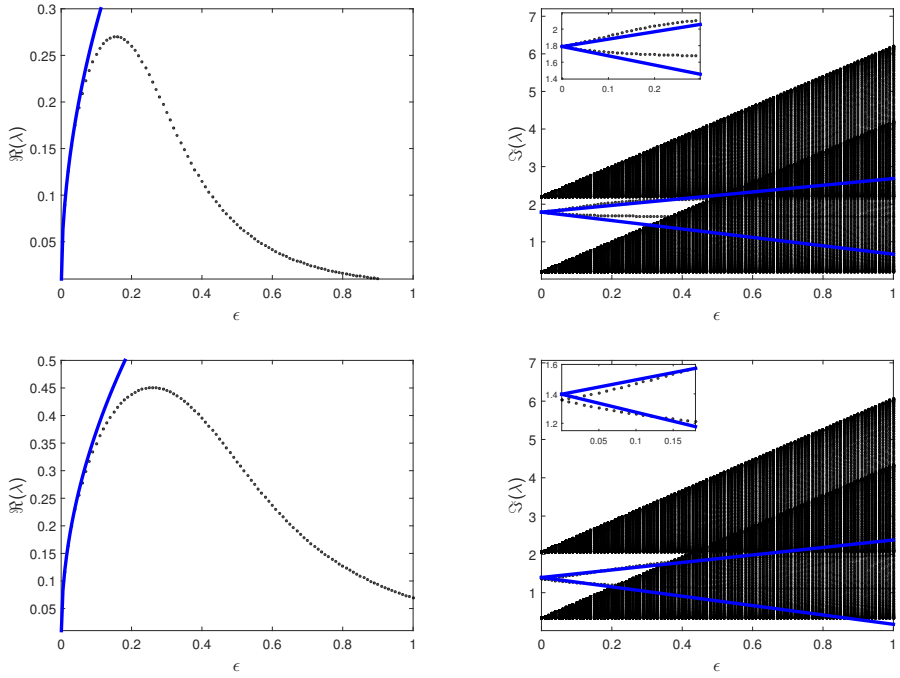

Figure 3.2: Eigenvalues of intersite soliton I with $\omega = 1.2$, $\gamma = 0$ (top panels) and 0.5 (bottom panels). Dots are from the numerics and solid lines are the asymptotic approximations in Section 3.4.2.1. The collection of dots forming black regions in the right column corresponds to the continuous spectrum.

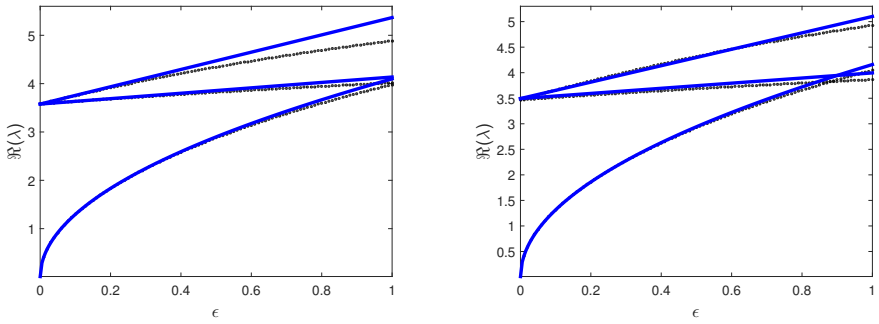

Figure 3.3: The same as in Fig. 3.2 with $\gamma = 0$ (left) and $\gamma = 0.5$ (right), but for $\omega = 5.2$. In this case, all the eigenvalues are real.

First, we consider the discrete intersite soliton I. We show in Fig. 3.2 the spectrum of the soliton as a function of the coupling constant ϵ for $\omega = 1.2$ and $\gamma = 0, 0.5$. On the real axis, one can observe that there is only one unstable eigenvalue that bifurcates from the origin. As the coupling increases, the bifurcating eigenvalue enters the origin again when $\epsilon \to \infty$. Hence, in that limit we obtain a stable soliton I (i.e. a stable symmetric soliton). The dynamics of the non-zero eigenvalues as a function of the coupling constant is shown in the right panels of the figure, where one can see that the eigenvalues are on the imaginary axis and simply enter the continuous spectrum as ϵ increases.

In Fig. 3.3, we plot the eigenvalues for ω large enough. Here, in the uncoupled limit, all the three pairs of eigenvalues are on the real axis. As the coupling increases, two pairs go back toward the origin, while one pair remains on the real axis (not shown here). In the continuum limit $\epsilon \to \infty$, we therefore obtain an unstable soliton I (i.e. an unstable symmetric soliton).

In both figures, we also plot the approximate eigenvalues in solid (blue) curves, where good agreement is obtained for small ϵ.

From numerical computations, we conjecture that if in the limit $\epsilon \to 0$ all the nonzero

eigenvalues λ satisfy $\lambda^2 > \lambda_{1-}^2$ (see (3.15-3.16)), then we will obtain unstable soliton I in the continuum limit $\epsilon \to \infty$. However, when in the anticontinuum limit $\epsilon \to 0$ all the nonzero eigenvalues λ satisfy $\lambda_{1+}^2 < \lambda^2 < \lambda_{2-}^2$, we may either obtain a stable or an unstable soliton I in the continuum limit.

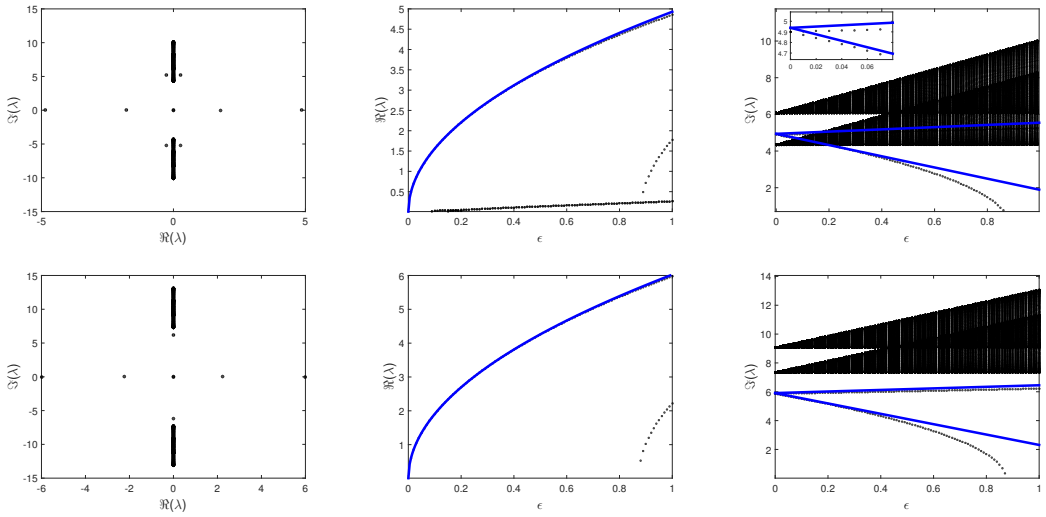

Figure 3.4: The spectra of intersite soliton II with $\omega = 5.2$ (top) and 8.2 (bottom) and $\gamma = 0.5$. The most left panels are the spectra in the complex plane for $\epsilon = 1$. Middle and right panels present the eigenvalues as a function the coupling constant. Solid blue curves are the asymptotic approximations.

Next, we consider intersite solitons II (i.e. antisymmetric intersite solitons). Shown in Fig. 3.4 is the spectrum of the discrete solitons for two values of ω. In both cases, there is an eigenvalue bifurcating from the origin. For the smaller value of ω (the top panels of the figure), we have the condition that all the nonzero eigenvalues λ satisfy $\lambda^2 < \lambda_{2-}^2$ in the anticontinuum limit $\epsilon \to 0$. The collision between the eigenvalues and the continuous spectrum as the coupling increases creates complex eigenvalues. In the second case using larger ω (lower panels of the figure), the nonzero eigenvalues λ satisfy $\lambda^2 > \lambda_{1-}^2$ when $\epsilon = 0$. Even though not seen in the figure, the collision between one of the nonzero eigenvalues and the continuous spectrum also creates a pair of complex eigenvalues. Additionally, in

the continuum limit both values of ω as well as the other values of the parameter that we computed for this type of discrete solitons yield unstable solutions.

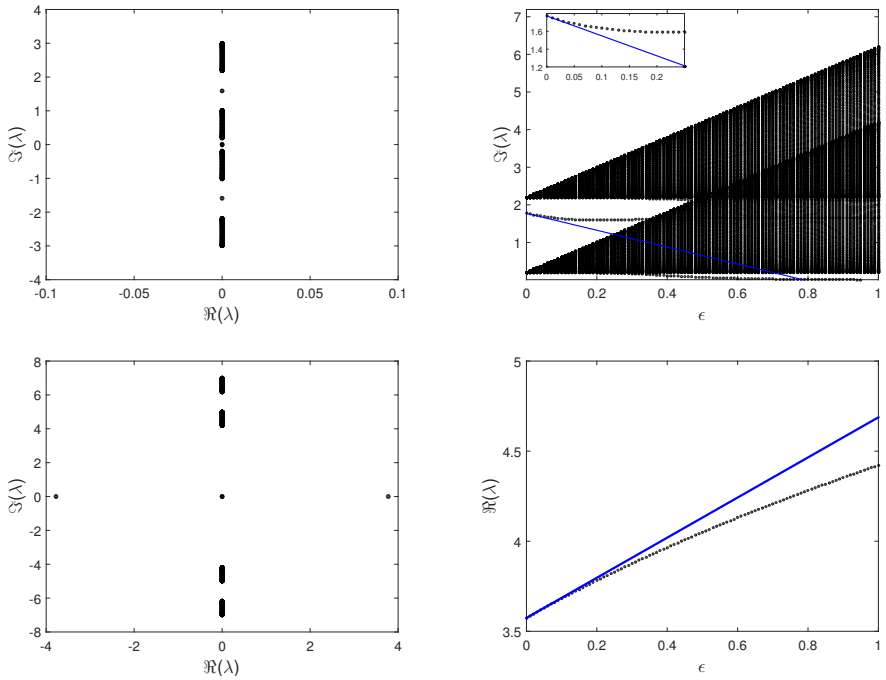

Figure 3.5: Left panels depict the spectrum of onsite soliton I in the complex plane for $\epsilon = 0.2$. Right panels show the eigenvalue as a function of the coupling and its approximation from Section 3.4.2.3. Top and bottom panels are for $\omega = 1.2$ and 5.2, respectively. Here, $\gamma = 0.1$.

We also study onsite solitons. Shown in Figs. 3.5 and 3.6 is the stability of discrete solitons type I and II, respectively.

In Fig. 3.5, the top left panel shows that for $(\omega - \sqrt{1-\gamma^2})$ small enough we will obtain stable discrete solitons. For coupling constant ϵ small, we indeed show it through our analysis depicted as the blue solid line. Numerically we obtain that this soliton is also stable in the continuum limit $\epsilon \to \infty$. However, when ω is large enough compared to $\sqrt{1-\gamma^2}$, even though initially in the uncoupled limit the nonzero eigenvalue λ satisfies $\lambda^2 < \lambda_{2-}^2$, one may obtain an exponential instability (i.e. instability due to a real eigenvalue). The bottom left panel shows the case when the discrete soliton is already unstable even in

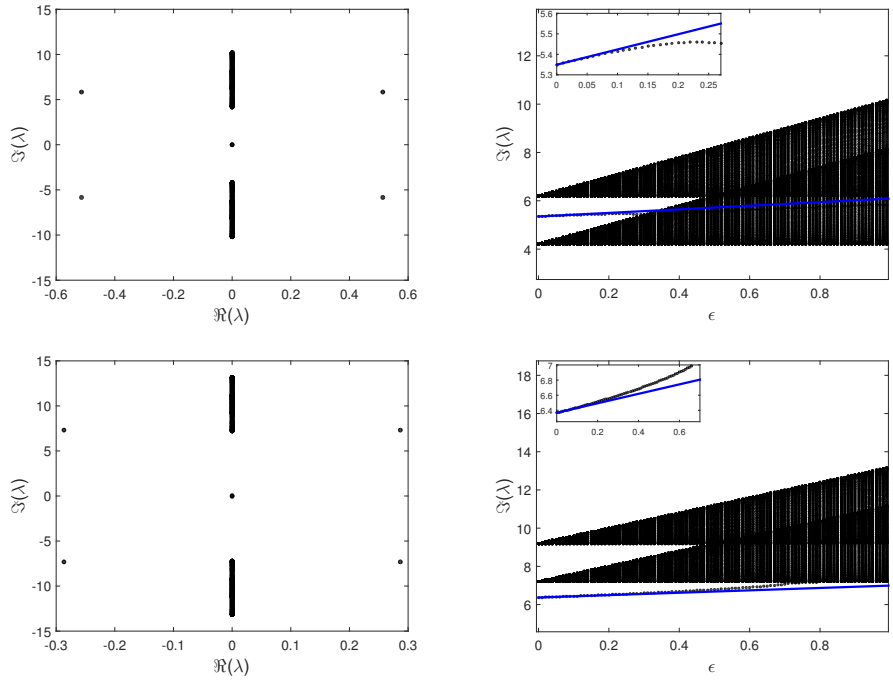

Figure 3.6: The same as in Fig. 3.5 but for onsite soliton II with $\omega = 5.2$ (top panels) and $\omega = 8.2$ (bottom panels) with $\epsilon = 1$.

the uncoupled limit due to the nonzero eigenvalue that is already real-valued.

Fig. 3.6 shows that the antisymmetric solitons are generally unstable due to a quartet of complex eigenvalues, as shown in the left panels of the figure. When the coupling is increased further, there will be an eigenvalue bifurcating from $\pm\lambda_{1-}$ that will move towards the origin and later becomes a pair of real eigenvalues. These solitons are also unstable in the continuum limit.

Unlike intersite discrete solitons that are always unstable, onsite discrete solitons may be stable. In Fig. 3.7, we present the (in)stability region of the two types of discrete solitons in the (ϵ, ω)-plane for three values of the gain-loss parameter γ. Discrete solitons are unstable above the curves in the left panel and between the curves in the right panel. Indeed as we mentioned before, for soliton I there is a critical ω that depends on γ below which the soliton is stable in the continuum limit, while soliton II is always unstable in that limit.

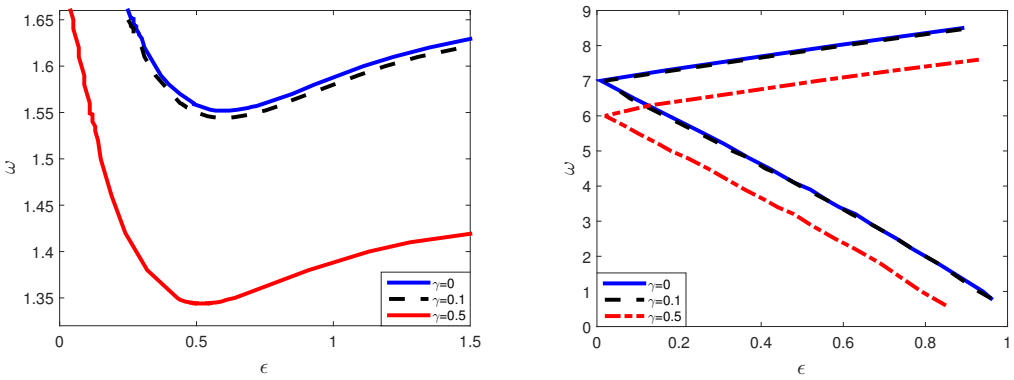

Figure 3.7: The stability region of the onsite soliton type I (left) and II (right) in the (ϵ, ω)-plane for several values of γ. The solutions are unstable above the curves in the left panel and between the curves in the right panel.

Another difference between the two figures is that the stability curves in the left panel generally corresponds to an eigenvalue crossing the origin that becomes real-valued, while the curves in the other panel are due to the appearance of a quartet of complex eigenvalues. In general, we obtain that the gain-loss term can be parasitic as it reduces the stability region of the discrete solitons.

Finally, we present in Fig. 3.8 the time dynamics of some of the unstable solutions shown in the previous figures. What we obtain is that typically there are two kinds of dynamics, i.e. in the form of travelling discrete solitons or solution blow-ups. The first type was the typical dynamics of the intersite soliton I. The second dynamics is typical for the other types of unstable discrete solitons.

3.6 Conclusion

We have presented a systematic method to determine the stability of discrete solitons in a $\mathcal{PT}$-symmetric coupler by computing the eigenvalues of the corresponding linear eigenvalue problem using asymptotic expansions. The computation is based on the so-

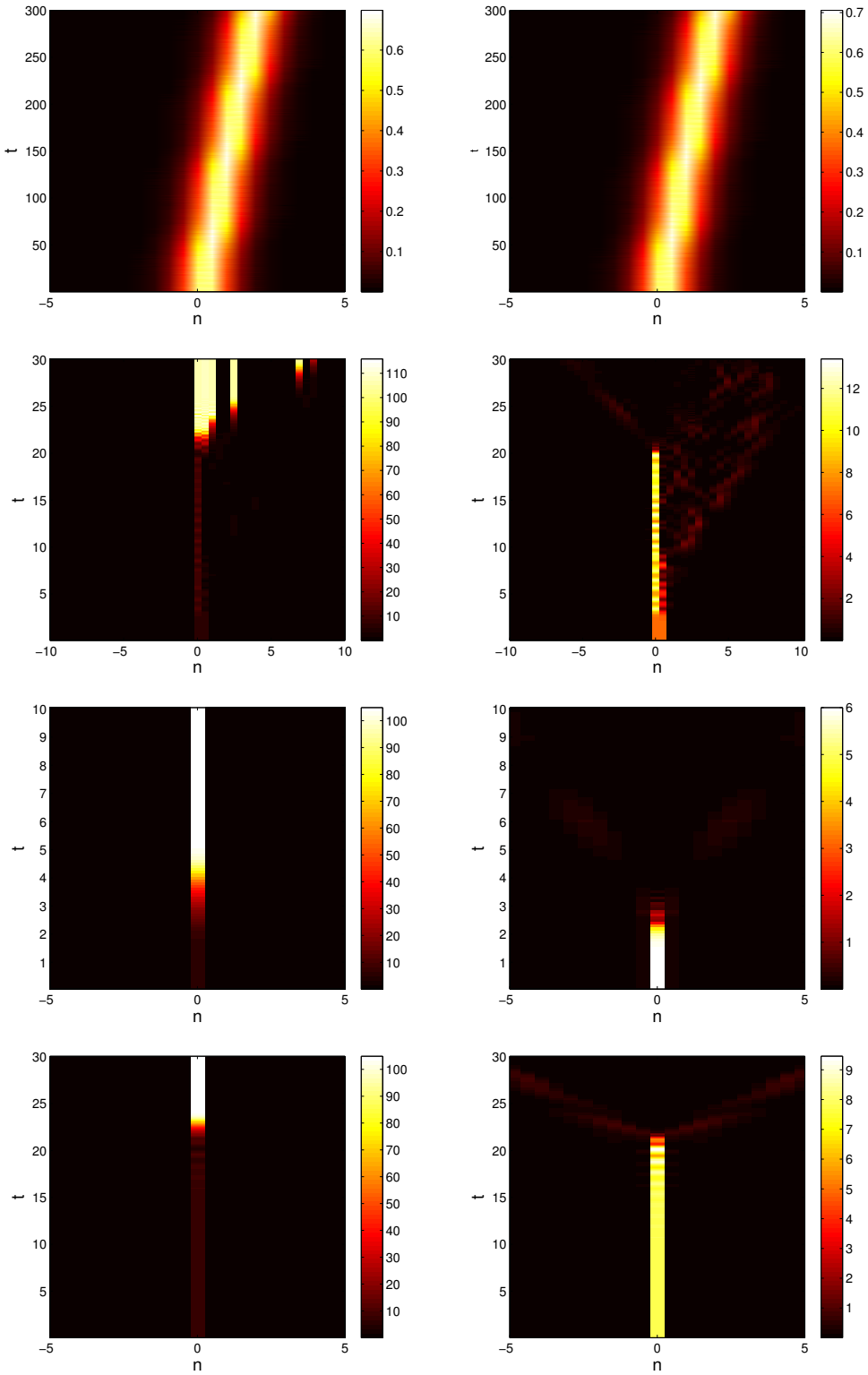

Figure 3.8: The typical dynamics of the instability of the discrete solitons in the previous Figs. Here, $\gamma = 0.5$ and $\epsilon = 1$. Depicted in the left and right panels are $|u_n|^2$ and $|v_n|^2$, respectively. From top to bottom panels, shown are the dynamics of intersite soliton I with $\omega = 1.2$, intersite soliton II with $\omega = 5.2$, and onsite soliton I and II both with $\omega = 5.2$.

called method of weak coupling or anti-continuum limit. While no explicit expression of the asymptotic series of the eigenvalues for the stability of discrete solitons had been presented before, in our work here explicit computations of the asymptotic series of the eigenvalues became possible. This is due to our approach, where in addition to the assumption of weak coupling between the dimers, we also proposed to consider expansions in the coefficient of the gain-loss terms. We have compared the analytical results that we obtained with numerical computations, where good agreement is obtained. From the numerics, we have also established the mechanism of instability as well as the stability region of the discrete solitons. We have produced the stability regions for all the fundamental solitons numerically. We have also presented the typical dynamics of solitons in the unstable parameter ranges by direct numerical integrations of the governing equation.

Chapter 4

Solitons in a chain of $\mathcal{CP}$-symmetric dimers

4.1 Introduction

Charge-parity ($\mathcal{CP}$) symmetry is one of the fundamental principles in physics of elementary particles [92,93]. It holds for all interactions, except for the small violation by weak nuclear forces [94]. The $\mathcal{CP}$ operator is composed of two factors: the parity transformation, $\mathcal{P}$, reverses the coordinates, and the charge conjugation, $\mathcal{C}$, which interchanges particles and antiparticles, i.e., essentially, positive and negative electric charges.

While the usual derivation of the $\mathcal{CP}$ symmetry is performed for Hermitian Hamiltonians, this symmetry does not hold solely for Hamiltonians which are necessarily Hermitian [95]. In fact, Hamiltonians which commute with another symmetry operator, *viz.*, the parity-time one, $\mathcal{PT}$ ($\mathcal{T}$ is the time-inverting transform), may include an anti-Hermitian spatially antisymmetric (odd) part, provided that the Hermitian one has a spatially even

structure [96]. The spectrum of energy eigenvalues, generated by such a $\mathcal{PT}$-symmetric Hamiltonian, may be purely real (i.e., physically relevant) up to a critical strength of the anti-Hermitian term, at which the $\mathcal{PT}$ symmetry is broken, making the system (in most cases) physically irrelevant above this point.

It is well known that non-Hermitian $\mathcal{PT}$-symmetric Hamiltonians may be emulated theoretically [97–103] and experimentally [68, 104–106] in the context of classical optics (without any actual connection to the quantum theory), making use of the fundamental fact that the usual paraxial propagation equation is essentially the same as the quantum-mechanical Schrödinger equation. Accordingly, the spatially even and odd Hermitian and anti-Hermitian terms of the underlying Hamiltonian correspond, severally, to symmetric and antisymmetric spatial patterns of the local refractive index, and of the local gain and loss in the waveguide.

Furthermore, the presence of the Kerr nonlinearity, which is ubiquitous in optics, has suggested the consideration of Hamiltonians which include the corresponding quartic terms too. The nonlinearity readily gives rise to families of $\mathcal{PT}$-symmetric solitons, that have been explored in various contexts, see recent reviews [69,70]. In particular, a natural setting for the prediction of such one- and two-dimensional solitons is provided by $\mathcal{PT}$-symmetric dual-core waveguides [79, 82, 107–109].

The emulation of the non-Hermitian $\mathcal{PT}$ symmetry in optics suggests to seek for a possibility to realise non-Hermitian Hamiltonians featuring the $\mathcal{CP}$ symmetry in appropriately designed optical settings. This was proposed in [110], using a model of a dual-core optical fiber, with opposite signs of the group-velocity dispersion (GVD) in the two cores and phase-velocity mismatch between them. The non-Hermitian ingredient of the system is the

specific intercore coupling, which, in a phenomenological form, can represent gain and loss in the system, assuming that the coupler is embedded into an "active" medium [73, 111]. Alternatively, the same coupling can be derived directly for two fundamental-frequency components of a nondegenerate (three-wave) second-harmonic-generating system, assuming that the depletion of the second-harmonic pump remains negligible [110]. In terms of this system, the $\mathcal{P}$ transform implies the swap of the two cores, and simultaneous inversion of the sign of the temporal variable in the transmission equations, while $\mathcal{C}$ amounts to the replacement of the wave amplitude by its complex-conjugate counterpart. The nonlinear version of the $\mathcal{CP}$-symmetric system, derived in [110], gives rise to a family of stable *gap solitons*, even if the Kerr nonlinearity breaks the $\mathcal{CP}$ symmetry. Another possibility to implement non-Hermitian $\mathcal{CP}$ symmetry in the semi-classical (mean-field) context was elaborated in terms of a two-component atomic Bose-Einstein condensate with the spin-orbit coupling between the components, assuming that one of them carries the gain, and the other one is subject to the action loss with the same strength [112].

In this work, we aim to derive a discrete version of the $\mathcal{CP}$-invariant system, which, unlike the continuum one, was not considered before, and demands a new physical realisation, in terms of optics. The system is realised as an array of dual-core optical waveguides in the spatial domain, with the temporal-domain GVD replaced by the discrete diffraction [113] in two parallel guiding arrays (two cores) of the system. While in dual-core fibers it is easy to realise the setting with opposite signs of the temporal GVD in the parallel cores [114–116], the implementation of opposite signs of the discrete diffraction is a challenging element of the model. As we discuss it below, it can be realised by means of the diffraction-management technique [117]. We construct families of discrete solitons in the

framework of the obtained system, which includes in the framework of Kerr nonlinearity. The soliton families are obtained in an approximate analytical and full numerical forms, starting from the anticontinuum limit (uncoupled array). One family continues, as a completely stable one, into the above-mentioned gap solitons found in the continuum-limit variant of the system. Other families terminate before reaching the continuum limit, and one hits a boundary of oscillatory instability.

The chapter is organised as follows. In Section 4.2, we present the model. We then use the perturbation theory for weak couplings to analyse fundamental discrete solitons in Section 4.3. In addition to the weak coupling between the sites ($\mathcal{CP}$ symmetric dimers), the analysis is also performed for a small gain coefficient, which accounts for the coupling between the cores. The existence and stability of the solitons is then considered by means of numerical methods in Section 4.4 by solving time-independent equations, and the corresponding eigenvalue problem for small perturbations around them. Results of the numerical calculations are also compared to their analytical counterparts. In particular, we produce stability regions for the fundamental onsite solitons. We also explore dynamics of unstable solitons by means of direct simulations. The chapter is concluded by Section 4.5.

4.2 The model

The chains of dimers we consider is described by the coupled equations

$$\begin{aligned} \dot{u}_n &= i|u_n|^2 u_n + i\epsilon\Delta_2 u_n + \gamma v_n - iqu_n, \\ \dot{v}_n &= i|v_n|^2 v_n - i\epsilon\Delta_2 v_n + \gamma u_n + iqv_n, \end{aligned} \tag{4.1}$$

where the dot stands for the derivative with respect to evolution variable t, which may actually be propagation distance in the arrays of optical waveguides, the cubic terms represent the usual Kerr nonlinearity, and $\epsilon > 0$ is the coefficient of the horizontal linear coupling with opposite signs, acting along each chain between adjacent sites, $\Delta_2 u_n = (u_{n+1} - 2u_n + u_{n-1})$ and $\Delta_2 v_n = (v_{n+1} - 2v_n + v_{n-1})$ being the respective finite-difference second derivatives, which represent the discrete spatial diffraction in the parallel arrays ($\epsilon < 0$ may be replaced by $\epsilon > 0$ simply by renaming $u_n \longleftrightarrow v_n$).

The opposite signs of the discrete diffraction in the two arrays (with spacing d), which is an essential ingredient of the present system, may be realised by means of the *diffraction-management* technique [117], i.e., coupling into one of the arrays a light beam with a small perpendicular component $\kappa_\perp = \pi/(2d)$ of the wave vector [the effective discrete-diffraction coefficient is $\sim \cos(\kappa_\perp d)$]. Another essential peculiarity in the present model is that the vertical coupling between the parallel chains, represented by real coefficient $\gamma > 0$ ($\gamma < 0$ may be replaced by $\gamma > 0$ by replacing $v_n \to -v_n$), acts as gain/loss in the active system [73]. The last terms in Eq. (4.1), with coefficient $q \gtrless 0$, which may be normalised to be ± 1, represent a phase-velocity mismatch between the cores. It is straightforward to check that the linearised version of Eq. (4.1) is symmetric under the above-mentioned $\mathcal{CP}$ transformation $u_n \to v_n^*$, $v_n \to u_n^*$, where * stands for the complex conjugation, i.e., the linear system supports the $\mathcal{CP}$ symmetry, while it is easy to see that the Kerr terms are not compatible with the transformation [110]. Our objective is to construct discrete solitons in the full nonlinear system satisfying the localisation conditions, $u_n, v_n \to 0$ at $n \to \pm\infty$.

In the continuum limit $\epsilon \to \infty$, system (4.1) was considered numerically and analytically in [110]. In the uncoupled limit, i.e. when $\epsilon = 0$, the chain (4.1) becomes isolated dimers

with a complex coupling that was studied in details in [73].

Stationary solutions of Eq. (4.1) are sought in the usual form

$$u_n = A_n e^{i\omega t}, \quad v_n = B_n e^{i\omega t}, \tag{4.2}$$

with real propagation constant ω and complex amplitudes A_n, B_n obeying the coupled algebraic equations

$$\begin{aligned} \omega A_n &= A_n^2 A_n^* + \epsilon(A_{n+1} - 2A_n + A_{n-1}) - i\gamma B_n - qA_n, \\ \omega B_n &= B_n^2 B_n^* - \epsilon(B_{n+1} - 2B_n + B_{n-1}) - i\gamma A_n + qB_n. \end{aligned} \tag{4.3}$$

In particular, looking for solutions to the linearised version of Eq. (4.3) in the natural form of plane waves, $(A_n, B_n) = (A_0, B_0)\, e^{ikn}$ with real wavenumber k, we obtain the dispersion relation for the linearised system:

$$\omega^2 = \left[q + 4\epsilon \sin^2(k/2)\right]^2 - \gamma^2. \tag{4.4}$$

An essential corollary of Eq. (4.4) is that the stability of the zero solution, which plays the role of the background for bright solitons, holds under condition $\omega^2 \geq 0$, i.e.,

$$q \geq \gamma, \tag{4.5}$$

for positive q, and

$$q \leq -(4\epsilon + \gamma), \tag{4.6}$$

for negative q. These conditions demonstrate that the presence of the phase-velocity mismatch, $q > 0$ or $q < 0$, is necessary for the stability of localised states (recall that we have set $\gamma > 0$ and $\epsilon > 0$).

If condition (4.5) holds, the existence of discrete solitons may be expected in spectral *bandgaps*, i.e., intervals of values of ω^2 which cannot be covered by Eq. (4.4) at $\sin^2(k/2) \leq 1$. These are

$$\omega^2 < q^2 - \gamma^2 \text{ or } \omega^2 > (q + 4\epsilon)^2 - \gamma^2, \tag{4.7}$$

in the case defined by Eq. (4.5), and

$$\omega^2 < (q + 4\epsilon)^2 - \gamma^2 \text{ or } \omega^2 > q^2 - \gamma^2, \tag{4.8}$$

in the case of Eq. (4.6).

Using the invariance of Eq. (4.3) with respect to the phase shift, one can infer that localised stationary solutions correspond to real-valued A_n and purely imaginary B_n, i.e. $B_n = i\Im(B_n)$. The stability of stationary states is determined by solving the corresponding problem for linear eigenvalue λ (generally, it is a complex one). To this end, we introduce the linearisation ansatz for the perturbed solution, $u_n = \left[A_n + \zeta(K_n + iL_n)e^{\lambda t}\right]e^{i\omega t}$, $v_n = \left[B_n + \zeta(P_n + iQ_n)e^{\lambda t}\right]e^{i\omega t}$, where ζ is an amplitude of small perturbations with real form factors K_n, L_n and P_n, Q_n, and substitute this into Eq. (4.1) to derive the linearised equations:

$$\begin{aligned}
\lambda K_n &= -(A_n^2 - \omega - q)L_n - \epsilon(L_{n+1} - 2L_n + L_{n-1}) + \gamma P_n, \\
\lambda L_n &= (3A_n^2 - \omega - q)K_n + \epsilon(K_{n+1} - 2K_n + K_{n-1}) + \gamma Q_n, \\
\lambda P_n &= (-3\Im(B_n)^2 + \omega - q)Q_n + \epsilon(Q_{n+1} - 2Q_n + Q_{n-1}) + \gamma K_n, \\
\lambda Q_n &= (\Im(B_n)^2 - \omega + q)P_n - \epsilon(P_{n+1} - 2P_n + P_{n-1}) + \gamma L_n,
\end{aligned} \tag{4.9}$$

which have to be solved for λ and the corresponding eigenvector $[K_n, L_n, P_n, Q_n]^T$. The solution is linearly stable under condition $\Re(\lambda) \leq 0$ for all eigenvalues, and unstable otherwise.

4.3 Analytical calculations

4.3.1 The anticontinuum limit

In the decoupled array, with $\epsilon = 0$ (the *anticontinuum limit* [55, 118, 119]), the stationary solution satisfying Eq. (4.3) can be written as $A_n^{(0)} = \tilde{a}_0$ and $B_n^{(0)} = i\tilde{b}_0$, with real $\tilde{a}_0$ and $\tilde{b}_0$. Upon substitution this into Eq. (4.3), one obtains

$$\tilde{b}_0 = -\frac{\tilde{a}_0(\tilde{a}_0^2 - \omega - q)}{\gamma}, \tag{4.10}$$

where $\tilde{a}_0$ solves the polynomial equation,

$$\tilde{a}_0^9 - 3(\omega + q)\tilde{a}_0^7 + 3(\omega + q)^2\tilde{a}_0^5 + [-\gamma^2(\omega - q) - (\omega + q)^3]\tilde{a}_0^3 + [\gamma^4 - \gamma^2(q^2 + \omega^2)]\tilde{a}_0 = 0. \tag{4.11}$$

One solution of (4.11) is clearly the trivial state $\tilde{a}_0 = \tilde{b}_0 = 0$. The non-trivial states are then roots of a quartic polynomial, which can be solved analytically. However, the expressions would not be simple [120]. Note that (4.11) simplifies for γ and $q = \pm 1$. Therefore instead we will consider special parameter values and solve the equation perturbatively for small γ.

Considering $q = 1 - \hat{q}\gamma$, one obtains up to $O(\gamma^2)$

$$\tilde{a}_0 = -\frac{\gamma\hat{q} - 2(\omega+1)}{2\sqrt{\omega+1}} + \ldots, \quad \tilde{b}_0 = \frac{\sqrt{\omega+1}\gamma}{1-\omega} + \ldots, \tag{4.12}$$

$$\tilde{a}_0 = \frac{\gamma\sqrt{\omega-1}}{\omega+1} + \ldots, \quad \tilde{b}_0 = \sqrt{\omega-1} + \ldots, \tag{4.13}$$

$$\begin{aligned} \tilde{a}_0 &= \sqrt{\omega+1} \pm \frac{\sqrt{\omega-1} - \hat{q}\gamma\sqrt{\omega+1}}{2(\omega+1)} + \ldots, \\ \tilde{b}_0 &= \mp\sqrt{\omega-1} + \ldots. \end{aligned} \tag{4.14}$$

Similarly for $q = -1 - \hat{q}\gamma$, one will obtain

$$\tilde{a}_0 = -\frac{\gamma\hat{q} - 2(\omega-1)}{2\sqrt{\omega-1}} + \ldots, \quad \tilde{b}_0 = 0, \tag{4.15}$$

$$\tilde{a}_0 = -\frac{\gamma\sqrt{\omega+1}}{1-\omega} + \ldots, \quad \tilde{b}_0 = \sqrt{\omega+1} + \ldots, \tag{4.16}$$

$$\begin{aligned} \tilde{a}_0 &= \sqrt{\omega-1} \pm \frac{\sqrt{\omega+1} - \hat{q}\gamma\sqrt{\omega-1}}{2(\omega-1)} + \ldots, \\ \tilde{b}_0 &= \mp\sqrt{\omega+1} + \ldots. \end{aligned} \tag{4.17}$$

4.3.2 Discrete solitons in the weakly-coupled arrays

Because solutions $\tilde{a}_0$, $\tilde{b}_0$ at each site n are mutually independent in the anticontinuum limit, one can construct infinitely many combinations, using the different solutions of $\tilde{a}_0$ and $\tilde{b}_0$. Here, we focus on fundamental onsite bright solitons for the case of weak coupling, i.e.,

small ϵ, which can be constructed by the continuation of the modes available at $\epsilon = 0$, which is a well-known method for finding various modes in discrete systems [1]. Up to order ϵ^2, such solitons are constructed in an approximate form,

$$A_n = \begin{cases} \tilde{a}_0 + \epsilon\tilde{a}_{0,1}, & n = 0, \\ \epsilon\tilde{a}_{1,1}, & n = \pm 1, \\ 0, & n \neq 0, \pm 1, \end{cases} \quad B_n = \begin{cases} i\tilde{b}_0 + \epsilon i\tilde{b}_{0,1}, & n = 0, \\ i\epsilon\tilde{b}_{1,1}, & n = \pm 1, \\ 0, & n \neq 0, \pm 1, \end{cases} \tag{4.18}$$

where, $\tilde{a}_0$, $\tilde{b}_0 \neq 0$ is one of the nonzero pairs given by Eqs. (4.12)-(4.17), and next-order terms are obtain perturbatively from Eq. (4.3), following [121]:

$$\tilde{a}_{0,1} = \frac{2\gamma\tilde{b}_0 + 2\tilde{a}_0(q - \omega + 3\tilde{b}_0^2)}{\gamma^2 - (q + \omega - 3\tilde{a}_0^2)(q - \omega + 3\tilde{b}_0^2)}, \tag{4.19}$$

$$\tilde{b}_{0,1} = \frac{2\gamma\tilde{a}_0 + 2\tilde{b}_0(q + \omega - 3\tilde{a}_0^2)}{\gamma^2 - (q + \omega - 3\tilde{a}_0^2)(q - \omega + 3\tilde{b}_0^2)}, \tag{4.20}$$

$$\tilde{a}_{1,1} = \frac{\gamma\tilde{b}_0 - \tilde{a}_0(q - \omega)}{\gamma^2 - (q^2 + \omega^2)}, \; \tilde{b}_{1,1} = \frac{-\gamma\tilde{a}_0 - \tilde{b}_0(q + \omega)}{\gamma^2 - (q^2 + \omega^2)}. \tag{4.21}$$

4.3.3 Stability eigenvalues of the discrete solitons

Following the weak-coupling perturbation used in subsections 4.3.1 and 4.3.2, we use similar asymptotic expansions to analytically solve the eigenvalue problem given by Eq. (4.9), i.e., we set

$$\square = \square^{(0)} + \sqrt{\epsilon}\square^{(1)} + \epsilon\square^{(2)} + \ldots, \tag{4.22}$$

with $\square = \lambda, K_n, L_n, P_n, Q_n$. Then, we substitute the expansions into the eigenvalue problem (4.9).

Due to the expansion of the anticontinuum-limit solutions in γ, we need to further expand Eqs. (4.22) as

$$\square^{(j)} = \square^{(j,0)} + \gamma\square^{(j,1)} + \gamma^2\square^{(j,2)} + \dots, \tag{4.23}$$

$j = 0, 1, 2, \dots$. Thus, we deal with two independent small parameters, i.e., the intersite and intercore couplings, ϵ and γ. Details of the respective calculations are not shown here, as they directly follow the method presented in [121]. Below, we report final results produced by this approach.

Due to the phase invariance, the discrete solitons have a trivial eigenvalue $\lambda = 0$. Additionally, for the discrete soliton (4.18), when $q = 1 - \hat{q}\gamma$ with $\tilde{a}_0$ and $\tilde{b}_0$ taken as per Eq. (4.12), it has a nonzero eigenvalue given, in the present approximation, by

$$\lambda = i\left[(-\omega + 1) - \gamma\hat{q} + \dots\right] + i\epsilon\left[2 + \dots\right] + \dots, \tag{4.24}$$

while for $\tilde{a}_0$ and $\tilde{b}_0$ taken as per Eq. (4.13), a nonzero stability eigenvalue is

$$\lambda = i\left[(-1 - \omega) + \gamma\hat{q} + \dots\right] + i\epsilon\left[-2 + \dots\right] + \dots, \tag{4.25}$$

When we consider $q = -1 - \hat{q}\gamma$, the discrete soliton (4.18), with $\tilde{a}_0$ and $\tilde{b}_0$ taken as per Eq. (4.15), it has a nonzero eigenvalue given by

$$\lambda = i\left[(-\omega - 1) - \gamma\hat{q} + \dots\right] + i\epsilon\left[2 + \dots\right] + \dots, \tag{4.26}$$

while for $\tilde{a}_0$ and $\tilde{b}_0$ taken as per Eq. (4.16), it is

$$\lambda = i\left[(-\omega + 1) + \gamma\hat{q} + \dots\right] + i\epsilon\left[-2 + \dots\right] + \dots, \tag{4.27}$$

In the present approximation, we obtain the discrete solitons are stable, as the corresponding eigenvalues are imaginary.

Unfortunately we are not able to obtain the non-trivial eigenvalues of the discrete soliton with $\tilde{a}_0$, $\tilde{b}_0$ given by (4.14) and (4.17) using the method discussed in [121]. It is because the expansion for q above, i.e. $q = \pm 1 - \hat{q}\gamma$, yields a degenerate case where in the unperturbed limit $\gamma \to 0$, the eigenvalues are all at the origin.

4.4 Numerical results

We have solved the steady-state Eq. (4.3) numerically using Newton-Raphson method, and analysed the stability of the numerical solutions by solving the eigenvalue problem (4.9). Below, we present numerical results, as well as their comparisons with the analytical calculations obtained above.

First, we consider the discrete soliton that are given in the approximate form by Eq. (4.18), with $\tilde{a}_0$ and $\tilde{b}_0$ taken as per Eq. (4.12). Using the approximate solution, we must have that $\omega > -1$. Together with the condition (4.5) and the first inequality of (4.7), one then obtains an interval of ω where such localised solutions can be continued to the strong-coupling regime of $\epsilon \gg 1$, indicating that the soliton continues into the continuum limit, where it goes over into the stable gap solitons reported in [110].

In Fig. 4.1, we display the numerical results of this class of solitons showing that the

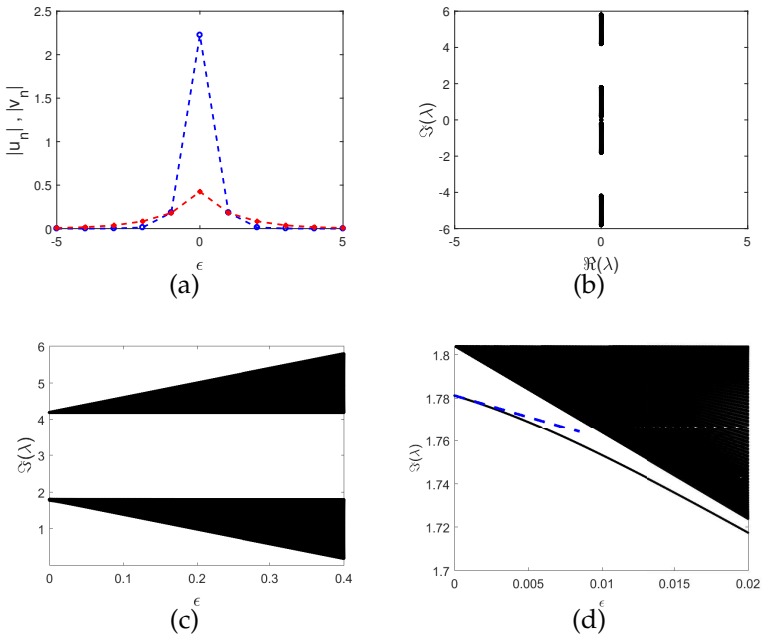

Figure 4.1: The discrete soliton given in the approximate form by Eqs. (4.18) and (4.12), and its stability for $\omega = 3$, $\gamma = 0.1$ and $q = 1.2$. (a) The solution profile for $\epsilon = 0.4$, blue and red dashed lines represent $|u_n|$ and $|v_n|$ respectively. (b) The corresponding spectrum of the solution in panel (a) in the complex plane. (c) Imaginary eigenvalues as a function of ϵ. (d) Zoom-in of panel (c) showing the nonzero eigenvalue and its approximation given by Eq. (4.24) (the dashed line).

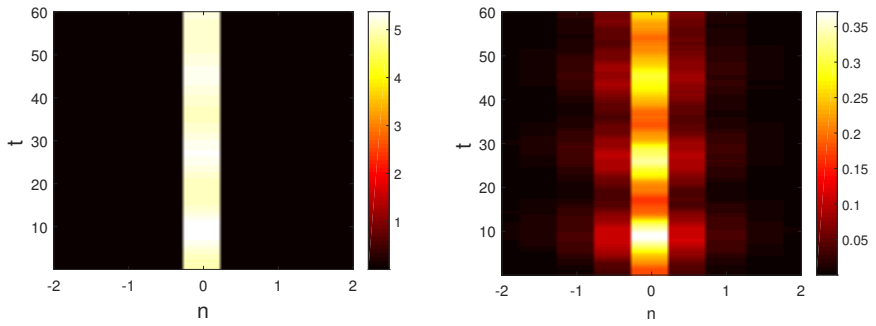

Figure 4.2: The dynamics of discrete solitons corresponding to those displayed in Fig. 4.1(a) past the critical coupling $\epsilon = 0.5$. Depicted in the left and right panels are $|u_n|^2$ and $|v_n|^2$, respectively.

solution is linearly stable. Here, we take the parameter value ω satisfying the second inequality in (4.7). In this case, there is a maximum coupling constant ϵ, above which the inequality is no longer satisfied. Numerical results cannot continue the solution beyond the critical value. In Fig. 4.1, the critical coupling corresponds to the moment when the lower branch of the continuous spectrum (see panel (c)) touches the horizontal axis.

In Fig. 4.2, we plot the typical dynamics of a discrete soliton past the critical coupling constant, i.e. we use the discrete soliton right before the critical coupling as the initial condition of the time integration code for the coupling right after the critical value. One can observe the 'breathing' dynamics of the solution, which creates radiation travelling towards the boundary. As time evolves, the soliton amplitude will decrease and eventually vanishes.

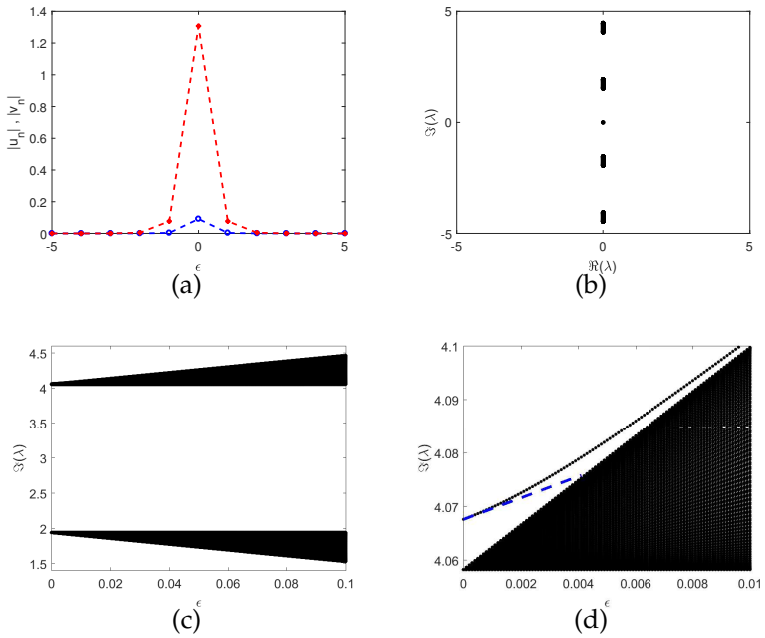

Figure 4.3: The same as Fig. 4.1, but for the discrete soliton given in the approximate form by Eqs. (4.18) and (4.13), and its stability for $\omega = 3$, $\gamma = 0.3$ and $q = 1.1$. The approximation of the nonzero eigenvalue is given by Eq. (4.25) (the dashed line).

Next, we consider the discrete soliton approximately given by Eq. (4.18) with $\tilde{a}_0$ and

$\tilde{b}_0$ taken as per Eq. (4.13). The solution profile and its stability are displayed in Fig. 4.3. Analytical approximation (4.25) is also shown, showing good agreement with the numerical findings. Note that this type of the solution exists only for $\omega > 1$ and it ceases to exist beyond a critical value of ϵ, i.e. because the possible values of ω can only be made to satisfy the second inequality of (4.7).

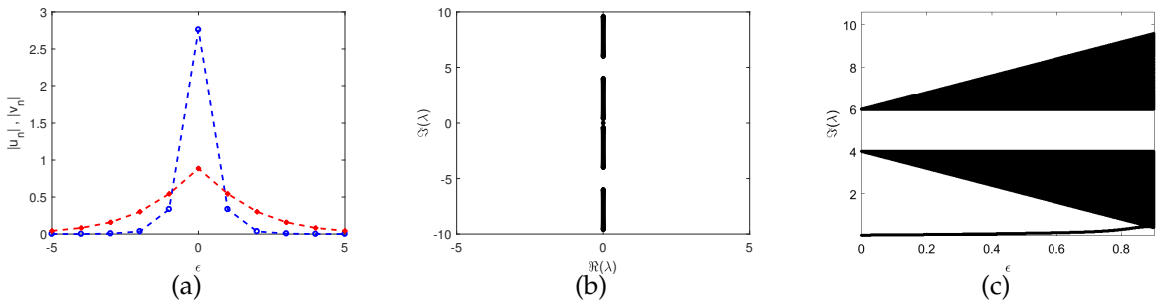

Figure 4.4: The discrete soliton for out-of-phase solitons corresponding to the approximate solution Eqs. (4.18) and (4.14), with the + and - *signs* for $\tilde{a}_0$ and $\tilde{b}_0$, respectively. Here, parameters are for $\omega = 3$, $\gamma = 0.1$ and $q = 1.2$. (a) The solution profile for $\epsilon = 0.9$, blue and red dashed lines represent $|u_n|$ and $|v_n|$ respectively. (b) The spectrum corresponding stability eigenvalues in the complex plane. (c) Imaginary eigenvalues as a function of ϵ.

Finally, we consider discrete solitons that correspond to the approximate expression (4.18) with $\tilde{a}_0$ and $\tilde{b}_0$ given by Eq. (4.14), which also requires $\omega > 1$ for its existence. Due to the ± sign in Eq. (4.14), there are two types of the solutions, that we refer to as the in-phase and out-of-phase solitons, for the solutions with signs + and − in $\tilde{b}_0$, respectively.

The profile and stability of the out-of-phase soliton are shown in Fig. 4.4, where one can see that the soliton is stable in its existence region. Further, we depict the profile and stability of the in-phase soliton in Fig. 4.5. Differently from the previous solutions, this solution becomes unstable beyond a critical point. The instability is caused by the collision of two eigenvalues on the imaginary axis (where one of them bifurcates from the continuous spectrum), thus creating a quartet of complex eigenvalues, i.e., oscillatory instability, which

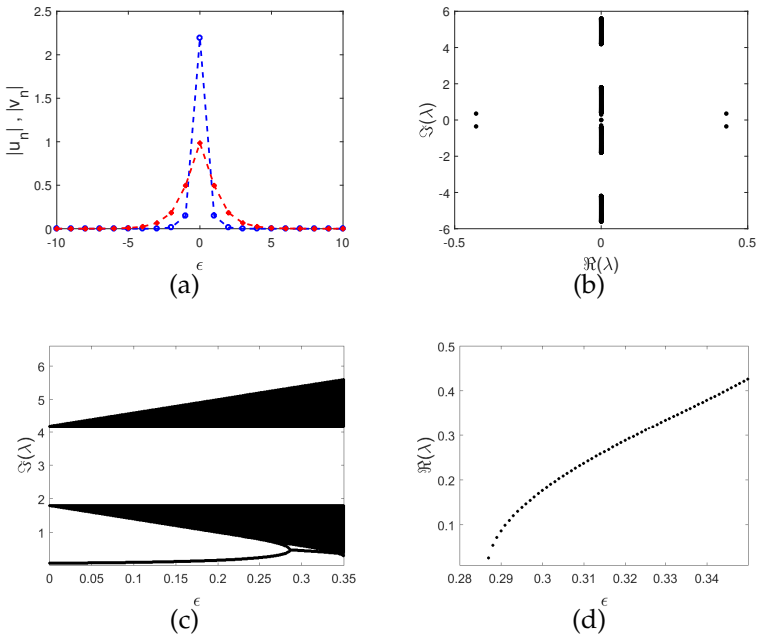

Figure 4.5: The same as Fig. 4.1, with $\epsilon = 0.35$ but for in-phase solitons corresponding to the approximate solution given by Eqs. (4.18) and (4.14), with the + and - *signs* for $\tilde{a}_0$ and $\tilde{b}_0$, respectively. In addition, panel (d) shows the real part of the spectrum as a function of the intersite coupling.

is a known generic scenario of the onset of instability of discrete solitons, [122] and [121]. The evolution initiated by the instability is shown in Fig. 4.6. It is clearly seen that the solution amplitude increases while oscillating, indicating an eventual blow-up.

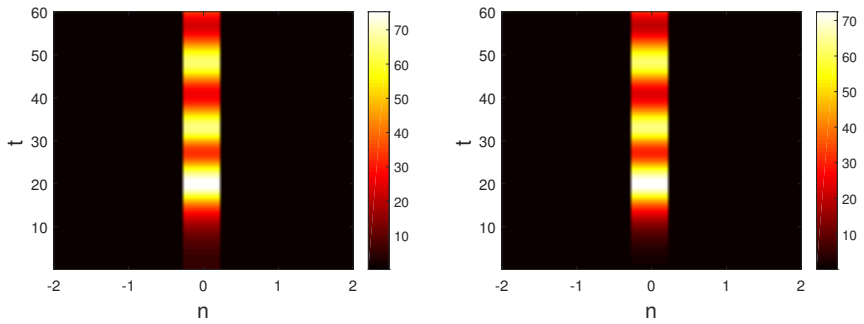

Figure 4.6: The dynamics of unstable in-phase discrete solitons, whose stationary shape is displayed in Fig. 4.5(a). Depicted in the left and right panels are $|u_n|^2$ and $|v_n|^2$, respectively.

We have also considered the case $q < 0$. Note that due to the condition (4.6), discrete solitons in this case will not be continuable towards the continuum limit $\epsilon \to \infty$, i.e.

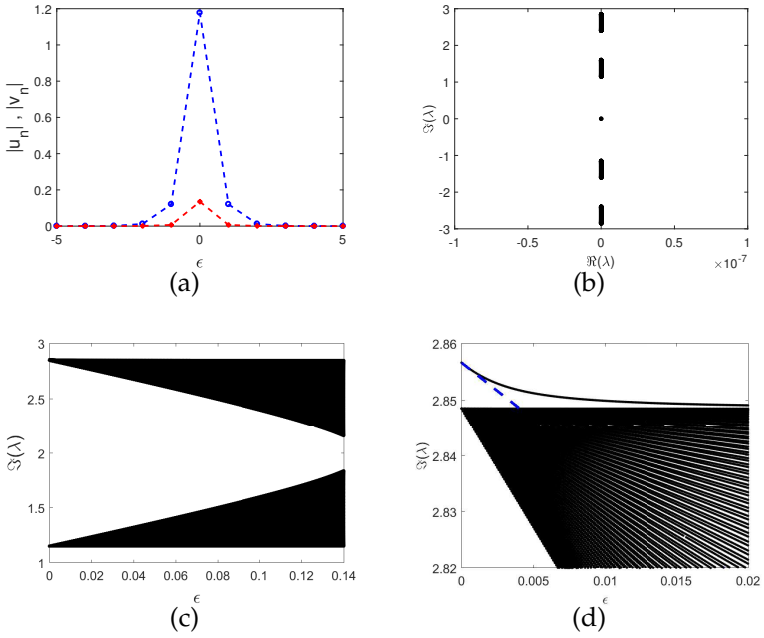

Figure 4.7: The same as Fig. 4.1, but for the discrete soliton given in the approximate form by Eqs. (4.18) and (4.13), and its stability for $\omega = 2$, $\gamma = 0.3$ and $q = -0.9$. The approximation of the nonzero eigenvalue is given by Eq. (4.26) (the dashed line).

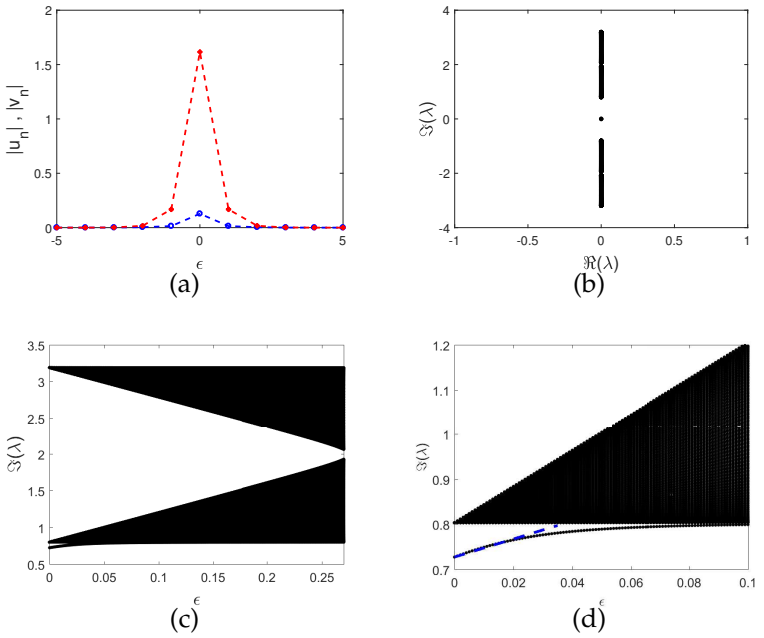

Figure 4.8: The same as Fig. 4.1, but for the discrete soliton given in the approximate form by Eqs. (4.18) and (4.13), and its stability for $\omega = 2$, $\gamma = 0.1$ and $q = -1.2$. The approximation of the nonzero eigenvalue is given by Eq. (4.27) (the dashed line).

whatever value of q we take initially, there will be a critical coupling ϵ above which the inequality is no longer satisfied.

For the sake of completeness, we depict in Figs. 4.7 and 4.8 the discrete soliton approximately given by Eq. (4.18) with $\tilde{a}_0$ and $\tilde{b}_0$ taken as per Eqs. (4.15) and (4.16), respectively. We also plot our approximation to the non-zero eigenvalue given by Eqs. (4.26) and (4.27), where good agreement is also obtained. In panel (c) of both figures, the critical coupling constant above which the condition (4.6) is violated corresponds to the moment when the two branches of the continuous spectrum merge. Here, we did not present the numerical results for discrete solitons approximately given by Eq. (4.18) with $\tilde{a}_0$ and $\tilde{b}_0$ taken as per Eqs. (4.17) because they yield the same qualitative pictures as those in Figs. 4.7 and 4.8.

4.5 Conclusion

In this work we have introduced the model of the dual-core waveguiding array, which can be realised as an optical system featuring the $\mathcal{CP}-$symmetry. Characteristic features of the system are the opposite sign of the discrete diffraction in the two parallel arrays (cores), that may be implemented by means of the diffraction-management technique, and the active coupling between the arrays, which accounts for the gain and loss in the system, the stability of the zero state being provided by a sufficiently phase-velocity mismatch between the parallel arrays. Our analytical results, obtained by means of the extension from the anticontinuum limit, and numerical findings show the existence of several families of stationary discrete solitons in the system. On the contrary to the continuous limit of the present setting, considered in [110], the discrete system supports different types of

solitons, with the propagation constant falling into the bandgap of the corresponding linear spectrum. Most soliton families are stable, although only one of them extends to the continuum limit, while others terminate by leaving the bandgap and crossing into the spectral bands. One discrete-soliton family develops the oscillatory instability past a critical value of the intersite coupling.

Chapter 5

Snakes in a $\mathcal{PT}$-symmetric chain of dimers

5.1 Introduction

Many nonlinear dynamical systems, such as spatially extended nonlinear dissipative systems [123], vertical-cavity semiconductor optical amplifiers [124], nematic liquid crystal layers with spatially modulated input beam [125], and magnetic fluids [126], exhibit spatially localised patterns and a snaking structure in their bifurcation diagrams in the plane of the length of the localised solution against a control parameter. This phenomenon of snaking is referred to as homoclinic snaking [127–129], where the spatial structure of such a localised state departs from and then returns to a uniform state. By definition, it has infinitely many turning points due to saddle-node bifurcations which form the boundaries (fronts) of the snaking region. Such snaking region is also called the pinning region since the fronts at either end 'pin' or 'lock' to the structure within the localised state, and an

infinite number of localised states exist in the entire interval of the pinning region.

In most of previous works devoted to localised states and snaking in continuous systems, the Swift-Hohenberg equation has been widely used as a model for pattern formation since it is the simplest model equation that illustrates the pinning effect [129–133]. In general, the pinning effect cannot be described by conventional multiple-scale asymptotic method due to the fact that the length of the pinning region is exponentially small in a parameter which is related to the pattern amplitude [127]. Recently the Swift-Hohenberg with quadratic-cubic nonlinearities and cubic-quintic nonlinearities have been successfully studied with the help of the exponential asymptotics [134–136]. The calculations, however, are rather cumbersome and unfortunately require two fitting parameters. Alternatively, variational methods to obtain scaling laws for the structure of the snaking region have been proposed and demonstrated, for example, in the system modelled by the cubic-quintic Swift-Hohenberg equation [137].

Like spatially continuous systems, several discrete systems can display the snaking behavior with the locking effect, however, being attributed to the imposed lattice. Examples include the discrete bistable nonlinear Schrödinger equation [138–140], which leads to a subcritical Allen-Cahn equation [141], optical cavity solitons [142, 143], discrete systems with a weakly broken pitchfork bifurcation [144] and in patterns on networks appearing due to Turing instabilities [145]. The pinning region in this case was studied analytically by Matthews and Susanto [146] and Dean et al. [147]. In this chapter, we consider localised structures in a $\mathcal{PT}$ symmetric chain of dimers that has two arms with each arm described by a discrete nonlinear Schrödinger equation with gain or loss. To the best of our knowledge, the effect of the gain and loss term in a $\mathcal{PT}$-symmetric chain of dimers to the snaking

regime has not been explored yet.

A system of equations is $\mathcal{PT}-$symmetric when it is invariant regarding combined parity ($\mathcal{P}$) and time-reversal ($\mathcal{T}$) transformation [14, 18, 66]. Such symmetry is of great interest as it forms a particular class of non-Hermitian Hamiltonians in quantum mechanics and has been widely studied [65]. Among these, dimers are the most basic and important $\mathcal{PT}-$symmetric systems because the concept of $\mathcal{PT}-$symmetry was first demonstrated experimentally on dimers, which are composed of two coupled optical waveguides [67,68] (see also [71] and references therein). In particular, when nonlinear dimers are put in arrays where elements with gain and loss are linearly coupled to the elements of the same type belonging to adjacent dimers, one can obtain a distinctive feature in the form of the existence of solutions localised in space as continuous families of their energy parameter [74]. The nonlinear localised solutions, which loosely are also referred to as bright discrete solitons, and their stability have been studied in [121] analytically and numerically (see also the references therein for localised solutions in systems of coupled nonlinear Schrödinger equations).

This chapter is devoted to a detailed numerical and analytical study of homoclinic snaking in a $\mathcal{PT}$-symmetric chain of dimers with cubic-quintic nonlinearity. The continuum limit of the same set-up has been considered in [107, 109]. In optical media, such nonlinearity can be obtained from a saturation of the Kerr response, which with the increase of the intensity will introduce a self-defocusing quintic term in the expansion of the refractive index [148, 149]. In the continuous case [107, 108], it was shown that the presence of gain-loss terms only influences the stability of the localised solutions. Here, it will be shown that the discrete set-up admits homoclinic snaking. We show that the

critical gain/loss parameter corresponding to the 'broken $\mathcal{PT}$-symmetry' phase, i.e. the linear system counterpart has a complex-valued spectrum, is related to the merging of two snaking regions. The width of the snaking region is discussed analytically in two different regimes, i.e. weak and strong coupling between the dimers. In the strong coupling region, we use a variational method following [146], but with a different approach yielding a simple expression of the width that was not obtainable in [146]. When the coupling is weak, we introduce a one-active-site approximation following [150].

This chapter is outlined as follows. In Section 5.2, we present the mathematical model. In Section 5.3, we present the numerical solution using Newton-Raphson method and analysed the stability. The analytical approximations of the solitons is then considered in Section 5.4. Conclusion the main finding in the chapter is in Section 5.5.

5.2 Mathematical model

The governing equations describing $\mathcal{PT}$-symmetric chains of dimers are of the form

$$\begin{aligned} i\dot{u}_n &= \left(\epsilon\Delta_2 - \omega + |u_n|^2 - Q\,|u_n|^4 + i\gamma\right) u_n + v_n, \\ i\dot{v}_n &= \left(\epsilon\Delta_2 - \omega + |v_n|^2 - Q\,|v_n|^4 - i\gamma\right) v_n + u_n. \end{aligned} \tag{5.1}$$

The derivative with respect to the evolution variable (i.e., the propagation distance, if we consider their application in fiber optics) is denoted by the overdot, $u_n = u_n(t)$, $v_n = v_n(t)$ are complex-valued wave function at site $n \in \mathbb{Z}$ with the propagation constant $\omega \in \mathbb{R}$, $\epsilon > 0$ is the constant coefficient of the horizontal linear coupling (coupling constant between two adjacent sites), $\Delta_2 u_n = (u_{n+1} - 2u_n + u_{n-1})$ and $\Delta_2 v_n = (v_{n+1} - 2v_n + v_{n-1})$ are the discrete

Laplacian term in one spatial dimension, the gain and loss acting on complex variables u_n, v_n are represented by the positive coefficient γ, i.e. $\gamma > 0$. The cubic nonlinearity coefficient has been scaled to +1, while Q is the coefficient of the quintic nonlinearity. Discrete solitons satisfy the localisation conditions $u_n, v_n \to 0$ as $n \to \pm\infty$. In the continuum limit $\epsilon \to \infty$, Eqs. (5.1) were studied in [108] and [107] for the one-dimensional and two-dimensional problems, respectively.

Here, we consider standing wave solutions of (5.1) that can be obtained from substituting $u_n = A_n$, $v_n = B_n e^{i\phi}$ into (5.1) to yield the equations

$$\begin{aligned} \left(\epsilon\Delta_2 - \omega + A_n^2 - QA_n^4 + i\gamma\right) A_n + B_n e^{i\phi} = 0, \\ \left(\epsilon\Delta_2 - \omega + B_n^2 - QB_n^4 - i\gamma\right) B_n + A_n e^{-i\phi} = 0. \end{aligned} \tag{5.2}$$

Here, $A_n, B_n, \phi \in \mathbb{R}$. We can assume that u_n is real-valued because of the phase invariance of the governing equations (5.1).

Simplifying the equations by splitting the real and the imaginary parts of the equation will yield

$$\Omega A_n = \epsilon \left(A_{n+1} - 2A_n + A_{n-1}\right) + A_n^3 - QA_n^5, \tag{5.3}$$

which is also known as the discrete Allen-Cahn equation, where $B_n = -A_n$, $\Omega = \omega \pm \sqrt{1-\gamma^2}$ with $\phi = \arcsin\gamma$ for the plus sign and $\phi = \pi - \arcsin\gamma$ for the minus sign, which corresponds to the so-called antisymmetric and symmetric configuration between the arms, respectively. Eq. (5.3) has uniform solutions $A_n \equiv A$ that are given by

$$A = 0,\ A^2 = \frac{1 \pm \sqrt{1 - 4Q\Omega}}{2Q}. \tag{5.4}$$

Note that (5.3) will have no real solution when $|\gamma| > 1$. This is the broken region of $\mathcal{PT}$-symmetry. The uniform solution (5.4) also requires $4Q\Omega < 1$ to exist.

The linear stability of a solution of (5.1) is determined by solving a corresponding linear eigenvalue problem of (5.1). To do so, we introduce the linearisation ansatz $u_n = A_n + \zeta(K_n + iL_n)e^{\lambda t}$, $v_n = B_n e^{i\phi} + \zeta(P_n + iQ_n)e^{\lambda t}$, $|\zeta| \ll 1$, and substitute this into Eq. (5.1) to obtain from the equations at $O(\zeta)$ the eigenvalue problem

$$\begin{aligned}
\lambda K_n &= (\epsilon\Delta_2 - \omega + A_n^2 - QA_n^4)L_n + \gamma K_n + Q_n, \\
-\lambda L_n &= (\epsilon\Delta_2 - \omega + 3A_n^2 - 5QA_n^4)K_n - \gamma L_n + P_n, \\
\lambda P_n &= (\epsilon\Delta_2 - \omega + B_n^2(1-\gamma^2)(1 - QB_n^2(1-\gamma^2)))Q_n \\
&\quad + (2B_n^2\gamma\sqrt{1-\gamma^2}(1 - 2QB_n^2(1-\gamma^2)) - \gamma)P_n + L_n, \\
-\lambda Q_n &= (\epsilon\Delta_2 - \omega + B_n^2(1-\gamma^2)(3 - 5QB_n^2(1-\gamma^2)))P_n \\
&\quad + \gamma Q_n + K_n,
\end{aligned} \tag{5.5}$$

which have to be solved for the eigenvalue λ and the corresponding eigenvector $[K_n, L_n, P_n, Q_n]^T$. One can note that if λ is a spectrum, so are $-\lambda$ and $\pm\overline{\lambda}$ [121]. Therefore, a solution is (linearly) stable only when $\Re(\lambda) = 0$ for all eigenvalues λ.

The spectrum of the uniform solutions (5.4) can be obtained by introducing the plane-wave ansatz $K_n = \hat{k}e^{ikn}, L_n = \hat{l}e^{ik}, P_n = \hat{p}e^{ikn}, Q_n = \hat{q}e^{ikn}$, $k \in \mathbb{R}$, and substitute the ansatz into (5.5) to yield the dispersion relations. The continuous spectrum is obtained from the dispersion relation by setting $k = 0$ and $k = \pi$ in the equation. However, rather than showing the lengthy expressions of the dispersion relations, for the sake of simplicity we only plot the uniform solutions and indicate their stability. In Fig. 5.1, we show

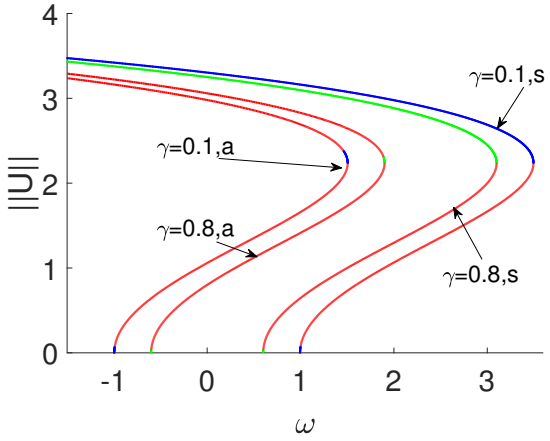

Figure 5.1: The bifurcation diagram of the uniform solutions (5.4) for $\gamma = 0.1$ and $\gamma = 0.8$ with $\epsilon = 0.1$. The notation 'a' and 's' denotes the antisymmetric ($\phi = \arcsin\gamma$) and symmetric ($\phi = \pi - \arcsin\gamma$) configuration between the arms, respectively.

the bifurcation diagram of the nonzero solutions (5.4) for $\epsilon = 0.1$. The solution when unstable is shown as dashed line. Note that the antisymmetric solutions are unstable almost everywhere in their existence region. We will need these observations later.

5.3 Numerical methods

We solve the steady-state Eq. (5.2) numerically using Newton-Raphson method and analysed the stability of the numerical solution by solving the eigenvalue problem (5.5).

It is well-known that there are two natural fundamental solutions representing bright discrete solitons that may exist for any coupling constant ϵ, from the anticontinuum to the continuum limit, i.e. an intersite (or bond-centred) and onsite (or site-centred) discrete mode.

Fixing the coupling ϵ and varying the propagation constant ω, we obtain the bifurcation diagrams of the two types of discrete modes in Fig. 5.2. One can note that for each symmetric and antisymmetric configuration between u_n and v_n, there are two branches that correspond

to the site-centred and bond-centred solutions. More importantly, the bifurcation diagrams form a snaking structure. Even though such structures have been reported before [138, 139,141,146,151], the stability behaviour along the curves are different due to the different setup of equations considered herein. The region between the boundaries of the snakes is the pinning region. Additionally, there are also branches of asymmetric solutions, called ladders, connecting the snaking branches of onsite and intersite modes. Comparing the two panels of Fig. 5.2, one can note that in agreement with the continuous case reported in [107,108] the gain-loss parameter tends to destabilise the localised solutions, shown by the dashed curve that tends to expand in the second panel.

In Fig. 5.3 we plot the profiles of several localised solutions and their spectrum in the complex plane. One can note that some of the solutions are unstable shown by the fact that there is a spectrum with nonzero real part. This corresponds to the red dashed segment in Fig. 5.2.

It is interesting to note that up in the snaking structures (represented by point 5 and 6 in Fig. 5.2(a)), the stability of the branches is similar to those in Fig. 5.1. This is due to the fact that as we move up in the snaking, the corresponding localised solutions have longer and longer plateau of nonzero uniform solutions, i.e. the stability may be determined by the continuous spectrum.

We show in Fig. 5.4 the time evolution of the unstable solutions of Fig. 5.3. While in Fig. 5.5 indicates a clear blow up of the wave field with gain, which is typical in $\mathcal{PT}$-systems [71], panel (a) shows intensity oscillations. The fact that the oscillations persist for quite a while is interesting by itself as $\mathcal{PT}$-symmetric dimers with cubic nonlinearity are known to have oscillations that blow up [71]. Similar oscillations in the continuum limit

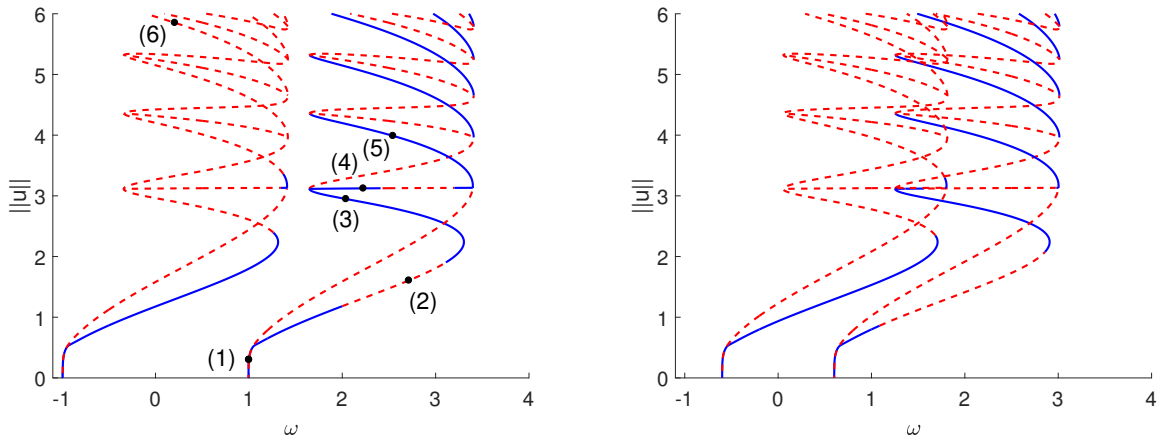

Figure 5.2: The bifurcation diagram of the fundamental localised solutions. We plot the norm $\|u\| = \sqrt{\sum_n u_n^2}$ as ω varies. Stable branches are represented by solid blue lines and unstable branches by dashed red lines. There are two principle branches, one corresponding to site-centered solutions and one for bond-centered solutions. The two principle branches are connected via asymmetric solutions at points of stability change. Here, (a) $\gamma = 0.1$ and (b) $\gamma = 0.8$ with $\epsilon = 0.1$.

$\epsilon \to \infty$ were also reported in [108], where the bounded oscillations were attributed to the quintic nonlinearity that may have suppressed the blow up. However, whether the long-live oscillation is a genuine cycle is still unknown and is addressed for future work. The instability of the solution at point (2) when $\gamma = 0$ is actually due to a symmetry breaking (or pitchfork) bifurcation, i.e. asymmetric solutions between the arms ($|A_n| \neq |B_n|$) emanate from the points of stability change. When $\gamma \neq 0$, the instability persists, however in the case of dimers with cubic nonlinearity only the bifurcating solution is usually called the 'ghost-state', i.e. nonlinear asymmetric solutions with complex-valued ω [152]. Whether such ghost states exist in the presence of quintic nonlinearity (considering the persisting oscillation in Fig. 5.4, instead of the normal blow up in the cubic dimers) is also addressed for future work.

Regarding the snaking region, we observe that the width does not depend on γ. As the

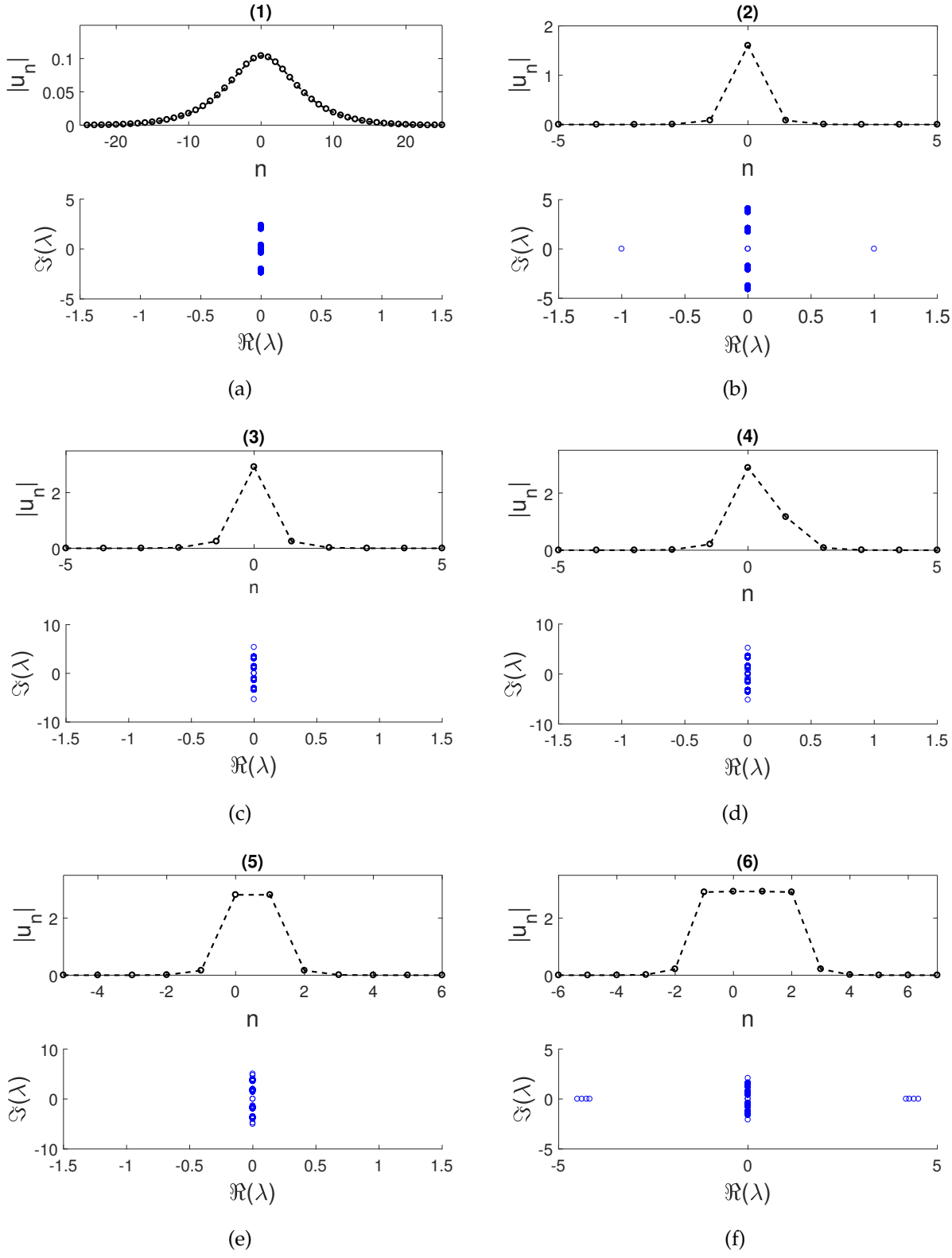

Figure 5.3: Plot of the corresponding localised solutions on the bifurcation diagram shown in Fig. 5.2 and their spectrum in the complex plane. Panels (a,b,c): site-centred solutions. Panels (e,f): bond-centred solutions. Panel (d): asymmetric solution, which is an intermediate between two symmetric profiles.

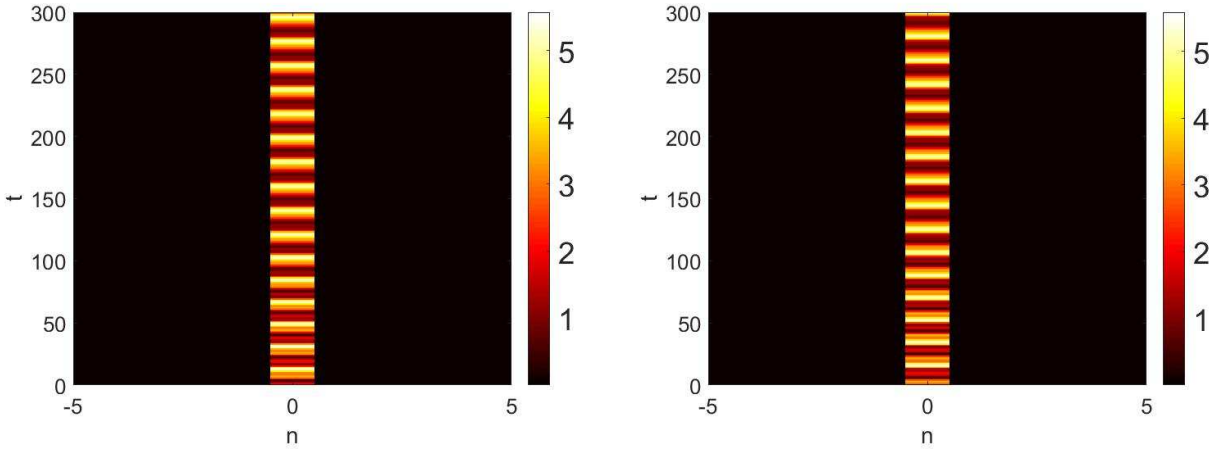

(a) Point (2) (b) Point (2)

Figure 5.4: Dynamics view of the unstable solutions in panels (b) and (f) of Fig. 5.3 when $\epsilon = 0.1$, $\gamma = 0.1$ and $\omega = 2.7133$. Left panel is for $|u_n(t)|^2$ and right panel is for $|v_n(t)|^2$.

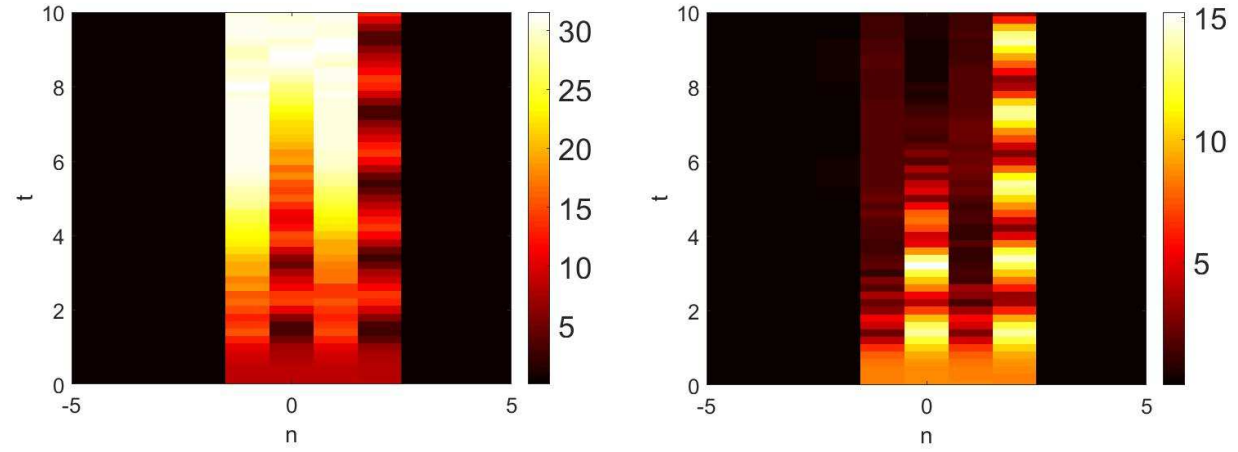

(a) Point (6) (b) Point (6)

Figure 5.5: Dynamics view of the unstable solutions in panels (b) and (f) of Fig. 5.3 when $\epsilon = 0.1$, $\gamma = 0.1$ and $\omega = 0.20623$. Left panel is for $|u_n(t)|^2$ and right panel is for $|v_n(t)|^2$.

parameter increases towards the critical value $\gamma \to 1$, Fig. 5.2 shows that the branches of the symmetric and asymmetric solutions become closer. At the critical value, they overlap. This is due to the fact that when studying time-independent solutions, the governing equation (5.1) reduces nicely to the discrete Allen-Cahn equation (5.3) that is rather independent of γ and the parameter Ω for the symmetric and antisymmetric solutions becomes the same when $\gamma = 1$.

Next, it is interesting to analyse the width of the snaking region as a function of, e.g., the coupling constant ϵ.

5.4 Analytical approximations

In this section, we will derive an asymptotic approximation of the width of the snaking region in Fig. 5.2. The approach is distinguished in two different regions, i.e. small and large coupling.

5.4.1 Small coupling case

When ϵ is small, as we follow the snaking structure upward (see Fig. 5.2), actually there is only one site that is 'active' as ω varies, with the remaining sites being either at 0 or at the plateau of a uniform solution. Such behaviours were observed and exploited in many ways before, see, e.g., [153, 154], but not in the context of snaking.

From (5.3) and (5.4), the one-active-site approximation is given by

$$f(a) := Qa^5 - a^3 + (\Omega + 2\epsilon)a - \epsilon\sqrt{\frac{1 + \sqrt{1 - 4Q\Omega}}{2Q}} = 0. \tag{5.6}$$

Note that we only use the '+' sign for the uniform solution forming the plateau.

In general (5.6) will have five roots. The roots relevant to our study are the positive ones. As Ω varies, two of the roots will collide in a saddle-node bifurcation. This condition corresponds to the boundaries of the snaking region. The condition for the collision is when a local maximum or minimum of the function $f(a)$ crosses the horizontal axis. The critical points of $f(a)$ are given by

$$f'(a) := 5Qa^4 - 3a^2 + (\Omega + 2\epsilon) = 0, \tag{5.7}$$

i.e.

$$a = \sqrt{\frac{3 \pm \sqrt{9 - 20Q(\Omega + 2\epsilon)}}{10Q}}. \tag{5.8}$$

Substituting (5.8) into (5.6) and solving the resulting equation for Ω asymptotically give us

$$\Omega = \frac{1}{4Q} - \epsilon + O(\epsilon^2),\ 3\sqrt[3]{\frac{\epsilon^2}{4Q}} + O(\epsilon^{4/3}). \tag{5.9}$$

the snaking width W is then given approximately by the difference between the two functions.

5.4.2 Large coupling case

In the large coupling case, i.e. close to the continuous limit, following [155, 156], (5.3) can also be obtained from

$$\epsilon A_{xx} + \sum_{n=-\infty}^{\infty} \delta(x - n)\left(-\Omega A + A^3 - QA^5\right) = 0, \tag{5.10}$$

where $A_n = A(x = n)$.

We then write the summation $\sum_{n=-\infty}^{\infty} \delta(x-n) = 1 + 2\sum_{k=1}^{\infty} \cos(2\pi k x)$, which does not converge uniformly. Taking only the first harmonic, (5.10) then becomes

$$\epsilon A_{xx} + (1 + 2\cos(2\pi x))\left(-\Omega A + A^3 - Q A^5\right) = 0, \tag{5.11}$$

which can be expected to approximate (5.3) for $\epsilon \gg 1$ [155].

Without the periodic potential $2\cos(2\pi x)$, Eq. (5.11) at the Maxwell point, that corresponds to the condition when $A_n \equiv A = 0$ has the same 'energy' (or the value of the first integral) with the nonzero solution (5.4) with the '+' sign, i.e.

$$\Omega A^2 = \frac{1}{2}A^4 - \frac{Q}{3}A^6,$$

which is attained at

$$\Omega = \frac{3}{16Q}, \tag{5.12}$$

has a front solution given by

$$A(x) = \sqrt{\frac{3}{4Q\left(1 + e^{\sqrt{\frac{3}{4Q\epsilon}}x}\right)}}. \tag{5.13}$$

Following [137, 146], we approximate the solutions along the snaking structure by

$$A(x) = \sqrt{\frac{3}{4Q\left(1 + e^{\sqrt{\frac{3}{4Q\epsilon}}(|x-\phi|-l)}\right)}}, \tag{5.14}$$

where ϕ is the phase-shift distinguishing the two branches, i.e. $\phi = 0, 1/2$ for the on-site and intersite solutions, respectively. l is the length of the plateau, which is presently an unknown variable.

Using the variational argument, requiring (5.14) to be an optimal solution of (5.11) implies that l must satisfy the equation (see [157] for the derivation in a general set-up)

$$\int_{-\infty}^{\infty} \left[\epsilon A_{xx} + (1 + 2\cos(2\pi x))\left(-\Omega A + A^3 - QA^5\right)\right] \frac{\partial A}{\partial l}\, dx = 0, \tag{5.15}$$

where Ω is set to be near the Maxwell point (5.12), i.e. $\Omega = 3/(16Q) + \Delta\Omega$.

Equation (5.15) can be simplified at the leading order for $l \gg 1$ to

$$\begin{aligned}\Delta\Omega &= \lim_{l\to\infty} \frac{-2\epsilon \int_0^\infty \cos(2\pi x) A_{xx} \frac{\partial A}{\partial l}\, dx}{\int_0^\infty A \frac{\partial A}{\partial l}\, dx} \\ &= \frac{\epsilon\pi^3}{3} \operatorname{csch}\left(\frac{4\pi^2\sqrt{\epsilon Q}}{\sqrt{3}}\right)\left[4\pi\sqrt{3\epsilon Q}\cos(2\pi l) + 3\sin(2\pi l)\right].\end{aligned} \tag{5.16}$$

The width of the snaking region is then simply given by

$$W = \frac{2\epsilon\pi^3}{3} \operatorname{csch}\left(\frac{4\pi^2\sqrt{\epsilon Q}}{\sqrt{3}}\right)\sqrt{48\pi^2\epsilon Q + 9}, \tag{5.17}$$

$$\approx 16\pi^4\epsilon^{3/2}\sqrt{\frac{Q}{3}}e^{-\frac{4\pi^2\sqrt{\epsilon Q}}{\sqrt{3}}}, \tag{5.18}$$

which is exponentially small. Note that [146], that used the explicit expression of the Lagrangian without approximating the discrete Laplacian with the second derivative, was not able to obtain the explicit expression and only provided the exponential scale.

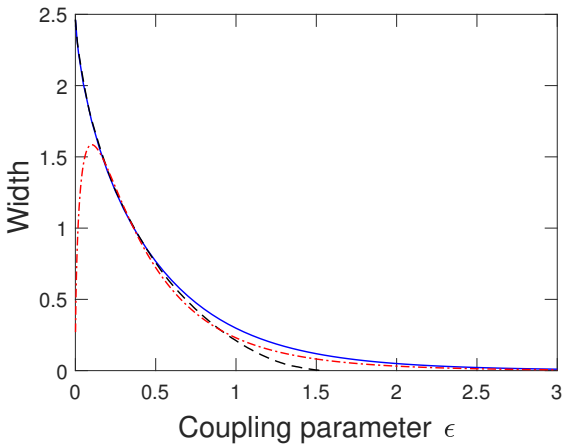

Figure 5.6: The width of the snaking region as a function of the coupling constant ϵ for $Q = 0.1$. The solid curve is obtained from the numeric and the dashed and dash-dotted lines are the approximations.

5.4.3 Snaking width

We show in Fig. 5.6 the width of the snaking region computed numerically and our approximations (5.9) and (5.17). One can see good agreement between them.

5.5 Conclusion

Localised solutions (site-centered and bond-centered modes) and their bifurcation diagrams that form a snaking structure in a $\mathcal{PT}$-symmetric coupler composed by a chain of dimers have been discussed. It has been shown that the gain-loss coefficient does not influence the width of the snakes, and the critical gain/loss coefficient above which the $\mathcal{PT}-$symmetry is broken corresponds to the overlapping bifurcation diagrams.

Asymptotic approximations of the width of the snaking region have been derived in two different limits, i.e. strong and weak coupling between the dimers. The approximations have been compared with the numerical results where good agreement is obtained.

Chapter 6

Conclusion and future work

6.1 Conclusion

In this thesis, a systematic method to determine the stability of discrete solitons in a $\mathcal{PT}$-symmetric coupler by computing the eigenvalues of the corresponding linear eigenvalue problem using asymptotic expansions has been presented. We used perturbation expansion method for small coupling constant ϵ to analyse the existence and stability of the solitons. Also a comparison between the analytical results that we obtained with numerical computations shows good agreement. From the numerics, we have established the mechanism of instability as well as the stability region of the discrete solitons.

We have also analysed a model of a dual-core waveguide which may implement an optical system featuring the $\mathcal{CP}-$symmetry. Our study shows the presence of a general family of stationary discrete solitons in the nonlinear system, that have been also found and checked for the stability in the numerical form. On the contrary to the continuous case discussed in [110], the lattice system may support different types of solitary pulses

with propagation constants above the upper edge of the spectrum band. Asymptotic expansions have been presented as well where good agreement with the numerical results was obtained.

Localised solutions in a $\mathcal{PT}$-symmetric coupler composed by a chain of dimers were studied in this work, that is modelled by linearly coupled discrete nonlinear Schrödinger equations with gain and loss terms and with a cubic-quintic nonlinearity. We consider site-centered and bond-centered localised solutions and show that the resulting bifurcation diagrams when a parameter is varied form a snaking behaviour. Each localised solution has symmetric and antisymmetric configurations between the arms. The critical gain/loss coefficient above which the $\mathcal{PT}-$symmetry is broken corresponds to the overlapping bifurcation diagrams. We analyse the width of the snaking region and provide asymptotic approximations in the limit of strong and weak coupling where good agreement is obtained. It has been shown that the gain-loss coefficient does not influence the width of the snakes, and the critical gain/loss coefficient above which the $\mathcal{PT}-$symmetry is broken corresponds to the overlapping bifurcation diagrams.

6.2 Future work

The application of the higher dimensional $\mathcal{PT}/\mathcal{CP}$-symmetric couplers in Chapter 3 and 4 (see, e.g., [158]) is a natural extension of the problem that is addressed for future work. Additionally we also address the computation of eigenvalues of discrete solitons in the neighbourhood of broken $\mathcal{PT}$-symmetry as future investigations.

An unstable solution was shown in Chapter 5 to yield a long-live oscillation. As such

oscillations would lead to blow up in the cubic dimers, it is not clear yet if the oscillation is a genuine cycle and related to the quintic nonlinearity or only a transient dynamics. The oscillation as a typical dynamics of the instability is also related to the mechanism of the instability of the localised solution, i.e. whether it is a symmetry breaking (or pitchfork) bifurcation with a 'ghost-state'. These questions are addressed for future work.

Bibliography

[1] P. G. Kevrekidis, "The discrete nonlinear Schrödinger equation: Mathematical analysis, numerical computations and physical perspectives", vol. 232. Springer Science & Business Media, 2009.

[2] N. J. Zabusky and M. D. Kruskal, "Interaction of solitons in a collisionless plasma and the recurrence of initial states", Physical Review Letters, vol. 15, no. 6, pp. 240–243, 1965.

[3] P. G. Drazin and R. S. Johnson, "Solitons: an introduction", vol. 2. Cambridge university press, 1989.

[4] A. Scott, "Encyclopedia of nonlinear science", Routledge, 2004.

[5] J. S. Russell, "Report on waves," in 14th meeting of the British association for the advancement of science", vol. 311, p. 390, 1844.

[6] L. Rayleigh, "On waves", Philos. Mag, vol. 1, no. 5, pp. 257–279, 1876.

[7] D. J. Korteweg and G. De Vries, "Xli. on the change of form of long waves advancing in a rectangular canal, and on a new type of long stationary waves", The London, Edinburgh, and Dublin Philosophical Magazine and Journal of Science, vol. 39, no. 240, pp. 422–443, 1895.

[8] E. Fermi, J. Pasta, and S. Ulam, "Studies of nonlinear problems", 1955.

[9] C. S. Gardner, J. M. Greene, M. D. Kruskal, and R. M. Miura, "Method for solving the korteweg-devries equation", Physical Review Letters vol. 19, no. 19, p. 1095, 1967.

[10] A. Shabat and V. Zakharov, "Exact theory of two-dimensional self-focusing and one-dimensional self-modulation of waves in nonlinear media", Soviet Physics JETP, vol. 34, pp. 62–69, 1972.

[11] R. K. Dodd, J. C. Eilbeck, J. D. Gibbon, and H. C. Morris, "Solitons and nonlinear wave equations", 1982.

[12] A. Scott, "Nonlinear Science: Emergence and Dynamics of Coherent Structures", Oxford texts in applied and engineering mathematics, Oxford University Press, 2003.

[13] M. J. Ablowitz, D. J. Kaup, A. Newell, and H. Segur, "Method for solving the sine-gordon equation", Physical Review Letters, vol. 30, no. 25, p. 1262, 1973.

[14] C. M. Bender and S. Boettcher, "Real spectra in non-hermitian hamiltonians having $\mathcal{PT}$ symmetry", Physical Review Letters, vol. 80, no. 24, p. 5243, 1998.

[15] C. M. Bender, "$\mathcal{PT}$ symmetry in quantum physics: From a mathematical curiosity to optical experiments", Europhysics News, vol. 47, no. 2, pp. 17–20, 2016.

[16] A. Millican-Slater, "Aspects of $\mathcal{PT}$-symmetric quantum mechanics", PhD thesis, Durham University, 2004.

[17] C. M. Bender, D. C. Brody, and H. F. Jones, "Complex extension of quantum mechanics", Physical Review Letters, vol. 89, no. 27, p. 270401, 2002.

[18] C. M. Bender, "Making sense of non-hermitian hamiltonians", Reports on Progress in Physics, vol. 70, no. 6, p. 947, 2007.

[19] S. Weigert, "Completeness and orthonormality in $\mathcal{PT}$-symmetric quantum systems", Physical Review A, vol. 68, no. 6, p. 062111, 2003.

[20] G. C. Branco, L. Lavoura, J. P. Silva, I. Bigi, A. Sanda, and A. Falk, "$\mathcal{CP}$ violation", Physics Today, vol. 53, no. 8, pp. 50–52, 2000.

[21] J. H. Christenson, J. W. Cronin, V. L. Fitch, and R. Turlay, "Evidence for the 2π decay of the k_2^0 meson", Physical Review Letters, vol. 13, no. 4, p. 138, 1964.

[22] Y. I. Frenkel and T. Kontorova, "The model of dislocation in solid body", Zh. Eksp. Teor. Fiz, vol. 8, no. 1340, 1938.

[23] N. W. Ashcroft and N. D. Mermin, "Solid state physics (holt, rinehart and winston, new york, 1976)", Google Scholar, vol. 403, 2005.

[24] M. Toda, "Vibration of a chain with nonlinear interaction", Journal of the Physical Society of Japan, vol. 22, no. 2, pp. 431–436, 1967.

[25] M. Toda, "Mechanics and statistical mechanics of nonlinear chains", Journal of the Physical Society of Japan, vol. 27, no. 6, pp. 1704B–1704B, 1969.

[26] S. Aubry, "A unified approach to the interpretation of displacive and order-disorder systems. ii. displacive systems", The Journal of Chemical Physics, vol. 64, no. 8, pp. 3392–3402, 1976.

[27] J. Krumhansl and J. Schrieffer, "Dynamics and statistical mechanics of a one-dimensional model hamiltonian for structural phase transitions", Physical Review B, vol. 11, no. 9, p. 3535, 1975.

[28] M. A. Collins, "Solitons in chemical physics", Advances of Chemical Physics, vol. 532, pp. 225–280, 1983.

[29] M. A. Collins and D. P. Craig, "A model of localization, soliton propagation, and self-trapping in an electronically excited atomic lattice", Chemical Physics, vol. 75, no. 2, pp. 191–214, 1983.

[30] A. Davydov and N. Kislukha, "Solitary excitons in one-dimensional molecular chains", Physica Status Solidi (b), vol. 59, no. 2, pp. 465–470, 1973.

[31] F. K. Abdullaev, B. Baizakov, S. Darmanyan, V. Konotop, and M. Salerno, "Nonlinear excitations in arrays of bose-einstein condensates", Physical Review A, vol. 64, no. 4, p. 043606, 2001.

[32] A. Trombettoni and A. Smerzi, "Discrete solitons and breathers with dilute bose-einstein condensates", Physical Review Letters, vol. 86, no. 11, p. 2353, 2001.

[33] A. Davydov, "The theory of contraction of proteins under their excitation", Journal of Theoretical Biology, vol. 38, no. 3, pp. 559–569, 1973.

[34] A. S. Davydov, Biology & Quantum Mechanics, vol. 109. Pergamon, 1982.

[35] M. Peyrard and J. Farago, "Nonlinear localization in thermalized lattices: application to dna", Physica A: Statistical Mechanics and its Applications, vol. 288, no. 1, pp. 199–217, 2000.

[36] P. Russell, "Photonic crystal fibers", Science, vol. 299, no. 5605, pp. 358–362, 2003.

[37] D. N. Christodoulides, F. Lederer, and Y. Silberberg, "Discretizing light behaviour in linear and nonlinear waveguide lattices", Nature, vol. 424, no. 6950, pp. 817–823, 2003.

[38] D. Mandelik, H. Eisenberg, Y. Silberberg, R. Morandotti, and J. Aitchison, "Band-gap structure of waveguide arrays and excitation of floquet-bloch solitons", Physical Review Letters, vol. 90, no. 5, p. 053902, 2003.

[39] H. F. Taylor and A. Yariv, "Guided wave optics", Proceedings of the IEEE, vol. 62, no. 8, pp. 1044–1060, 1974.

[40] A. Yariv, "Coupled-mode theory for guided-wave optics", IEEE Journal of Quantum Electronics, vol. 9, no. 9, pp. 919–933, 1973.

[41] A. L. Jones, "Coupling of optical fibers and scattering in fibers", Journal of the Societuy of America, vol. 55, no. 3, pp. 261–271, 1965.

[42] S. Somekh, E. Garmire, A. Yariv, H. Garvin, and R. Hunsperger, "Channel optical waveguide directional couplers", Applied Physics Letters, vol. 22, no. 1, pp. 46–47, 1973.

[43] D. Christodoulides and R. Joseph, "Discrete self-focusing in nonlinear arrays of coupled waveguides", Optics Letters, vol. 13, no. 9, pp. 794–796, 1988.

[44] H. Eisenberg, Y. Silberberg, R. Morandotti, A. Boyd, and J. Aitchison, "Discrete spatial optical solitons in waveguide arrays", Physical Review Letters, vol. 81, no. 16, p. 3383, 1998.

[45] J. W. Fleischer, M. Segev, N. K. Efremidis, and D. N. Christodoulides, "Observation of two-dimensional discrete solitons in optically induced nonlinear photonic lattices", Nature, vol. 422, no. 6928, pp. 147–150, 2003.

[46] R. Iwanow, R. Schiek, G. Stegeman, T. Pertsch, F. Lederer, Y. Min, and W. Sohler, "Observation of discrete quadratic solitons", Physical Review Letters, vol. 93, no. 11, p. 113902, 2004.

[47] A. Fratalocchi, G. Assanto, K. A. Brzdakiewicz, and M. A. Karpierz, "Discrete propagation and spatial solitons in nematic liquid crystals", Optics letters, vol. 29, no. 13, pp. 1530–1532, 2004.

[48] J. Eilbeck and M. Johansson, "Conference on localization and energy transfer in nonlinear systems", World Scientific, 2003.

[49] M. Syafwan, "The existence and stability of solitons in discrete nonlinear Schrödinger equations", PhD thesis, University of Nottingham, 2012.

[50] J. Perring and T. Skyrme, "A model unified field equation", Nuclear Physics, vol. 31, pp. 550–555, 1962.

[51] J. Frenkel and T. Kontorova, "On the theory of plastic deformation and twinning", Izv. Akad. Nauk, Ser. Fiz., vol. 1, pp. 137–149, 1939.

[52] T. Holstein, "Studies of polaron motion: Part i. the molecular-crystal model", Annals of Physics, vol. 8, no. 3, pp. 325–342, 1959.

[53] A. Scott and L. Macneil, "Binding energy versus nonlinearity for a "small" stationary soliton", Physics Letters A, vol. 98, no. 3, pp. 87–88, 1983.

[54] R. MacKay and S. Aubry, "Proof of existence of breathers for time-reversible or hamiltonian networks of weakly coupled oscillators", Nonlinearity, vol. 7, no. 6, p. 1623, 1994.

[55] S. Aubry, "Breathers in nonlinear lattices: Existence, linear stability and quantization", Physica D: Nonlinear Phenomena, vol. 103, no. 1-4, pp. 201–250, 1997.

[56] J. C. Eilbeck, P. Lomdahl, and A. Scott, "The discrete self-trapping equation", Physica D: Nonlinear Phenomena, vol. 16, no. 3, pp. 318–338, 1985.

[57] J. Eilbeck, "Nonlinear vibrational modes in a hexagonal molecule", Physics of Many-Particle Systems, vol. 12, pp. 41–51, 1987.

[58] A. M. Morgante, M. Johansson, G. Kopidakis, and S. Aubry, "Standing wave instabilities in a chain of nonlinear coupled oscillators", Physica D: Nonlinear Phenomena, vol. 162, no. 1, pp. 53–94, 2002.

[59] Y. S. Kivshar and M. Peyrard, "Modulational instabilities in discrete lattices", Physical Review A, vol. 46, no. 6, p. 3198, 1992.

[60] I. Daumont, T. Dauxois, and M. Peyrard, "Modulational instability: first step towards energy localization in nonlinear lattices", Nonlinearity, vol. 10, no. 3, pp. 617–630, 1997.

[61] J. Carr and J. Eilbeck, "Stability of stationary solutions of the discrete self-trapping equation", Physics Letters A, vol. 109, no. 5, pp. 201–204, 1985.

[62] M. Syafwan, H. Susanto, and S. Cox, "Solitons in a parametrically driven damped discrete nonlinear schrödinger equation", in Spontaneous symmetry breaking, Self-Trapping, and Josephson oscillations, pp. 601–638, Springer, 2013.

[63] B. Orr and J. Ward, "Perturbation theory of the non-linear optical polarization of an isolated system", Molecular Physics, vol. 20, no. 3, pp. 513–526, 1971.

[64] P. Grisvard, "Elliptic problems in nonsmooth domains", vol. 69. SIAM, 2011.

[65] N. Moiseyev, "Non-Hermitian quantum mechanics", Cambridge University Press, 2011.

[66] C. M. Bender, S. Boettcher, and P. N. Meisinger, "$\mathcal{PT}$-symmetric quantum mechanics", Journal of Mathematical Physics, vol. 40, no. 5, pp. 2201–2229, 1999.

[67] A. Guo, G. Salamo, D. Duchesne, R. Morandotti, M. Volatier-Ravat, V. Aimez, G. Siviloglou, and D. Christodoulides, "Observation of $\mathcal{PT}$-symmetry breaking in complex optical potentials", Physical Review Letters, vol. 103, no. 9, p. 093902, 2009.

[68] C. E. Rüter, K. G. Makris, R. El-Ganainy, D. N. Christodoulides, M. Segev, and D. Kip, "Observation of parity-time symmetry in optics", Nature Physics, vol. 6, no. 3, pp. 192–195, 2010.

[69] S. V. Suchkov, A. A. Sukhorukov, J. Huang, S. V. Dmitriev, C. Lee, and Y. S. Kivshar, "Nonlinear switching and solitons in $\mathcal{PT}$-symmetric photonic systems", Laser & Photonics Reviews, vol. 10, no. 2, pp. 177–213, 2016.

[70] V. V. Konotop, J. Yang, and D. A. Zezyulin, "Nonlinear waves in $\mathcal{PT}$-symmetric systems", Reviews of Modern Physics, vol. 88, no. 3, p. 035002, 2016.

[71] J. Pickton and H. Susanto, "Integrability of $\mathcal{PT}$-symmetric dimers", Physical Review A, vol. 88, no. 6, p. 063840, 2013.

[72] P. G. Kevrekidis, D. E. Pelinovsky, and D. Y. Tyugin, "Nonlinear dynamics in $\mathcal{PT}$-symmetric lattices", Journal of Physics A: Mathematical and Theoretical, vol. 46, no. 36, p. 365201, 2013.

[73] I. Barashenkov, G. Jackson, and S. Flach, "Blow-up regimes in the $\mathcal{PT}$-symmetric coupler and the actively coupled dimer", Physical Review A, vol. 88, no. 5, p. 053817, 2013.

[74] S. V. Suchkov, B. A. Malomed, S. V. Dmitriev, and Y. S. Kivshar, "Solitons in a chain of $\mathcal{PT}$-invariant dimers", Physical Review E, vol. 84, no. 4, p. 046609, 2011.

[75] P. L. Chu, B. A. Malomed, and G.-D. Peng, "Soliton switching and propagation in nonlinear fiber couplers: analytical results", Journal of Optical Society of America B, vol. 10, no. 8, pp. 1379–1385, 1993.

[76] E. M. Wright, G. Stegeman, and S. Wabnitz, "Solitary-wave decay and symmetry-breaking instabilities in two-mode fibers", Physical Review A, vol. 40, no. 8, p. 4455, 1989.

[77] N. Akhmediev and J. Soto-Crespo, "Propagation dynamics of ultrashort pulses in nonlinear fiber couplers", Physical Review E, vol. 49, no. 5, p. 4519, 1994.

[78] B. A. Malomed, I. Skinner, P. Chu, and G. Peng, "Symmetric and asymmetric solitons in twin-core nonlinear optical fibers", Physical Review E, vol. 53, no. 4, p. 4084, 1996.

[79] R. Driben and B. A. Malomed, "Stability of solitons in $\mathcal{PT}$-symmetric couplers", Optics Letters, vol. 36, no. 22, pp. 4323–4325, 2011.

[80] F. K. Abdullaev, V. Konotop, M. Ögren, and M. P. Sørensen, "Zeno effect and switching of solitons in nonlinear couplers", Optics Letters, vol. 36, no. 23, pp. 4566–4568, 2011.

[81] R. Driben and B. Malomed, "Stabilization of solitons in $\mathcal{PT}$ models with supersymmetry by periodic management", EPL (Europhysics Letters), vol. 96, no. 5, p. 51001, 2011.

[82] N. Alexeeva, I. Barashenkov, A. A. Sukhorukov, and Y. S. Kivshar, "Optical solitons in $\mathcal{PT}$-symmetric nonlinear couplers with gain and loss", Physical Review A, vol. 85, no. 6, p. 063837, 2012.

[83] P. Li, L. Li, and B. A. Malomed, "Multisoliton newton's cradles and supersolitons in regular and parity-time-symmetric nonlinear couplers", Physical Review E, vol. 89, no. 6, p. 062926, 2014.

[84] J. D'Ambroise, P. G. Kevrekidis, and B. A. Malomed, "Staggered parity-time-symmetric ladders with cubic nonlinearity", Physical Review E, vol. 91, no. 3, p. 033207, 2015.

[85] G. Herring, P. Kevrekidis, B. Malomed, R. Carretero-González, and D. Frantzeskakis, "Symmetry breaking in linearly coupled dynamical lattices", Physical Review E, vol. 76, no. 6, p. 066606, 2007.

[86] A. Chernyavsky and D. E. Pelinovsky, "Breathers in hamiltonian (*pt*)-symmetric chains of coupled pendula under a resonant periodic force", Symmetry, vol. 8, no. 7, p. 59, 2016.

[87] C. M. Bender, B. K. Berntson, D. Parker, and E. Samuel, "Observation of pt phase transition in a simple mechanical system", American Journal of Physics, vol. 81, no. 3, pp. 173–179, 2013.

[88] A. Chernyavsky and D. E. Pelinovsky, "Long-time stability of breathers in hamiltonian (pt)-symmetric lattices", Journal of Physics A: Mathematical and Theoretical, vol. 49, no. 47, p. 475201, 2016.

[89] V. Konotop, D. Pelinovsky, and D. Zezyulin, "Discrete solitons in $\mathcal{PT}$-symmetric lattices", EPL (Europhysics Letters), vol. 100, no. 5, p. 56006, 2012.

[90] D. E. Pelinovsky, D. A. Zezyulin, and V. V. Konotop, "Nonlinear modes in a generalized $\mathcal{PT}$-symmetric discrete nonlinear schrödinger equation", Journal of Physics A: Mathematical and Theoretical, vol. 47, no. 8, p. 085204, 2014.

[91] K. Li and P. Kevrekidis, "$\mathcal{PT}$-symmetric oligomers: analytical solutions, linear stability, and nonlinear dynamics", Physical Review E, vol. 83, no. 6, p. 066608, 2011.

[92] J. Bernabeu, "$\mathcal{T}$ and $\mathcal{CPT}$ symmetries in entangled neutral meson systems", in Journal of Physics: Conference Series, vol. 335, p. 012011, IOP Publishing, 2011.

[93] A. Aguilar-Arevalo, C. Anderson, A. Bazarko, S. Brice, B. Brown, L. Bugel, J. Cao, L. Coney, J. Conrad, D. Cox, et al., "Test of lorentz and cpt violation with short baseline neutrino oscillation excesses", Physics Letters B, vol. 718, no. 4, pp. 1303–1308, 2013.

[94] L. G. Yaffe, "Particles and symmetries", University of Washington, 2013.

[95] C. M. Bender, "Properties of non-hermitian quantum field theories", in Annales de l'institut Fourier, vol. 53, pp. 997–1008, 2003.

[96] C. Bender, A. Fring, U. Günther, and H. Jones, "Quantum physics with non-hermitian operators", Journal of Physics A: Mathematical and Theoretical, vol. 45, no. 44, p. 440301, 2012.

[97] A. Ruschhaupt, F. Delgado, and J. Muga, "Physical realization of $\mathcal{PT}$-symmetric potential scattering in a planar slab waveguide", Journal of Physics A: Mathematical and General, vol. 38, no. 9, p. L171, 2005.

[98] Z. Musslimani, K. G. Makris, R. El-Ganainy, and D. N. Christodoulides, "Optical solitons in $\mathcal{PT}$ periodic potentials", Physical Review Letters, vol. 100, no. 3, p. 030402, 2008.

[99] K. G. Makris, R. El-Ganainy, D. N. Christodoulides, and Z. H. Musslimani, "Beam dynamics in $\mathcal{PT}$-symmetric optical lattices", Physical Review Letters, vol. 100, no. 10, p. 103904, 2008.

[100] S. Longhi, "Spectral singularities and bragg scattering in complex crystals", Physical Review A, vol. 81, no. 2, p. 022102, 2010.

[101] Z. Lin, H. Ramezani, T. Eichelkraut, T. Kottos, H. Cao, and D. N. Christodoulides, "Unidirectional invisibility induced by $\mathcal{PT}$-symmetric periodic structures," Physical Review Letters, vol. 106, no. 21, p. 213901, 2011.

[102] X. Zhu, H. Wang, L.-X. Zheng, H. Li, and Y.-J. He, "Gap solitons in parity-time complex periodic optical lattices with the real part of superlattices," Optics Letters, vol. 36, no. 14, pp. 2680–2682, 2011.

[103] K. Makris, R. El-Ganainy, D. Christodoulides, and Z. H. Musslimani, "$\mathcal{PT}$-symmetric periodic optical potentials," International Journal of Theoretical Physics, vol. 50, no. 4, pp. 1019–1041, 2011.

[104] L. Feng, M. Ayache, J. Huang, Y.-L. Xu, M.-H. Lu, Y.-F. Chen, Y. Fainman, and A. Scherer, "Nonreciprocal light propagation in a silicon photonic circuit," Science, vol. 333, no. 6043, pp. 729–733, 2011.

[105] A. Regensburger, C. Bersch, M.-A. Miri, G. Onishchukov, D. N. Christodoulides, and U. Peschel, "Parity-time synthetic photonic lattices," Nature, vol. 488, no. 7410, p. 167, 2012.

[106] L. Razzari and R. Morandotti, "Optics: Gain and loss mixed in the same cauldron," Nature, vol. 488, no. 7410, pp. 163–164, 2012.

[107] G. Burlak and B. A. Malomed, "Stability boundary and collisions of two-dimensional solitons in $\mathcal{PT}$-symmetric couplers with the cubic-quintic nonlinearity," Physical Review E, vol. 88, no. 6, p. 062904, 2013.

[108] G. Burlak, S. Garcia-Paredes, and B. A. Malomed, "$\mathcal{PT}$-symmetric couplers with competing cubic-quintic nonlinearities," Chaos: An Interdisciplinary Journal of Nonlinear Science, vol. 26, no. 11, p. 113103, 2016.

[109] H. Sakaguchi and B. A. Malomed, "One-and two-dimensional solitons in $\mathcal{PT}$-symmetric systems emulating spin-orbit coupling," New Journal of Physics, vol. 18, no. 10, p. 105005, 2016.

[110] B. Dana, A. Bahabad, and B. A. Malomed, "$\mathcal{CP}$ symmetry in optical systems," Physical Review A, vol. 91, no. 4, p. 043808, 2015.

[111] S. Karthiga, V. Chandrasekar, M. Senthilvelan, and M. Lakshmanan, "Systems that become $\mathcal{PT}$-symmetric through interaction," Physical Review A, vol. 94, no. 2, p. 023829, 2016.

[112] Y. Kartashov, V. Konotop, and D. Zezyulin, "$\mathcal{CPT}$-symmetric spin-orbit-coupled condensate," EPL (Europhysics Letters), vol. 107, no. 5, p. 50002, 2014.

[113] F. Lederer, G. I. Stegeman, D. N. Christodoulides, G. Assanto, M. Segev, and Y. Silberberg, "Discrete solitons in optics," Physics Reports, vol. 463, no. 1, pp. 1–126, 2008.

[114] A. Boardman and K. Xie, "Bright spatial soliton dynamics in a symmetric optical planar waveguide structure," Physical Review A, vol. 50, no. 2, p. 1851, 1994.

[115] D. Kaup and B. Malomed, "Gap solitons in asymmetric dual-core nonlinear optical fibers," Journal of the Optical Society of America B, vol. 15, no. 12, pp. 2838–2846, 1998.

[116] B. Dana, B. A. Malomed, and A. Bahabad, "Breathing solitary-pulse pairs in a linearly coupled system," Optics Letters, vol. 39, no. 7, pp. 2175–2178, 2014.

[117] H. Eisenberg, Y. Silberberg, R. Morandotti, and J. Aitchison, "Diffraction management," Physical Review Letters, vol. 85, no. 9, p. 1863, 2000.

[118] J. Marin and S. Aubry, "Breathers in nonlinear lattices: Numerical calculation from the anticontinuous limit," Nonlinearity, vol. 9, no. 6, p. 1501, 1996.

[119] D. Chen, S. Aubry, and G. Tsironis, "Breather mobility in discrete φ 4 nonlinear lattices," Physical Review Letters, vol. 77, no. 23, p. 4776, 1996.

[120] R. Nickalls, "The quartic equation: invariants and euler's solution revealed," The Mathematical Gazette, vol. 93, no. 526, pp. 66–75, 2009.

[121] O. B. Kirikchi, A. A. Bachtiar, and H. Susanto, "Bright solitons in a $\mathcal{PT}$-symmetric chain of dimers," Advances in Mathematical Physics, vol. 2016, no. 9514230,, 2016.

[122] B. Malomed and P. Kevrekidis, "Discrete vortex solitons," Physical Review E, vol. 64, no. 2, p. 026601, 2001.

[123] H.-G. Purwins, H. Bödeker, and S. Amiranashvili, "Dissipative solitons," Advances in Physics, vol. 59, no. 5, pp. 485–701, 2010.

[124] S. Barbay, X. Hachair, T. Elsass, I. Sagnes, and R. Kuszelewicz, "Homoclinic snaking in a semiconductor-based optical system," Physical Review Letters, vol. 101, no. 25, p. 253902, 2008.

[125] F. Haudin, R. Rojas, U. Bortolozzo, S. Residori, and M. Clerc, "Homoclinic snaking of localized patterns in a spatially forced system," Physical Review Letters, vol. 107, no. 26, p. 264101, 2011.

[126] D. J. Lloyd, C. Gollwitzer, I. Rehberg, and R. Richter, "Homoclinic snaking near the surface instability of a polarisable fluid," Journal of Fluid Mechanics, vol. 783, pp. 283–305, 2015.

[127] Y. Pomeau, "Front motion, metastability and subcritical bifurcations in hydrodynamics," Physica D: Nonlinear Phenomena, vol. 23, no. 1, pp. 3–11, 1986.

[128] P. Coullet, C. Riera, and C. Tresser, "Stable static localized structures in one dimension," Physical Review Letters, vol. 84, no. 14, p. 3069, 2000.

[129] P. Woods and A. Champneys, "Heteroclinic tangles and homoclinic snaking in the unfolding of a degenerate reversible hamiltonian–hopf bifurcation," Physica D: Nonlinear Phenomena, vol. 129, no. 3, pp. 147–170, 1999.

[130] H. Sakaguchi and H. R. Brand, "Stable localized solutions of arbitrary length for the quintic swift-hohenberg equation," Physica D: Nonlinear Phenomena, vol. 97, no. 1-3, pp. 274–285, 1996.

[131] J. Burke and E. Knobloch, "Localized states in the generalized swift-hohenberg equation," Physical Review E, vol. 73, no. 5, p. 056211, 2006.

[132] J. Burke and E. Knobloch, "Homoclinic snaking: structure and stability," Chaos: An Interdisciplinary Journal of Nonlinear Science, vol. 17, no. 3, p. 037102, 2007.

[133] J. Burke and E. Knobloch, "Snakes and ladders: localized states in the swift–hohenberg equation," Physics Letters A, vol. 360, no. 6, pp. 681–688, 2007.

[134] S. J. Chapman and G. Kozyreff, "Exponential asymptotics of localised patterns and snaking bifurcation diagrams," Physica D: Nonlinear Phenomena, vol. 238, no. 3, pp. 319–354, 2009.

[135] G. Kozyreff and S. J. Chapman, "Asymptotics of large bound states of localized structures," Physical Review Letters, vol. 97, no. 4, p. 044502, 2006.

[136] A. D. Dean, P. Matthews, S. Cox, and J. King, "Exponential asymptotics of homoclinic snaking," Nonlinearity, vol. 24, no. 12, p. 3323, 2011.

[137] H. Susanto and P. Matthews, "Variational approximations to homoclinic snaking," Physical Review E, vol. 83, no. 3, p. 035201, 2011.

[138] R. Carretero-González, J. Talley, C. Chong, and B. Malomed, "Multistable solitons in the cubic-quintic discrete nonlinear schrödinger equation," Physica D: Nonlinear Phenomena, vol. 216, no. 1, pp. 77–89, 2006.

[139] C. Chong, R. Carretero-González, B. Malomed, and P. Kevrekidis, "Multistable solitons in higher-dimensional cubic-quintic nonlinear schrödinger lattices," Physica D: Nonlinear Phenomena, vol. 238, no. 2, pp. 126–136, 2009.

[140] C. Chong and D. E. Pelinovsky, "Variational approximations of bifurcations of asymmetric solitons in cubic-quintic nonlinear schrödinger lattices," arXiv preprint arXiv:0904.3387, 2009.

[141] C. Taylor and J. H. Dawes, "Snaking and isolas of localised states in bistable discrete lattices," Physics Letters A, vol. 375, no. 1, pp. 14–22, 2010.

[142] A. Yulin, A. Champneys, and D. Skryabin, "Discrete cavity solitons due to saturable nonlinearity," Physical Review A, vol. 78, no. 1, p. 011804, 2008.

[143] A. Yulin and A. R. Champneys, "Discrete snaking: Multiple cavity solitons in saturable media," SIAM Journal on Applied Dynamical Systems, vol. 9, no. 2, pp. 391–431, 2010.

[144] M. G. Clerc, R. G. Elías, and R. G. Rojas, "Continuous description of lattice discreteness effects in front propagation," Philosophical Transactions of the Royal Society of London A: Mathematical, Physical and Engineering Sciences, vol. 369, no. 1935, pp. 412–424, 2011.

[145] N. McCullen and T. Wagenknecht, "Pattern formation on networks: from localised activity to turing patterns," Scientific Reports, vol. 6, 2016.

[146] P. Matthews and H. Susanto, "Variational approximations to homoclinic snaking in continuous and discrete systems," Physical Review E, vol. 84, no. 6, p. 066207, 2011.

[147] A. D. Dean, P. C. Matthews, S. M. Cox, and J. R. King, "Orientation-dependent pinning and homoclinic snaking on a planar lattice," SIAM Journal on Applied Dynamical Systems, vol. 14, no. 1, pp. 481–521, 2015.

[148] J.-L. Coutaz and M. Kull, "Saturation of the nonlinear index of refraction in semiconductor-doped glass," Journal of the Optical Society of America B, vol. 8, no. 1, pp. 95–98, 1991.

[149] E. Smirnov, C. E. Rüter, M. Stepić, D. Kip, and V. Shandarov, "Formation and light guiding properties of dark solitons in one-dimensional waveguide arrays," Physical Review E, vol. 74, no. 6, p. 065601, 2006.

[150] R. Kusdiantara and H. Susanto, "Homoclinic snaking in the discrete swift-hohenberg equation," Unpublished, 2017.

[151] Y. Chong, L. Ge, and A. D. Stone, "$\mathcal{PT}$-symmetry breaking and laser-absorber modes in optical scattering systems," Physical Review Letters, vol. 106, no. 9, p. 093902, 2011.

[152] A. Rodrigues, K. Li, V. Achilleos, P. Kevrekidis, D. Frantzeskakis, and C. M. Bender, "$\mathcal{PT}$-symmetric double well potentials revisited: bifurcations, stability and dynamics," Romanian Reports in Physics, vol. 65, no. 1, pp. 5–26, 2013.

[153] A. Carpio and L. L. Bonilla, "Depinning transitions in discrete reaction-diffusion equations," SIAM Journal on Applied Mathematics, vol. 63, no. 3, pp. 1056–1082, 2003.

[154] M. Wolfrum, "The turing bifurcation in network systems: Collective patterns and single differentiated nodes," Physica D: Nonlinear Phenomena, vol. 241, no. 16, pp. 1351–1357, 2012.

[155] S. Flach and K. Kladko, "Perturbation analysis of weakly discrete kinks," Physical Review E, vol. 54, no. 3, p. 2912, 1996.

[156] S. Usikov, Nonlinear Physics, vol. 4. CRC Press, 1988.

[157] J. H. Dawes and H. Susanto, "Variational approximation and the use of collective coordinates," Physical Review E, vol. 87, no. 6, p. 063202, 2013.

[158] Z. Chen, J. Liu, S. Fu, Y. Li, and B. A. Malomed, "Discrete solitons and vortices on two-dimensional lattices of $\mathcal{PT}$-symmetric couplers," Optics Express, vol. 22, no. 24, pp. 29679–29692, 2014.

Appendix A

Analytical calculation

As mentioned in Section 4.3.3, to solve the eigenvalue problem (3.12) analytically we expand the eigenvalue and eigenvector asymptotically as

$$\square = \square^{(0)} + \sqrt{\epsilon}\square^{(1)} + \epsilon\square^{(2)} + \dots, \tag{A.0.1}$$

with $\square = \lambda, K_n, L_n, P_n, Q_n$.

Performing the expansion in ϵ, at $O(\epsilon^0)$ we obtain the following set of equations

$$\lambda^{(0)}\underline{v}_n^{(0)} = \underbrace{\begin{bmatrix} \gamma & \omega - A_n^{(0)^2} & 0 & -1 \\ 3(A_n^{(0)})^2 - \omega & \gamma & 1 & 0 \\ 0 & -1 & k_1 & k_2 \\ 1 & 0 & k_3 & k_4 \end{bmatrix}}_{M_0} \underline{v}_n^{(0)}, \tag{A.0.2}$$

where

$$\underline{v}_n^{(j)} = \begin{bmatrix} K_n^{(j)} \\ L_n^{(j)} \\ P_n^{(j)} \\ Q_n^{(j)} \end{bmatrix},$$

$$k_1 = -(2\Re(B_n^{(0)})\Im(B_n^{(0)}) + \gamma), \quad k_2 = \omega - \Re(B_n^{(0)})^2 - 3\Im(B_n^{(0)})^2,$$
$$k_3 = 3\Re(B_n^{(0)})^2 + \Im(B_n^{(0)})^2 - \omega, \quad k_4 = 2\Re(B_n^{(0)})\Im(B_n^{(0)}) - \gamma.$$

At $O(\epsilon^{1/2})$ and $O(\epsilon^1)$, we obtain

$$\lambda^{(0)}\underline{v}_n^{(1)} = M_0\underline{v}_n^{(1)} - \lambda^{(1)}\underline{v}_n^{(0)}, \tag{A.0.3}$$

$$\begin{aligned}\lambda^{(0)}\underline{v}_n^{(2)} &= M_0\underline{v}_n^{(2)} - \lambda^{(1)}\underline{v}_n^{(1)} - \lambda^{(2)}\underline{v}_n^{(0)} \\ &+ \underbrace{\begin{bmatrix} 0 & 2\left(1 - A_n^{(0)}A_n^{(1)}\right) & 0 & 0 \\ 6A_n^{(0)}A_n^{(1)} - 2 & 0 & 0 & 0 \\ 0 & 0 & k_5 & 2 + k_6 \\ 0 & 0 & k_7 - 2 & k_8 \end{bmatrix}}_{M_1}\underline{v}_n^{(0)} \\ &+ \begin{bmatrix} 0 & -1 & 0 & 0 \\ 1 & 0 & 0 & 0 \\ 0 & 0 & 0 & -1 \\ 0 & 0 & 1 & 0 \end{bmatrix}\left(\underline{v}_{n+1}^{(1)} + \underline{v}_{n-1}^{(1)}\right),\end{aligned} \tag{A.0.4}$$

where

$$\begin{aligned} k_5 &= -2(\Re(B_n^{(0)})\Im(B_n^{(1)}) + \Re(B_n^{(1)})\Im(B_n^{(0)})), \\ k_6 &= -2(\Re(B_n^{(0)})\Re(B_n^{(1)}) + 3\Im(B_n^{(0)})\Im(B_n^{(1)})), \\ k_7 &= 2(3\Re(B_n^{(0)})\Re(B_n^{(1)}) + \Im(B_n^{(0)})\Im(B_n^{(1)})), \\ k_8 &= 2(\Re(B_n^{(0)})\Im(B_n^{(1)}) + \Re(B_n^{(1)})\Im(B_n^{(0)})). \end{aligned}$$

The steps of finding the coefficients $\lambda^{(j)}$ of the asymptotic expansions, $j = 0, 1, 2, \ldots$, are as follows.

1. Solve the eigenvalue problem (A.0.2), which is a 4×4 system of equations, for $\lambda^{(0)}$ and $\underline{v}_n^{(0)}$.

2. Determine $\lambda^{(1)}$ by taking the vector inner product of both sides of (A.0.3) with the null-space of the Hermitian transpose of the block matrix that consists of $\left(M_0 - \lambda^{(0)}I_4\right)$ along the diagonal, where I_4 is the 4×4 identity matrix.

3. Solve (A.0.3) for $\underline{v}_n^{(1)}$.

4. Determine $\lambda^{(2)}$ by taking the vector inner product of both sides of (A.0.4) with the null-space of the Hermitian transpose of the block matrix that consists of $\left(M_0 - \lambda^{(0)}I_4\right)$.

The procedure repeats if one would like to calculate the higher order terms.

The leading order eigenvalue $\lambda^{(0)}$ of (A.0.2) has been solved in [91]. However, the expression of the corresponding eigenvector $\underline{v}_n^{(0)}$ was very lengthy, that makes it almost

impractical to be used to determine the higher order corrections of $\lambda^{(j)}$. Therefore, in every equation at order $O(\epsilon^{\ell})$, $\ell = 0, 1/2, 1, \ldots$, obtained from (3.12), we also expand the variables in γ, i.e.

$$M_j = M_{j,0} + \gamma M_{j,1} + \gamma^2 M_{j,2} = \ldots, \; \square^{(j)} = \square^{(j,0)} + \gamma \square^{(j,1)} + \gamma^2 \square^{(j,2)} + \ldots,$$

where again $\square = \lambda, \underline{v}_n$, and obtain equations at order $O(\gamma^{\hat{\ell}})$, $\hat{\ell} = 0, 1, 2, \ldots$. The steps to determine $\lambda^{(j,k)}$ and $\underline{v}_n^{(j,k)}$ are the same as mentioned above.

Publications

- O. B. Kirikchi, A. A. Bachtiar, and H. Susanto, Bright solitons in a pt-symmetric chain of dimers, Advances in Mathematical Physics, vol. 2016, 9514230, (2016).
- O. B. Kirikchi, Boris A. Malomed, N. Karjanto, R. Kusdiantara, and H. Susanto, Solitons in a chain of $\mathcal{CP}$-symmetric dimers, submitted.